CARLOS AUGUSTO PRETE JUNIOR

ACOUSTIC EMISSION SIGNAL PROCESSING

São Paulo
2020

CARLOS AUGUSTO PRETE JUNIOR

ACOUSTIC EMISSION SIGNAL PROCESSING

Dissertação apresentada à Escola Politécnica da Universidade de São Paulo para obtenção do Título de Mestre em Ciências.

São Paulo
2020

CARLOS AUGUSTO PRETE JUNIOR

ACOUSTIC EMISSION SIGNAL PROCESSING

Versão Corrigida

Dissertação apresentada à Escola Politécnica da Universidade de São Paulo para obtenção do Título de Mestre em Ciências.

Orientador:
Vítor Heloiz Nascimento

Co-orientador:
Cássio Guimarães Lopes

São Paulo
2020

Este exemplar foi revisado e corrigido em relação à versão original, sob responsabilidade única do autor e com a anuência de seu orientador.

São Paulo, _____ de _____ de _____

Assinatura do autor: _____

Assinatura do orientador: _____

Catalogação-na-publicação

Prete Jr., Carlos Augusto
Acoustic Emission Signal Processing / C. A. Prete Jr. -- versão corr. -- São Paulo, 2020.
135 p.

Dissertação (Mestrado) - Escola Politécnica da Universidade de São Paulo. Departamento de Engenharia de Sistemas Eletrônicos.

1.Processamento de Sinais 2.Emissão Acústica 3.Localização de Fontes 4.Ensaios Não Destrutivos 5.Compressive Sensing I.Universidade de São Paulo. Escola Politécnica. Departamento de Engenharia de Sistemas Eletrônicos II.t.

ACKNOWLEDGMENTS

First of all, I would like to thank God for guiding me through all the stages of my life and for making this work possible.

I would also like to thank my advisors Vítor Heloiz Nascimento and Cássio Guimarães Lopes for helping me with indispensable technical advises along these years and for everything they have taught me.

I am deeply grateful to all the people that have supported me during my academic life, especially my father Carlos, my mother Stella and my beloved Tayná.

This work was supported by FAPESP (grant 2017/20933-2), CAPES and Embraer.

ABSTRACT

Acoustic Emission is a widely used structure health monitoring (SHM) method for monitoring large structures with high sensitivity. When an acoustic source is active (for example, during the expansion of a crack), it emits an elastic wave that reaches the sensors that are spread along the structure surface. The signals sampled by these sensors are processed and used to estimate the source position.

In this work, we study acoustic emission techniques based on the time of arrival (TOA) of the signals received by the sensors and develop methods to improve the source position estimate. More specifically, we derive the probability distribution of the TOA measured by the fixed threshold method, a popular TOA estimation algorithm, as well as an expression for its bias and consequently a TOA debiasing method. Moreover, we derive a nearly-optimal TOA-based source position estimator. Algorithms for anisotropic structures are also investigated.

In scenarios where multiple sources are active simultaneously, it is important to group signals (hits) from the same source to avoid using signals emitted by other sources in the localization algorithm. For this reason, we develop hit grouping techniques and compare them with existing methods.

We also create a source localization algorithm that directly uses the signals received by the sensors instead of TOAs to estimate the source position. This method takes into account the wave propagation model and also the sparsity of the source signal in a known dictionary to improve the localization performance using sparse reconstruction methods.

This work was partially supported by EMBRAER, which provided data of actual acoustic emission tests in complex structures.

Keywords – Acoustic Emission, Source Localization, Signal Processing, Time of Arrival, Structural Health Monitoring, Nondestructive Testing, Sparse Estimation, Compressive Sensing.

RESUMO

A Emissão Acústica é uma técnica de monitoramento de saúde de estruturas (structure health monitoring — SHM) amplamente usado na indústria, permitindo o monitoramento de grandes superfícies com alta sensitividade. Quando uma fonte acústica está ativa (por exemplo, durante a expansão de uma trinca), uma onda elástica é emitida por ela. Esta onda se propaga até os sensores espalhados na superfície da estrutura, que amostram os sinais recebidos para então serem processados e usados para estimar a posição da fonte acústica.

Neste trabalho, são estudadas técnicas de emissão acústica baseadas em tempo de chegada (time of arrival — TOA) dos sinais recebidos pelos sensores e desenvolvidos novos métodos com o objetivo de melhorar a estimativa da posição da trinca. Especificamente, deriva-se a função densidade de probabilidade dos TOAs quando estes são estimado pelo método do limiar fixo, um algoritmo popular de estimação de tempo de chegada, além de uma expressão para seu viés e consequentemente um método de remoção de viés. Além disso, deriva-se a expressão de um estimador de posição baseado em TOAs próximo ao estimador ótimo. Algoritmos para estruturas anisotrópicas também são investigados.

Em cenários onde múltiplas fontes acústicas estão ativas simultaneamente, é importante agrupar sinais (hits) provenientes da mesma fonte a fim de evitar utilizar sinais emitidos por outras fontes em algoritmos de localização. Por este motivo, neste trabalho desenvolve-se algoritmos de agrupamento de hits, que são comparados com outros métodos já existentes.

Também desenvolveu-se um algoritmo de localização que usa diretamente os sinais amostrados pelos sensores ao invés dos tempos de chegada para estimar a posição da fonte. Este método leva em consideração o modelo de propagação da onda e também o fato de que o sinal da fonte acústica é esparso em um dicionário conhecido para melhorar seu desempenho através de técnicas de reconstrução esparsa.

Este trabalho foi parcialmente financiado pela EMBRAER, que forneceu dados de ensaios reais de emissão acústica realizados em estruturas complexas.

Palavras-Chave – Emissão Acústica, Localização de Fontes, Processamento de Sinais, Tempo de Chegada, Monitoramento de Saúde de Estruturas, Ensaios Não Destrutivos, Estimação Esparsa, Compressive Sensing.

LIST OF FIGURES

LIST OF SYMBOLS

$\mathcal{F}\{\cdot\}$: Fourier Transform, defined here by $\mathcal{F}\{x\}(\Omega) = \int_{-\infty}^{+\infty} x(t)e^{-j\Omega t}\mathrm{d}t$.
$\mathcal{H}\{\cdot\}$: Hilbert Transform
$\mathbb{E}\{\cdot\}$: Expected Value
$\mathbb{P}(A)$: Probability of A
$*$: Convolution operator
$\Gamma(\cdot)$: The Gamma Function
$\lfloor\cdot\rfloor$: Floor operator
$\lceil\cdot\rceil$: Ceil operator
$\mathbf{A}_{:,k}$: A column-vector extracted from the k-th column of the matrix $\mathbf{A}$.
$\mathbf{A}_{k,:}$: A row-vector extracted from the k-th row of the matrix $\mathbf{A}$.
$\mathbf{A}^{\dagger}$: The pseudo-inverse of the matrix $\mathbf{A}$.
$\|\mathbf{x}\|_p$: The ℓ_p-norm of the $N \times 1$ vector $\mathbf{x}$, defined as

$$\|\mathbf{x}\|_p = \left[\sum_{i=1}^{N} |x_i|^p\right]^{\frac{1}{p}}$$

$\|\mathbf{x}\|_0$: The ℓ_0-pseudo-norm of the $N \times 1$ vector $\mathbf{x}$, defined as the number of nonzero entries of $\mathbf{x}$.
$\|\mathbf{A}\|_F$: The Frobenius norm of matrix $\mathbf{A}$, defined as $\|\mathbf{A}\|_F = \sqrt{\mathrm{tr}\{\mathbf{A}^T\mathbf{A}\}}$.
$|\mathcal{S}|$: The number of elements of the set $\mathcal{S}$.
$\mathrm{supp}\{\mathbf{x}\}$: The support I of the vector $\mathbf{x}$, defined as $I = \{i : \mathbf{x}_i \neq 0\}$
$\mathbf{1}_{\mathcal{S}}(x)$: The indicator function, equal to 1 if $x \in \mathcal{S}$ and 0 if $x \notin \mathcal{S}$.
$\mathbf{I}$: Identity matrix.
$\mathbf{1}$: Column vector whose entries are all equal to one.
$\mathbf{e}_k$: The vector whose k-th element is one, and all other elements are zero.

CONTENTS

1 INTRODUCTION TO ACOUSTIC EMISSION TESTING

Acoustic emission testing is a non-destructive testing method used to detect several kinds of faults in structures such as piping, bridges and aerospace structures. Its main advantages over other non-destructive testing methods are the high sensibility, the wide coverage region and the possibility of monitoring structures in real time [1–6]. Elastic waves that propagate through the medium are detected by acoustic emission sensors, and as the signal is acquired at each sensor its time of arrival is estimated and used to localize sources.

The objective of acoustic emission methods is to estimate the position of acoustic sources (such as cracks or rivets under stress) that emit elastic waves. This is done by scattering acoustic emission sensors along the structure to be monitored, and processing the received signal. In some applications it is also important to identify the nature of the source [7] (for example, classify the source as a growing crack, an active rivet, oscillation due to an external actuator or noise). This work aims at improving source localization algorithms, hence we are not interested in the source classification step.

In acoustic emission, a *hit* is a segment of the signal acquired by a sensor that is identified as a wave that reached it. Hits from different sensors are grouped (using a hit grouping algorithm) and used to localize the potential source, forming an *event*. A hit can occur not only due to physical faults, but also because of oscillation caused by actuators that stress the structure or simply noise.

Most acoustic emission methods extract the time of arrival (TOA) from the hits that belong to an event and use them to estimate the source position [7–12]. In these TOA-based methods, the estimated TOAs depend on the sampled signals, and the estimated position only depends on these estimated TOAs. On the other hand, there are authors who use directly the sampled signals to localize the source instead of estimating TOAs [13–16]. At first, we were interested in developing better TOA estimation methods. Although localization algorithms based on TOAs usually assume a Gaussian distribution

for the uncertainties in the TOA estimates [17–20], we observed that when applied to actual acoustic emission waveforms, the most popular TOA estimation method – the fixed threshold algorithm [21] – produces estimates with a non-Gaussian distribution and large bias in general, causing a considerable bias in the position estimate. For this reason, we model the TOA estimate probability distribution (and bias) for the fixed threshold method in Chapter 2, which is an extended version of the paper [22] (see Appendix), presented at EUSIPCO 2018. The TOA probability density function (pdf) is also derived in Chapter 2, as well as a debiasing technique.

In Chapter 3, localization techniques based on TOAs are studied on both isotropic and anisotropic structures, as well as an alternative TOA estimation method based on the Akaike Information Criterion (AIC) [23–25]. Then, in Chapter 4 we develop a position estimator using the debiased TOAs, which are obtained by subtracting the bias model (which is a deterministic variable) from TOAs (note that the variance of the estimates remain unchanged by the debiasing stage, so the total error is reduced). This localization method can be seen as a joint TOA and position estimation technique because TOA bias depends on the estimated source position, and we show that our position estimator is the optimal one when TOAs follow a Gaussian mixture distribution, which is approximately true for high sampling frequency, as discussed in Chapter 2.

In Chapter 5, we develop a source waveform estimation and source localization method that uses directly the signals acquired by the sensors to localize the fault, bypassing the TOA estimation step. One of the versions of the method presented in Chapter 5 uses a sparse estimation algorithm, which assumes the signals received by the sensors are sparse in a known dictionary. This method is also used to create a hit grouping algorithm, which is compared with other existing grouping methods.

In part of this work, data of real acoustic emission tests provided by Embraer is used to test localization methods. We also use simulated data generated using a simulator that we built as an improved version of the one developed in [26]. This simulator considers wave propagation models, sampling, non-white noise and custom source waveform generation, generating realistic TOAs that are used to test localization methods.

1.1 How Acoustic Emission Works

Consider we want to monitor a 2D structure such as a plate or shell using L sensors that are fixed at different points on the structure. Before detecting and localizing sources,

we have to learn intrinsic parameters of the structure that affect wave propagation, as the wave speed. For this, we must create artificial sources whose positions are known, which can be done in two ways: with a pencil-lead break (or Hsu-Nielsen test), or with an AST (Auto Sensor Testing) test. The pencil-lead break consists in breaking a pencil lead at 45° at a known position, generating a waveform that is similar to the one generated by a crack [27]. The AST test consists in using the sensors as actuators, one at a time, which is possible for many piezoelectric sensors [28].

Both in the AST and pencil-lead break tests, an artificial source with a known position emits a wave that propagates through the structure and reaches the sensors. The time the wave reaches each sensor is estimated, and is called Time of Arrival (TOA). These TOA's can be used to determine the wave velocity in the medium, as detailed in Chapter 3, and the waveforms each sensor samples can be used to determine other parameters that can be used in more complex localization methods, as explained in Chapter 5. The advantage of the pencil-lead break is that it is possible to create sources at any position, while the AST only lets us emulate sources at the sensor positions. On the other hand, the AST test can be done much faster (since it can be an automated process) and the waves it emits are much more similar to one another than the ones emitted by the pencil-lead break test. Furthermore, AST tests allow the generation of custom signals, unlike pencil-lead break tests.

Once the wave velocity in the medium is known, the structure is submitted to traction. When a crack occurs, it emits an elastic wave that propagates through the medium and reaches the sensors at different instants. For each sensor, the time of arrival is estimated using the sampled signals (or *hits*), and then converted in Time Difference of Arrival (TDOA) by subtracting the smallest TOA (i.e. the TOA estimated by the first sensor to detect a wave) from others. This process is illustrated in Figure 2, and an example of a *hit* captured by a sensor during a tensile test as a result of the expansion of a crack is shown in Figure 1.

Many TOA estimation algorithms are presented in the literature [25, 29–31], but the fixed threshold method [32] is one of the most popular techniques due to its simplicity. Suppose there are N sensors and define $r_i[n]$ as the signal sampled by the i-th sensor with period T_s such that $r_i[0]$ corresponds to the sample at the instant $t = t_0$. This method estimates the TOA t_i by comparing the absolute value of the signal to a fixed threshold K:

$$t_i = n_i T_s + t_0, \tag{1.1}$$

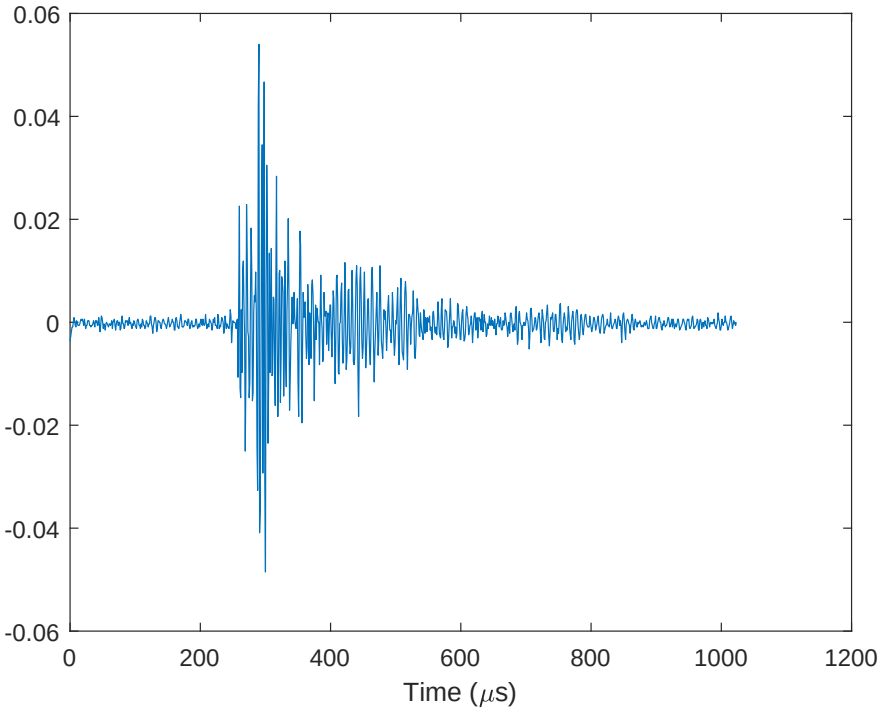

Figure 1: An example of a *hit* obtained by sampling an elastic wave emitted by a crack during a tensile test.

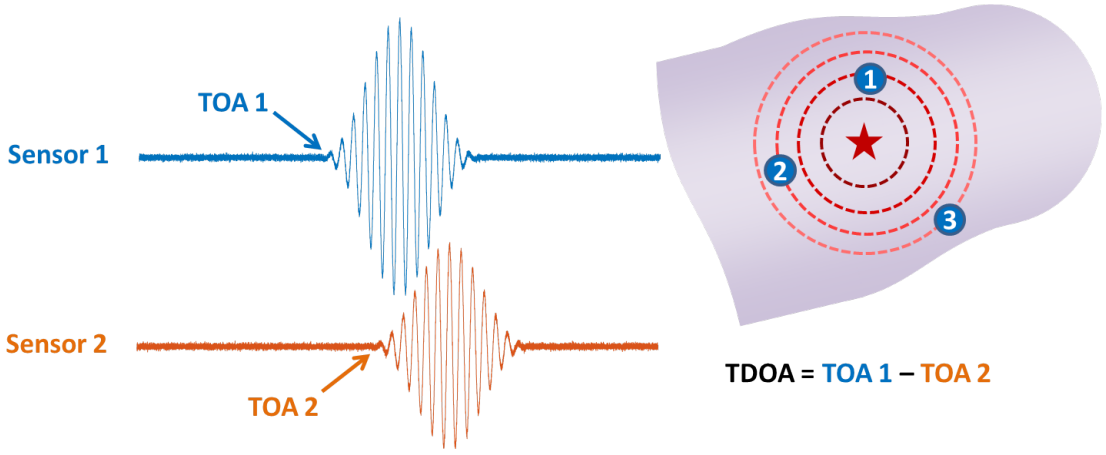

Figure 2: When a crack grows, it emits an elastic wave that is captured by sensors 1, 2 and 3. The TOAs are estimated and converted into TDOAs in order to determine the source position.

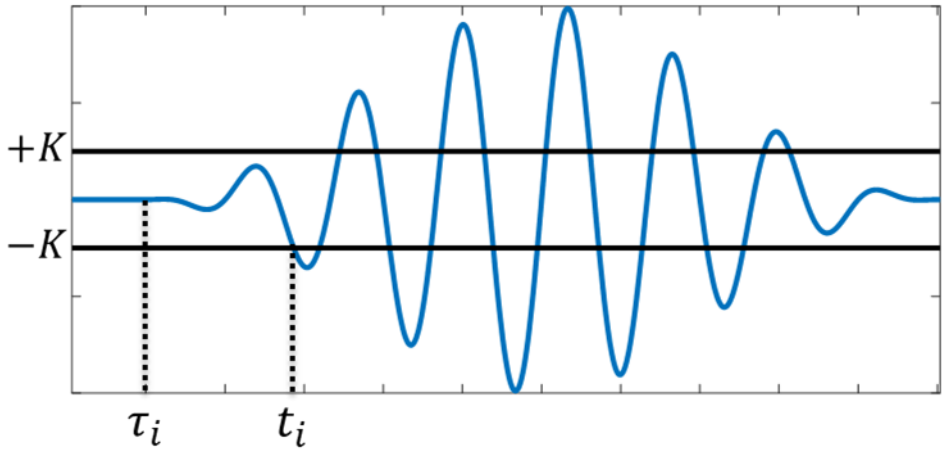

Figure 3: TOA estimation using the fixed threshold method. The signal sampled by each sensor is compared to a fixed threshold K, yielding a TOA estimate t_i, which is in general different than the actual time of arrival τ_i.

where n_i is such that

$$n_i = \min_n \{n : \ |r_i[n]| \geq K\} \tag{1.2}$$

Thus, the estimated TOA is the first time the absolute value of the signal crosses the threshold. This method only works if K is sufficiently higher than the noise level, but if it is set too high, incoming waves will not cross the threshold, so they will not be detected. An example of TOA estimation using the fixed threshold method is presented in Figure 3.

In Acoustic Emission Tests where different acoustic emission sources emit elastic waves at close time instants, sensors can receive multiple hits in a small time interval. In order to localize the source using TOA estimates, it is necessary to use hits generated by the same source. For this reason, hits are grouped into events using a hit grouping algorithm and TOAs that belong to the same event are used to localize a source. We propose a Hit Grouping technique in Chapter 5 and we compare it to other hit grouping techniques.

Once the TOAs $t_1, t_2, \cdots, t_N$ are determined and grouped into an event, the source position is determined by solving the following system of equations, illustrated in Figure 4:

$$\begin{cases} c(t_2 - t_1) = \sqrt{(x - x_2)^2 + (y - y_2)^2} - \sqrt{(x - x_1)^2 + (y - y_1)^2} \\ c(t_3 - t_1) = \sqrt{(x - x_3)^2 + (y - y_3)^2} - \sqrt{(x - x_1)^2 + (y - y_1)^2} \\ \vdots \\ c(t_2 - t_1) = \sqrt{(x - x_N)^2 + (y - y_N)^2} - \sqrt{(x - x_N)^2 + (y - y_N)^2} \end{cases}, \tag{1.3}$$

where (x, y) is the tentative source position, (x_k, y_k) is the position of the k-th sensor and

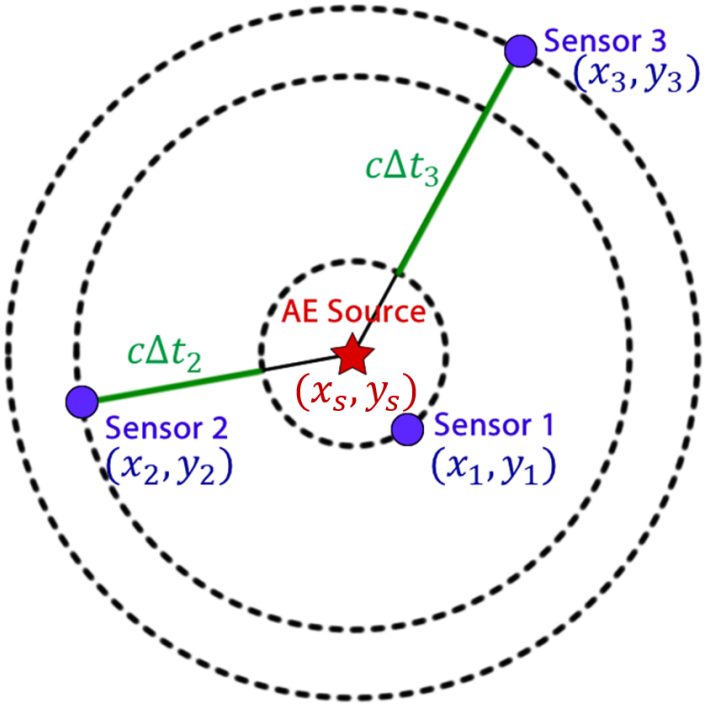

Figure 4: Illustration of (1.3) for three sensors. TDOAs are equated to the distances highlighted in green.

c is the wave velocity, a parameter that can be measured before the acoustic emission test. System 1.3 has two unknowns (x_s and y_s) and $N-1$ equations, thus if $N > 3$ the system is overdetermined (unless there are co-linear sensors). For this reason, the position is usually estimated through the minimization of a cost function. For example, the minimization of the cost function $J_{TDOA}(x, y)$ given by

$$J_{TDOA}(x,y) = \sum_{i=2}^{N} [(t_i - t_1) - \frac{1}{c}\sqrt{(x-x_i)^2 + (y-y_i)^2}]^2 \tag{1.4}$$

yields an estimate of the source position, where (x_i, y_i) is the position of the i-th sensor and c is the wave velocity. The quality of the position estimates depends on the choice of the cost function, and on the distribution of the uncertainty in the TOA estimates t_i. The use of cost functions to localize sources from TOA measurements is explored in Chapter 3.

Although most commercial acoustic emission systems use TOAs to estimate the source position, it is possible to bypass the TOA measurement and estimate the position directly from the waveforms sampled at the sensors, at the cost of a higher computational complexity and the need to store the waveforms if the localization is made offline. A waveform-based localization technique is presented in chapter 5.

1.1.1 Hit Segmentation

In acoustic emission tests, sensors sample continuously during the whole test, yielding a stream of samples that contains several waves generated by multiple sources. In order to locate them, hits must be extracted from these streams using hit segmentation methods that are run in real time. We use the term *hit* to describe a segmented part of the signal acquired by a sensor (that is, a part of the signal that was extracted by a hit segmentation method). A well-segmented hit is contains the wave produced by only one source. If a hit contains a wave generated by a second source, the TOA of this second wave will be badly estimated or not estimated at all, since only one TOA is estimated per hit.

All hits from actual acoustic emission tests used in this work were extracted using the Hit Definition Time/Hit Lockout Time (HLT/HDT) method [28], which is a popular hit segmentation method that uses a fixed threshold K (as in the fixed threshold method for TOA estimation) to determine the beginning of the hit, and then uses two predefined time intervals called *Hit Definition Time* (HDT) and *Hit Lockout Time* (HLT) to determine its ending.

Roughly, the HDT/HLT method determines the beginning of a hit at the first instant it crosses the fixed threshold, and it ends at the instant where there is no threshold crossing for a time interval HDT. Then, to avoid computing reflections in the next hit, the sensor stop identifying hits for a time interval HLT.

Now, let us describe the HDT/HLT more comprehensively. Suppose we want to segment the stream $y_i[n]$ captured by the i-th sensor. We will show how to extract the indexes n_1, n_2 so that the first hit is $y_i[n]$ for $n_1 \leq n \leq n_2$. We consider that HDT and HLT are measured in samples, but they can be converted into μs by multiplying them by the sampling period.

Let $d[n]$ be a binary sequence that assumes 1 or 0 depending on if $r[n]$ crosses the threshold K, that is,

$$d[n] = \begin{cases} 1, & |r[n]| \geq K \\ 0, & |r[n]| < K \end{cases} . \tag{1.5}$$

The hit begins at the first instant where the signal crosses the threshold, thus

$$n_1 = \min_n \{n : \ d[n] = 1\}. \tag{1.6}$$

The hit does not end until one of the following conditions happen:

1. The number of samples of the hit surpasses a predefined limit.

2. $r[n]$ did not cross the threshold for HDT samples, that is, $d[n] = d[n-1] = \cdots = d[n - \text{HDT} + 1] = 0$.

If one of the conditions above is satisfied at instant m, HLT samples are discarded to avoid identifying reflections of the same wave as another hit, and n_2 is set as

$$n_2 = m + \text{HLT}. \tag{1.7}$$

After the hit $\begin{bmatrix} r[n_1] & r[n_1+1] & \cdots, r[n_2] \end{bmatrix}^T$ is segmented and stored, the HDT/HLT algorithm is executed again, but the samples at instant $n \leq n_2$ are not taken into account for the new hit.

Even though the HDT/HLT technique is a naive method that cannot separate waves that reach a sensor simultaneously, it is extremely simple and computationally efficient, allowing it to be easily implemented in real time.

1.1.2 Anisotropic Media

In Section 1.1, we introduced the acoustic emission framework assuming that the wave velocity is constant. However, the wave velocity can be different at each point of the structure. When the wave speed depends only on the direction of propagation, we say the structure presents a direction-dependent anisotropy. The advantage of using models with direction-dependent anisotropy is that the velocity is constant along any straight line. Therefore, if the source occurs at the position (x_s, y_s), the time it takes to reach the sensor located at (x_i, y_i) is $\tau_i = \frac{1}{c_i}\sqrt{(x_s - x_i)^2 + (y_s - y_i)^2}$, where c_i is the velocity along the line that connects the points (x_s, y_s) and (x_i, y_i).

Writing the velocity along the line $y = \tan(\theta)x + b$ (i.e. the line that forms an angle θ with the x axis) as $c(\theta)$, the wave velocity along the line that connects (x_s, y_s) and (x_i, y_i) is $c_i = c(\theta_i)$, where θ_i is the angle this line forms with the x-axis.

A special case of direction-dependent anisotropy is the elliptical anisotropy, where $c(\theta)$ forms an ellipse for $\theta \in [0, 2\pi[$. This means that for some constants a, b and β, $c(\theta)$ satisfies

$$c(\theta) = \frac{ab}{\sqrt{a^2 \sin^2(\theta - \beta) + b^2 \cos^2(\theta - \beta)}}. \tag{1.8}$$

This anisotropy model, illustrated in Figure 5, was employed in [26, 33] and will be used in the following chapters.

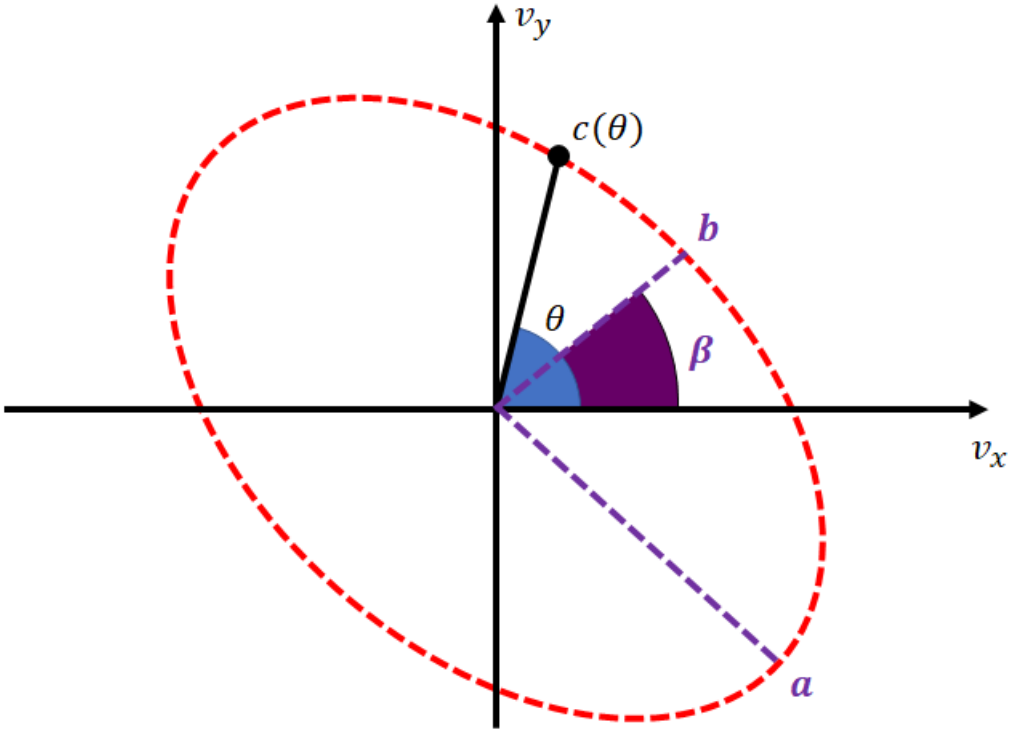

Figure 5: Illustration of the elliptical anisotropic model. The wave velocity $c(\theta)$ depends on the direction of propagation θ in such a way that $c(\theta)$ describes an ellipsis in polar coordinates. The axes represent the horizontal and vertical components of $c(\theta)$.

1.2 Wave Propagation Models for Acoustic Emission

In this work we are interested in waves propagating in planar solids, as plates or shells. When a crack grows, an elastic wave is emitted and propagates through the medium. In general, the waveform measured at a single point will not be a delayed version of the waveform measured at another point, even if we disregard the energy loss. In lossless 2D media, the energy of the whole wavefront must remain constant over time, so the energy measured at a given point of the wavefront will decay as a function of its distance from the source. Moreover, the velocity that each frequency propagates is not constant, so that different frequencies reach the sensors at different instants.

Many of the signal processing techniques we present in this work assume a specific propagation model. For this reason, in this section we discuss the main models described in the literature.

1.2.1 Constant Velocity Model

The Constant Velocity Model [34] is a simplified model where all frequencies propagate with the same velocity. Even though this is in general not true, this model is often used in applications that do not require high precision. This model can also be used for narrow-band signals because in this case the energy of the signal is concentrated in very close frequencies which propagate with similar velocities.

Consider an elastic wave propagating in an 1D medium (as in a wire) and assume that all frequencies propagate with the same velocity c. The elastic displacement waves $u(t, r_0)$ and $u(t, r)$ measured at distances r_0 and r from the source are related as

$$u(t, r) = u(t - \tau, r_0)e^{-\alpha(r-r_0)}, \tag{1.9}$$

where α is the linear attenuation coefficient and

$$\tau = \frac{r - r_0}{c} \tag{1.10}$$

is the time the wave takes to propagate through the distance $r - r_0$.

In isotropic 2D media, the energy spreads as the wave propagates so that the total energy of the wavefront decays with $e^{-2\alpha(r-r_0)}$. This can be used to derive the relation between $u(t, r)$ and $u(t, r_0)$. Defining $\mathcal{C}(r)$ as a circumference of radius r centered at the source position, the relation between the energy of the wavefronts $\mathcal{C}(r)$ and $\mathcal{C}(r_0)$ is

$$\oint_{\mathcal{C}(r)} u^2(t, r)\ \mathrm{d}\ell = e^{-2\alpha(r-r_0)} \oint_{\mathcal{C}(r_0)} u^2(t, r_0)\ \mathrm{d}\ell. \tag{1.11}$$

Since

$$\oint_{\mathcal{C}(r)} u^2(t, r)\ \mathrm{d}\ell = \int_{-\pi}^{\pi} u^2(t, r) r\ \mathrm{d}\theta = 2\pi r u^2(t, r) \tag{1.12}$$

and

$$\oint_{\mathcal{C}(r_0)} u^2(t, r_0)\ \mathrm{d}\ell = \int_{-\pi}^{\pi} u^2(t, r_0) r_0\ \mathrm{d}\theta = 2\pi r_0 u^2(t, r_0), \tag{1.13}$$

we have

$$2\pi r u^2(t, r) = 2\pi r_0 u^2(t, r_0)e^{-2\alpha(r-r_0)}, \tag{1.14}$$

hence

$$u(t, r) = u(t, r_0)e^{-\alpha(r-r_0)}\sqrt{\frac{r_0}{r}}. \tag{1.15}$$

The term $e^{-\alpha(r-r_0)}$ models the energy loss, and the term $\sqrt{\frac{r_0}{r}}$ models the energy spreading due to the expansion of the wavefront. Note that the only difference between the 2D model (1.15) and the 1D model (1.9) is the term $\sqrt{\frac{r_0}{r}}$.

It is also possible to substitute the square root by an exponent $\beta \approx \frac{1}{2}$, obtaining a relaxed model:

$$u(t,r) = u(t,r_0)e^{-\alpha(r-r_0)}\left[\frac{r_0}{r}\right]^{\beta}. \tag{1.16}$$

The relaxed model can be used instead of (1.15) in cases where (1.15) does not fit well the signals and it is not desired to use more complex models. Note that substituting $\beta = \frac{1}{2}$ in (1.16) yields the original equation (1.15), and using $\beta = 0$ yields the 1D propagation model (1.9), which considers that all attenuation is due to energy loss, modelled by the term $e^{-\alpha(r-r_0)}$.

1.2.2 Power-Law Attenuation Model

In practice, different frequencies propagate with different velocities, such that the wave deforms as it propagates throughout the medium. Employing (1.16) with a frequency-dependent attenuation coefficient $\alpha(\Omega)$ is a popular way to model this deformation. This model is known as Power-Law attenuation model [35], and considers

$$\alpha(\Omega) = \alpha_0|\Omega|^{\gamma}, \tag{1.17}$$

where $\gamma \in [0,2]$ is a constant that only depends on the material of the medium [36] and Ω is the frequency in $\frac{\text{rad}}{\text{s}}$.

Setting Ω_0 as a fixed frequency (for example, the center frequency of a band-pass sensor), $\alpha(\Omega)$ can be rewritten as

$$\alpha(\Omega) = \alpha(\Omega_0)\left|\frac{\Omega}{\Omega_0}\right|^{\gamma}. \tag{1.18}$$

Note that $\alpha_0 = \frac{\alpha(\Omega_0)}{\Omega_0^{\gamma}}$.

In the expression of the transfer function $H(\Omega)$ of the Power-Law Attenuation Model, the phase must be taken into account:

$$H(\Omega) = e^{-\alpha(\Omega)(r-r_0)}e^{-j\Omega(r-r_0)/V_p(\Omega)}\sqrt{\frac{r_0}{r}}, \tag{1.19}$$

where $V_p(\Omega)$ is the phase velocity for the frequency Ω in the medium. When converted to time domain, the term $e^{-j\Omega(r-r_0)/V_p(\Omega)}$ represents the time the wave component of frequency Ω takes to propagate through the distance $r-r_0$. For most functions $V_p(\Omega)$, the system whose frequency response is $H(\Omega)$ is not a causal system (the impulse response $h(t)$ is not zero for all $t < 0$). It is possible to choose $V_p(\Omega)$ that makes the system

causal [35,37], but in this work we derive a simpler approach using the Hilbert transform and using $V(\Omega) = c$ as a constant, as described below. Even thought our approach leads to an approximate model that is not exactly the Power-Law Attenuation Model, its implementation is much simpler than choosing $V_p(\Omega)$ as in [35,37].

1.2.2.1 Causal approximation for the Power-Law Attenuation Model

Let us decompose the system impulse response $h_c(t)$ into the sum of an even part $h_e(t)$ and an odd part $h_o(t)$:

$$h_c(t) = h_e(t) + h_o(t),$$

where

$$h_e(t) = \frac{h_c(t) + h_c(-t)}{2}$$

and

$$h_o(t) = \frac{h_c(t) - h_c(-t)}{2}.$$

If the system is causal, $h_c(-t) = 0$ for $t > 0$. Thus,

$$\begin{cases} h_e(t) &= \frac{h_c(t)}{2}, \qquad t > 0 \\ h_o(t) &= \frac{h_c(t)}{2}, \qquad t > 0. \end{cases} \tag{1.20}$$

On the other hand, if $t < 0$, $h_c(t) = 0$, hence

$$\begin{cases} h_e(t) &= \frac{h_c(t)}{2}, \qquad t < 0 \\ h_o(t) &= -\frac{h_c(t)}{2}, \qquad t < 0. \end{cases} \tag{1.21}$$

(1.20) and (1.21) can be combined into $h_o(t) = \frac{1}{2}\operatorname{sgn} h_e(t)$, thus

$$h_c(t) = h_e(t) + \operatorname{sgn}(t) h_e(t). \tag{1.22}$$

Taking the Fourier transform at both sides of (1.22), recalling that $\mathcal{F}\{\operatorname{sgn}(t)\} = -j\frac{2}{\Omega}$ and defining $H_e(\Omega) = \mathcal{F}\{h_e(t)\}(\Omega)$, we have

$$H_c(\Omega) = H_e(\Omega) - \frac{1}{2\pi}\left(-j\frac{2}{\Omega} * H_e(\Omega)\right) = H_e(\Omega) - j\left(\frac{1}{\pi\Omega} * H_e(\Omega)\right),$$

where $*$ denotes convolution. The convolution $\left(\frac{1}{\pi\Omega} * H_e(\Omega)\right)$ is the Hilbert Transform (denoted by $\mathcal{H}_c\{\cdot\}$) of $H_e(\Omega)$, thus $H_c(\Omega)$ is causal if and only if

$$H_c(\Omega) = H_e(\Omega) - j\mathcal{H}\{H_e(\Omega)\}. \tag{1.23}$$

In our causal approximation (used in Chapter 5), we first define a causal system whose frequency response is $H_c(\Omega)$ as in (1.23) using

$$H_e(\Omega) = e^{-\alpha(\Omega)(r-r_0)}\sqrt{\frac{r_0}{r}}, \tag{1.24}$$

so

$$H_0(\Omega) = \left(e^{-\alpha(\Omega)(r-r_0)} - j\mathcal{H}\{e^{-\alpha(\Omega)(r-r_0)}\}\right)\sqrt{\frac{r_0}{r}}. \tag{1.25}$$

This causal system has no delay: If an impulse is applied to the system, an output is measured instantaneously. However, the wave must take a time $\frac{r-r_0}{c}$ to propagate through the distance $r - r_0$. For this reason, we add a delay to $H_0(\Omega)$ by multiplying it by $e^{-j\Omega\frac{r-r_0}{c}}$, obtaining the frequency response $H(\Omega)$ of our causal approximation of the Power-Law Attenuation Model:

$$H(\Omega) = \left(e^{-\alpha(\Omega)(r-r_0)} - j\mathcal{H}\{e^{-\alpha(\Omega)(r-r_0)}\}\right)\sqrt{\frac{r_0}{r}}e^{-j\Omega(r-r_0)/c}. \tag{1.26}$$

Note that in our approximation for the Power-Law Attenuation Model, the phase of $H(\Omega)$ is not linear, so different frequencies propagate with different velocities.

1.2.3 Lossless isotropic model

It is possible to show that the equation that describes the wave propagation in lossless linear elastic media is [38]

$$\mu\nabla^2\mathbf{u} + (\mu+\lambda)\nabla(\nabla\cdot\mathbf{u}) + \mathbf{F} = \rho\frac{\partial^2\mathbf{u}}{\partial t^2}, \tag{1.27}$$

where λ is the Lamé parameter, μ is the Shear Modulus (or second Lamé parameter), $\mathbf{u}$ is the displacement vector, ρ is the density of the medium and $\mathbf{F}$ is the external force field. The symbol $\nabla\phi$ is the gradient of the scalar field ϕ, and the symbols $\nabla\cdot\mathbf{u}$ and $\nabla^2\mathbf{u}$ are respectively the divergent and Laplacian of vector $\mathbf{u} = \begin{bmatrix} u_1 \\ u_2 \\ u_3 \end{bmatrix}$. These operators are

defined as

$$\nabla\phi = \begin{bmatrix} \frac{\partial\phi}{\partial x} \\ \frac{\partial\phi}{\partial y} \\ \frac{\partial\phi}{\partial z} \end{bmatrix}, \tag{1.28}$$

$$\nabla \cdot \mathbf{u} = \frac{\partial u_1}{\partial x} + \frac{\partial u_2}{\partial y} + \frac{\partial u_3}{\partial z}, \tag{1.29}$$

$$\nabla^2\mathbf{u} = \begin{bmatrix} \nabla^2 u_1 \\ \nabla^2 u_2 \\ \nabla^2 u_3 \end{bmatrix} = \begin{bmatrix} \frac{\partial^2 u_1}{\partial x^2} + \frac{\partial^2 u_1}{\partial y^2} + \frac{\partial^2 u_1}{\partial z^2} \\ \frac{\partial^2 u_2}{\partial x^2} + \frac{\partial^2 u_2}{\partial y^2} + \frac{\partial^2 u_2}{\partial z^2} \\ \frac{\partial^2 u_3}{\partial x^2} + \frac{\partial^2 u_3}{\partial y^2} + \frac{\partial^2 u_3}{\partial z^2} \end{bmatrix}. \tag{1.30}$$

Lamé parameters can be written as a function of the Young Modulus E and the Poisson Coefficient ν, which are usually found in tables for each material, as follows

$$\lambda = \frac{\nu}{(1+\nu)(1-2\nu)}E, \tag{1.31}$$

$$\mu = \frac{E}{2(1+\nu)}. \tag{1.32}$$

Our objective here is to solve (1.27) for lossless isotropic plates to obtain a propagation model where distinct frequencies propagate with different velocities, unlike the Constant Velocity Model (given by (1.15)).

We can apply the Helmholtz Decomposition in $\mathbf{u}$ and $\mathbf{F}$, decomposing them as sum of divergent-free and curl-free fields:

$$\mathbf{u} = \nabla\Phi + \nabla \times \mathbf{\Psi}, \tag{1.33}$$

$$\mathbf{F} = \nabla\Phi_F + \nabla \times \mathbf{\Psi}_F. \tag{1.34}$$

The scalar field Φ is named Compression Potential, and the vector field $\mathbf{\Psi}$ is called Shear Potential. The symbol $\nabla \times \mathbf{\Psi}$ is the curl of $\mathbf{\Psi} = \begin{bmatrix} \Psi_1 \\ \Psi_2 \\ \Psi_3 \end{bmatrix}$, defined as

$$\nabla \times \mathbf{\Psi} = \begin{bmatrix} \frac{\partial\Psi_3}{\partial y} - \frac{\partial\Psi_2}{\partial z} \\ \frac{\partial\Psi_1}{\partial z} - \frac{\partial\Psi_3}{\partial x} \\ \frac{\partial\Psi_2}{\partial x} - \frac{\partial\Psi_1}{\partial y} \end{bmatrix}. \tag{1.35}$$

Substituting the decompositions at (1.27) and using the vector calculus properties

$\nabla \cdot (\nabla \times \boldsymbol{\Psi}) = \mathbf{0}$, $\nabla^2(\nabla\Phi) = \nabla(\nabla^2\Phi)$ and $\nabla^2(\nabla \times \boldsymbol{\Psi}) = \nabla \times (\nabla^2\boldsymbol{\Psi})$, we obtain

$$\mu\nabla(\nabla^2\Phi)+\mu\nabla\times(\nabla^2\boldsymbol{\Psi})+(\mu+\lambda)\nabla(\nabla^2\Phi)+\nabla\Phi_F+\nabla\times\boldsymbol{\Psi}_F = \rho\frac{\partial^2}{\partial t^2}(\nabla\Phi+\nabla\times\boldsymbol{\Psi}), \quad (1.36)$$

which can be rearranged into a sum of a curl-free and a divergence-free field:

$$\nabla\left((2\mu+\lambda)\nabla^2\Phi + \Phi_F - \rho\frac{\partial^2\Phi}{\partial t^2}\right) + \nabla\times\left(\mu\nabla^2\boldsymbol{\Psi} + \boldsymbol{\Psi}_F - \rho\frac{\partial^2\boldsymbol{\Psi}}{\partial t^2}\right) = \mathbf{0}. \quad (1.37)$$

The curl-free and the divergence-free components of (1.37) generate two independent wave equations:

$$\nabla^2\Phi - \frac{1}{c_\alpha^2}\frac{\partial^2\Phi}{\partial t^2} = -\frac{\Phi_F}{\lambda+2\mu} \qquad c_\alpha = \sqrt{\frac{\lambda+2\mu}{\rho}}, \quad (1.38)$$

$$\nabla^2\boldsymbol{\Psi} - \frac{1}{c_\beta^2}\frac{\partial^2\boldsymbol{\Psi}}{\partial t^2} = -\frac{\boldsymbol{\Psi}_F}{\mu} \qquad c_\beta = \sqrt{\frac{\mu}{\rho}}. \quad (1.39)$$

The term $(\mu+\lambda)\nabla(\nabla\cdot\mathbf{u})$ influences only the compression component of $\mathbf{u}$, and does not affect its shear component. As both equations are independent, two independent waves with different velocities are generated – The compressional wave (also called 'P-wave'), given by (1.38), and the shear wave (or 'S-wave'), given by (1.39). The compressional wave has higher velocity than the shear wave, but only the shear wave oscillates in the transverse axis (orthogonal to the surface of the structure). It is important to talk about compressional and shear waves because many sensors only measure deformations that are orthogonal to the surface of the structure, thus only the shear wave can be sensed by these sensors. In practice, sensors may measure compressional waves with small gain, implying that compressional waves are converted in signals with low amplitude.

Writing Lamé parameters in terms of E and ν as in (1.31), the ratio between the S-wave and P-wave velocities depends only on the Poisson coefficient:

$$\frac{c_\alpha}{c_\beta} = \sqrt{\frac{2-2\nu}{1-2\nu}}$$

For example, the Poisson coefficient of a 2024-T3 alluminium alloy is $\nu = 0.33$ [39], thus $c_\alpha = 2c_\beta$. Thus, compressional waves travel at higher velocity than shear waves. For this reason, when a crack grows, a small amplitude compressional wave may be captured by sensors before the shear wave arrives.

1.2.4 Fractional Zener Model

The Fractional Zener Model [40] is a much more complex model than those presented before, but the waveform deformation described by this model tends to be closer to reality. In this model, the displacement $u(t)$ in a fixed position is the solution of a linear differential equation that includes fractional derivatives:

$$\nabla^2 u - \frac{1}{c^2}\frac{\partial^2 u}{\partial t^2} + \tau_\sigma^a \frac{\partial^a}{\partial t^a}\nabla^2 u - \frac{\tau_\epsilon^b}{c^2}\frac{\partial^{b+2}}{\partial t^{b+2}}u, \tag{1.40}$$

where c is a constant that can be interpreted as the wave speed when the constants τ_ϵ and τ_σ are equal to zero, and a and b are constants. In this model, each frequency has its own velocity and attenuation. For the model to be physically consistent, we must have $a = b$, but a relaxed model can be obtained using $a \neq b$.

Note that despite the fractional derivatives, the Fractional Zener Model is still linear. Nevertheless, its main disadvantage is that it depends on many parameters that are not straightforward to estimate. For this reason, this model is not employed in this work.

Concluding remarks

In this chapter, we presented the framework of acoustic emission. The fixed threshold algorithm, which is a popular method for estimating TOAs in real time, was introduced. In order to obtain an estimate from the source position, TOAs from at least three sensors must be used, and if more than three sensors are available it is possible to minimize a cost function to generate a position estimate. If it is desired to store the waveform or extract parameters from it (as the energy), a hit segmentation algorithm as the HDT/HLT method must be used to define the instants of the first and last samples of the hit.

Propagation models of elastic waves were also presented. We introduced the elliptical anisotropic model, which considers that the velocity of the wave $c(\theta)$ depends on the angle of propagation such that $c(\theta)$ describes an ellipse. The Constant Velocity Model is a simple model that considers that all frequencies of the wave propagate with the same velocity, hence each hit is an attenuated and shifted version of another hit. On the other hand, the Power-Law model assumes that higher frequencies attenuate more than lower frequencies, deforming the wave as it propagates. A causal implementation of the Power-Law model is not straightforward, thus in this work we employ a causal approximation using the Hilbert transform.

2 MODELING TIME OF ARRIVAL PROBABILITY DISTRIBUTION AND TDOA BIAS

In acoustic emission tests, the time of arrival estimates are subjected to uncertainties caused by signal distortion and noise. While some authors evaluate and compare source localization algorithms using time of arrival estimates obtained by applying the fixed threshold method to simulated or real signals [16,41–43], others assume the time of arrival is Gaussian-distributed instead of processing the received signals [17–20]. To the best of our knowledge, the article we published [22] was the first one to calculate the actual time of arrival distribution expression. Knowing the time of arrival probability distribution function (pdf) expression would allow the development of new statistical source position estimators that may have better performance than traditional source localization methods. For this reason, in this chapter we derive the time of arrival pdf considering noise, sampling and waveform distortion, and show it is not Gaussian distributed. We also deduce an approximate and simplified expression for the pdf that depends on fewer parameters, being easier to apply in practical situations than the exact distribution.

The fixed threshold method is a popular detection algorithm in which the time of arrival is estimated as the first time the received signal absolute value crosses a fixed threshold [42]. However, sampling rate, attenuation and envelope modulation due to sensor frequency response can add bias to the estimated Time Difference of Arrival (TDOA) and consequently to the estimated position, since the position is estimated using TDOA measurements. It is interesting to reduce TDOA bias because it may lead to an estimated source position bias reduction, and thus to a smaller localization error. In [20], a bias reducing algorithm for TDOA-based localization is developed, but TDOA itself was assumed unbiased and Gaussian distributed. For this reason, we derive an approximate model for the TDOA bias for the fixed threshold algorithm considering our more realistic time of arrival model, as well as lower and upper bounds for it.

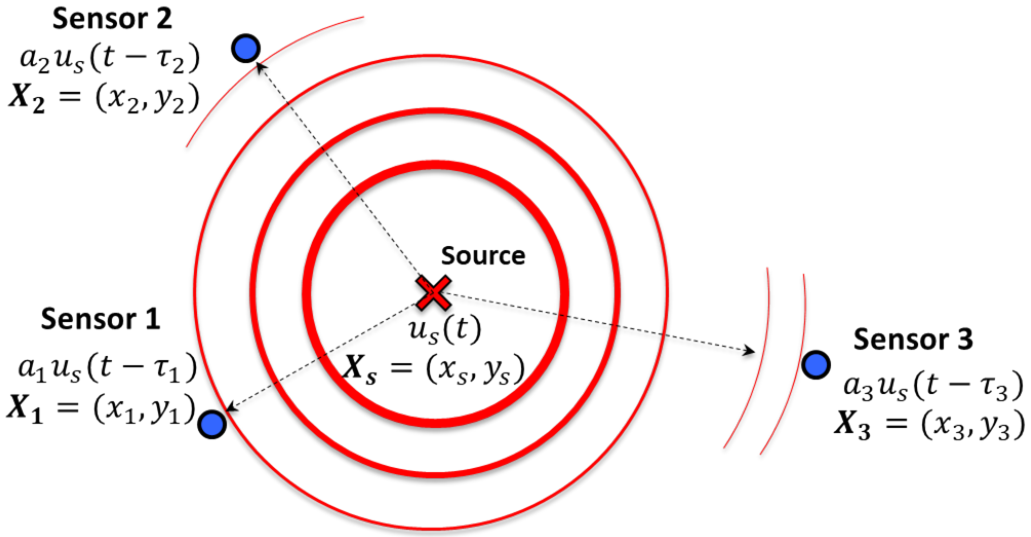

Figure 6: The elastic wave generated by the source at $t = 0$ reaches the sensors at different instants and with different amplitudes.

2.1 Time of arrival probability distribution

The objective of this section is to derive an expression for the probability distribution of the time of arrival estimates considering they were obtained using a fixed threshold. The threshold value is considered to be set high enough so that the noise has approximately zero probability of crossing it.

2.1.1 Signal Model

We consider an acoustic source located at a deterministic position $\mathbf{X} = (x_s, y_s)$ emitting an elastic wave at $t = 0$ that propagates throughout the 2D isotropic material with velocity c. Let $u_s(t)$ and $u_i(t)$ be the elastic displacement respectively at the source position and at the i-th sensor position $\mathbf{X}_i = (x_i, y_i)$. We adopt the constant velocity attenuation model presented in Chapter 1 and used in [34]:

$$u_i(t) = a_i u_s(t - \tau_i), \tag{2.1}$$

where

$$a_i = \frac{e^{-\alpha \|\mathbf{X}_s - \mathbf{X}_i\|}}{\|\mathbf{X}_s - \mathbf{X}_i\|^{\frac{1}{2}}}. \tag{2.2}$$

The constant α is the attenuation coefficient and $\tau_i = \frac{1}{c} \|\mathbf{X}_s - \mathbf{X}_i\|$ is the time the wave takes to propagate from the source to the i-th sensor, as illustrated in Figure 6. Assuming all sensors have the same frequency response $h(t)$, the electrical signal $r_i(t)$ sensed by the

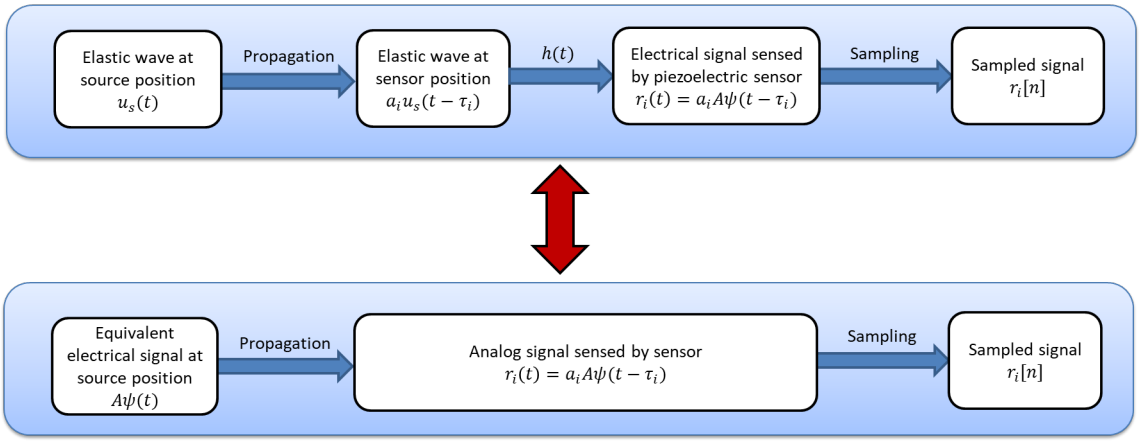

Figure 7: Equivalence between sampling the elastic wave and sampling the shifted equivalent source signal.

i-th sensor in a noiseless scenario is

$$r_i(t) = [h * u_i](t) = a_i[h * u_s](t - \tau_i) = a_i\psi_i(t), \tag{2.3}$$

where $\psi_i(t) = [h * u_s](t - \tau_i)$. Define the normalized received signal as $\psi(t-\tau_i) = \frac{\psi_i(t)}{\max_t \psi_i(t)}$ and denote $A = \max_t \psi(t)$ as the equivalent source amplitude. This way, $\psi_i(t) = A\psi(t - \tau_i)$, and the noiseless wave received by sensor i is

$$r_i(t) = a_i A\psi(t - \tau_i). \tag{2.4}$$

Assuming that the signal at each sensor is sampled at the instants $t = nT + t_0$, where n is a non-negative integer, $T = \frac{1}{F}$ is the sampling interval and t_0 is the initial sample instant, the signal sampled by sensor i and corrupted by a white noise $w_i[n]$ is

$$r_i[n] = a_i A\psi(nT + t_0 - \tau_i) + w_i[n]. \tag{2.5}$$

We call the term $A\psi(t)$ the equivalent source signal. It allows us to ignore the frequency response of the sensors and the elastic deformations, making it possible to work directly with the signals sampled at the sensors. The equivalent source signal is an auxiliary signal that does not exist physically, but it generates the waveforms $r_i(t)$ received by the sensors when it propagates from the source position to the sensors as shown in (2.4). The equivalence between sampling the elastic waves and sampling directly the attenuated and shifted equivalent source waveform is presented as a diagram in Figure 7.

Throughout this chapter, we assume that the noise probability density function $f_W(w)$ is symmetric, i.e. $f_W(w) = f_W(-w)$, or equivalently, $F_W(w) = 1 - F_W(-w)$, where $F_W(w)$ is the noise cumulative distribution function (cdf). We also assume that t_0 is uniformly

distributed in $[0, T]$. In addition, we consider the time of arrival was estimated using the fixed threshold method. This algorithm estimates the time of arrival at the i-th sensor as the smallest instant such that the $|r_i[n]|$ is greater than the threshold K.

2.1.2 Time of Arrival Probability Distribution

We first calculate the pdf of the time of arrival t_i given the initial sample time t_0. The TOA estimated by the fixed threshold method is the first instant where $|r_i[n]|$ crosses the fixed threshold K.

Let $\Phi_i(t)$ be the probability that the absolute value of a sample acquired at instant t be less than the threshold. Note that $\Phi_i(t)$ can only be calculated at the instants $t = nT + t_0$, where n is a non-negative integer. Denoting $\mathbb{P}\{A\}$ as the probability of the event A, $\Phi_i(t)$ can be expressed in terms of the noise cdf $F_W(w)$:

$$\begin{aligned}
\Phi_i(t) &= \mathbb{P}\{|r_i[n]| < K\}, \qquad n = \frac{t - t_0}{T} \\
&= \mathbb{P}\{-K < r_i[n] < K\} \\
&= \mathbb{P}\{-K < a_i A\psi(t - \tau_i) + w_i[n] < K\} \\
&= \mathbb{P}\{-K - a_i A\psi(t - \tau_i) < w_i[n] < K - a_i A\psi(t - \tau_i)\} \\
&= F_W(K - a_i A\psi(t - \tau_i)) - F_W(-K - a_i A\psi(t - \tau_i)).
\end{aligned} \tag{2.6}$$

As the threshold is assumed to be much larger than the noise standard deviation, we can approximate $F_W(K)$ and $1 - F_W(-K)$ to one (or, equivalently, $F_W(-K)$ to zero). This means in the case where $a_i A\psi(t - \tau_i) < 0$, $F_W(K - a_i A\psi(t - \tau_i)) \approx 1$ because $K - a_i A\psi(t - \tau_i) \geq K$, and $F_W(-K - a_i A\psi(t - \tau_i)) \approx 0$ is approximately zero in the case where $a_i A\psi(t - \tau_i) > 0$ because $-K - a_i A\psi(t - \tau_i) \leq -K$.

Assuming symmetrical noise, that is, $f_W(w) = f_W(-w)$, or equivalently $F_W(w) = 1 - F_W(-w)$, leads to a simplified approximation for $\Phi_i(t)$:

$$\Phi_i(t) \approx F_W(K - |a_i A\Psi(t - \tau_i)|). \tag{2.7}$$

Now, we use $\Phi_i(t)$ to derive an expression for the TOA distribution given t_0. The probability of the TOA be estimated at instant $t = nT + t_0$ is the probability of $|r_i[n]| \geq K$ and $|r_i[k]| < K$ for all $k < n$. Hence, the probability mass function (pmf) of the TOA t_i given t_0 is given by

$$\mathbb{P}\{t_i = t|t_0\} = (1 - \Phi_i(t)) \prod_{k=1}^{\infty} \Phi_i(t - kT), \tag{2.8}$$

where $(1-\Phi_i(t))$ is the probability of $|r_i[n]| \geq K$ and $\prod_{k=1}^{\infty}\Phi_i(t-kT)$ is the probability of $|r_i[k]| < K$ for all $k < n$ (recall that we assumed the noise $w[n]$ is independent and identically distributed). It is worth noting that the variable t in (2.8) is a discrete variable because it represents the instants where a sampling occurs (thus $t = nT + t_0$, where n is an integer).

Taking into account that $r_i(t) = |w_i[n]| < K$ for $t < \tau_i$, the upper limit in the product can be substituted by $\lfloor (t-\tau_i)/T \rfloor$ since $\Phi_i(t-kT) = 1$ for $k > (t-\tau_i)/T$ (recall that $\Phi_i(t) = 1$ for $t < 0$ because the wave is emitted at instant $t = 0$).

The time of arrival pdf $f_{t_i}(t)$ can be calculated using $\mathbb{P}\{t_i = t|t_0\}$ and the initial sample instant pdf $f_{t_0}(t)$. The joint distribution of TOA t_i and the initial sample instant t_0 is obtained through the Bayes Rule:

$$f_{t_i,t_0}(t,t_0) = f_{t_i|t_0}(t|t_0)f_{t_0}(t_0) = \left(\sum_{k=-\infty}^{+\infty}\mathbb{P}\{t_i = t|t_0\}\delta(t-(kT+t_0))\right)f_{t_0}(t_0), \tag{2.9}$$

where $\delta(\cdot)$ is the Dirac delta function. Thus, the TOA pdf is obtained by integrating the joint pdf $f_{t_i,t_0}(t,t_0)$ with respect to t_0:

$$f_{t_i}(t) = \int_{-\infty}^{+\infty} f_{t_i,t_0}(t,t_0)\,\mathrm{d}t_0 = \sum_{k=-\infty}^{+\infty}\mathbb{P}\{t_i = t|t_0 = t-kT\}f_{t_0}(t-kT). \tag{2.10}$$

As $f_{t_0}(t-kT) = 0$ for $t-kT \notin [0,T]$, all the elements of the sum are equal to zero, except for k such that $0 \leq t-kT \leq T$, which is only possible for $k = \lfloor Ft \rfloor$. Substituting the pmf in (2.8) into (2.10) yields

$$f_{t_i}(t) = \frac{1}{T}[1-\Phi_i(t)]\prod_{k=1}^{\lfloor (t-\tau_i)/T \rfloor}\Phi_i(t-kT). \tag{2.11}$$

We compare $f_{t_i}(t)$ from (2.11) with the experimental distribution obtained in simulation in section 2.3.

2.1.3 Simplified Case

Equation (2.11) is a complicated expression that describes the time of arrival pdf in terms of the noise cdf for any signal and for any symmetric noise distribution, and does not lead to closed-form solutions in general. A simple expression can be obtained assuming the noise level is low enough so that $\psi(t)$ can be approximated by a first-order Taylor polynomial centered at $\bar{t}_i$, where $\bar{t}_i$ is the noiseless time of arrival at the i-th sensor

(i.e., disregarding the effect of noise, but not the errors due to sampling and waveform attenuation. See Figure 8). Note that this hypothesis is not true if $\bar{t}_i - \tau_i$ occurs near a maximum of $|\psi(t)|$.

Let $\psi'(t) = \frac{\mathrm{d}\psi}{\mathrm{d}t}$ and consider the first-order Taylor approximation for the signal $\psi(t)$ centered at $\bar{t}_i - \tau_i$:

$$\psi(t) \approx \psi(\bar{t}_i - \tau_i) + \psi'(\bar{t}_i - \tau_i)(t - \bar{t}_i + \tau_i). \tag{2.12}$$

Assuming $\psi'(\bar{t}_i - \tau_i) \neq 0$ and defining the constants $b_i = \psi'(\bar{t}_i - \tau_i)$ and $\bar{\tau}_i = \bar{t}_i - \tau_i - \frac{\psi(\bar{t}_i - \tau_i)}{\psi'(\bar{t}_i - \tau_i)}$, this expression can be rewritten as

$$\psi(t) \approx b_i(t - \bar{\tau}_i). \tag{2.13}$$

We also need to approximate $F_W(w)$ in order to simplify the product in (2.11). $F_W(w)$ may be approximated as the first order Taylor polynomial centered at $w = 0$, if w is assumed to be bounded on an interval to guarantee that $0 \leq F_W(w) \leq 1$:

$$F_W(w) \approx \begin{cases} 0, & w < -\frac{1}{2f_W(0)}. \\ \frac{1}{2} + w f_W(0), & -\frac{1}{2f_W(0)} \leq w \leq \frac{1}{2f_W(0)}. \\ 1, & w > \frac{1}{2f_W(0)}. \end{cases} \tag{2.14}$$

Using this approximation for $F_W(w)$ is equivalent to approximating the noise distribution as a uniform distribution bounded between $-\Delta$ and $+\Delta$, with $\Delta = \frac{1}{2f_W(0)}$. Substituting these approximations in (2.11) and defining the constants $t_i^- = \bar{\tau}_i + \tau_i + \frac{K - \Delta}{|Ab_i|}$ and $t_i^+ = \bar{\tau}_i + \tau_i + \frac{K + \Delta}{|Ab_i|}$, we have

$$f_{t_i}(t) \approx \frac{B_i(t)}{T} \prod_{k=1}^{\lfloor (t - t_i^-)/T \rfloor} \frac{|b_i|}{2\Delta}(t_i^+ - t + kT), \tag{2.15}$$

where $B_i(t)$ is defined by

$$B_i(t) = \begin{cases} \frac{b_i(t - t_i^-)}{2\Delta}, & t_i^- \leq t \leq t_i^+. \\ 1, & t_i^+ < t < t_i^+ + T. \\ 0, & t < t_i^- \text{or } t \geq t_i^+ + T. \end{cases} \tag{2.16}$$

Applying the arithmetic progression product formula [44] to (2.15), we obtain

$$f_{t_i}(t) \approx \frac{B_i(t)}{T} \left[\frac{b_i T}{2\Delta} \right]^{N(t)} \frac{\Gamma(1 + (t_i^+ - t)/T + N(t))}{\Gamma(1 + (t_i^+ - t)/T)}, \tag{2.17}$$

where $N(t) = \lfloor (t - t_i^-)/T \rfloor$. This expression can be further simplified assuming the sample rate is high enough so that $N(t) \approx (t - t_i^-)/T$, resulting in

$$f_{t_i}(t) \approx \frac{B_i(t)}{T} \left[\frac{b_i T}{2\Delta} \right]^{(t-t_i^-)/T} \frac{\Gamma(1 + (t_i^+ - t_i^-)/T)}{\Gamma(1 + (t_i^+ - t)/T)}. \tag{2.18}$$

Unlike the exact time of arrival pdf expression (2.11), this approximated pdf does not depend on the entire source waveform, but only on the noiseless time of arrival and the source waveform derivative at that point. This closed-form approximation may simplify the development of better location estimators.

2.2 Time Difference of Arrival Bias

In the previous section an exact pdf for the estimated time of arrival was derived. We are also interested in obtaining the bias in the TDOA, which is more important than the time of arrival bias when the localization algorithm is based on the TDOA, since two time of arrival estimates with the same bias would produce an unbiased TDOA.

We can obtain the TDOA pdf using the time of arrival pdf expression in (2.11) or even its approximation in (2.18). However, this approach does not lead to a closed-form expression, so in the remaining of this section we concentrate on finding a closed-form approximation for TDOA bias.

The signal $\psi(t)$ is modeled here as an envelope $m(t)$ that is increasing and thus invertible in the interval $[0, t_{max}]$ and whose maximum is at $t = t_{max}$, modulated by a cosine whose frequency f_0 represents the sensor resonance frequency. Since the time of arrival has a low probability to be after the peak of the waveform, we do not make any restriction on $\psi(t)$ for $t > t_{max}$.

$$\psi(t) = m(t)\cos(2\pi f_0 t), \qquad 0 \le t \le t_{max} \tag{2.19}$$

The time τ_i it takes the wave to reach the sensor can be seen as the optimal value for t_i. The measured time of arrival deviation from τ_i can be approximately decomposed into a sum of errors caused by different factors:

$$t_i - \tau_i \approx \epsilon_{\text{thr}} + \epsilon_{\text{osc}} + \epsilon_{\text{samp}} + \epsilon_{\text{noise}}. \tag{2.20}$$

The factor $\epsilon_{\text{thr}} = m^{-1}(\frac{K}{Aa_i})$ is the time the wave envelope $m(t)$ takes to reach the threshold since the wave has arrived, ϵ_{osc} is the time the signal $\psi(t)$ takes to cross the threshold

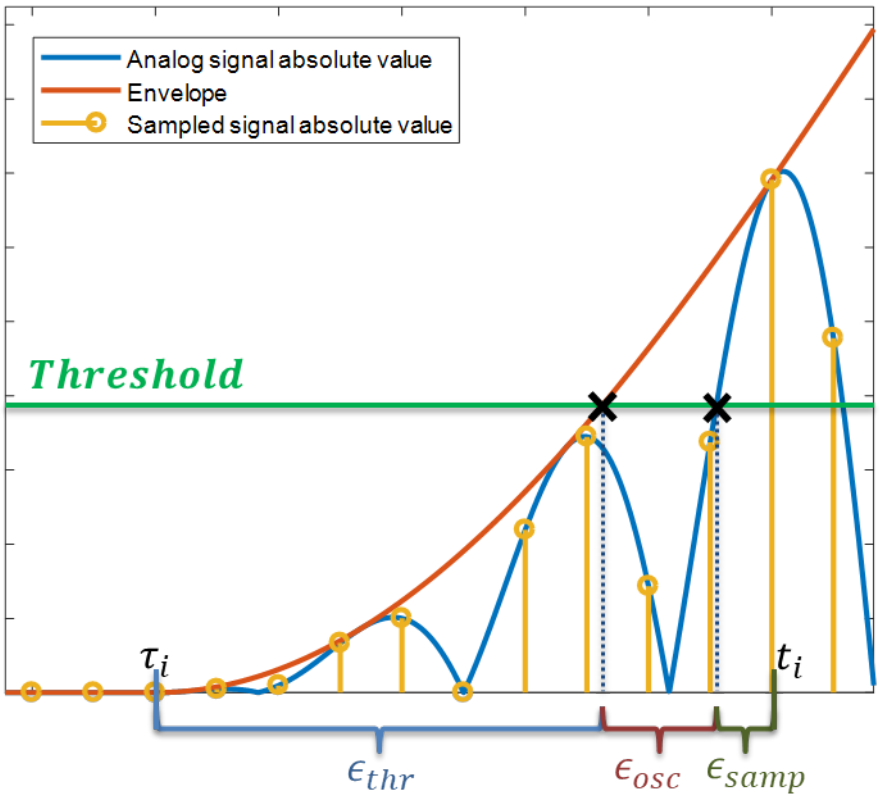

Figure 8: Illustration of (2.20) in a noiseless case

after $m(t)$ crosses it, ϵ_{samp} is the time the sampled signal takes to cross the threshold after the analog signal crosses it, and ϵ_{noise} is the time of arrival deviation cause by sampled noise. Figure 8 illustrates (2.20) in a noiseless case.

Consider the noise level is small enough so that $\psi(t)$ can be approximated by its tangent line at $t = \bar{t}_i - \tau_i$ as in equation (2.12). As $|Aa_i\psi(\bar{t}_i - \tau_i)| = K$, approximating the time of arrival deviation caused by sampled noise as the one caused by a zero-mean continuous-time noise $w_i(t)$ leads to

$$Aa_i\psi'(\bar{t}_i - \tau_i)(t_i - \bar{t}_i) + w_i(t) = 0. \tag{2.21}$$

Applying the expected value into both sides of the equation we obtain $\mathbb{E}\{t_i\} = \bar{t}_i$ and conclude that $\mathbb{E}\{\epsilon_{\text{noise}}\} \approx 0$.

Assuming the sampling rate is higher enough than f_0 so that the first time $|\psi(t)|$ crosses the threshold it has a high probability to stay above it for at least one sampling period, the deviation ϵ_{samp}, which is always positive, will have a high probability to be less than T.

Since $m(t)$ is an increasing function in $[0, t_{max}]$, the deviation ϵ_{osc}, which is also always positive, is limited by half of the oscillation period because in the worst case the signal

will be detected in the next period of $|\psi(t)|$. Hence, under the assumed hypothesis, the measured time of arrival deviation from τ_i is bounded by

$$m^{-1}\left(\frac{K}{Aa_i}\right) \leq t_i - \tau_i \leq T + \frac{1}{2f_0} + m^{-1}\left(\frac{K}{Aa_i}\right). \tag{2.22}$$

The TDOA bias bounds can then be calculated using (2.22):

$$-T - \frac{1}{2f_0} + \Delta\epsilon_{\text{thr}} \leq \Delta t - \Delta t^{opt} \leq T + \frac{1}{2f_0} + \Delta\epsilon_{\text{thr}}, \tag{2.23}$$

where $\Delta t^{opt} = \tau_2 - \tau_1$ is the optimal TDOA, $\Delta t = t_2 - t_1$ is the estimated TDOA and $\Delta\epsilon_{\text{thr}}$ is the time of arrival deviation due to the amplitude difference between received waves at different sources, given by

$$\Delta\epsilon_{\text{thr}} = m^{-1}\left(\frac{K}{Aa_2}\right) - m^{-1}\left(\frac{K}{Aa_1}\right). \tag{2.24}$$

If the attenuation factors a_1 and a_2 were the same, $\Delta\epsilon_{\text{thr}}$ would be zero. This would only happen if the source were equally distant from the sensors. Note that a_i and hence $\Delta\epsilon_{\text{thr}}$ depend on the source position.

The average of the lower and upper TDOA bias bounds, equal to $\Delta\epsilon_{\text{thr}}$, can be used as an estimator for the TDOA bias. This estimator should show good performance if $\Delta\epsilon_{\text{thr}} \gg T + \frac{1}{2f_0}$.

2.3 Simulations

2.3.1 Time of arrival probability distribution

In order to verify if (2.11) successfully represents the time of arrival distribution for a generic signal and to assess the approximation in (2.18), a noisy signal was generated and detected by one sensor in simulation. The signal $\psi(t)$ was modeled as in (2.19), and the envelope was chosen as a hanning window $m(t) = \sin(\frac{\pi t}{L}),\ 0 \leq t \leq L$, as done in [42].

We used the following parameters: $f_0 = 150$kHz (a common resonance frequency for Acoustic Emission sensors), $L = 50\mu$s, $Aa_i = 0.04$, sampling frequency $F = 1$MHz, threshold $K = 0.0178$ (equivalent to a 45dB threshold when the reference is 100 μV) and $\tau_i = 100\mu$s (equivalent to a source whose distance from the sensor is 0.5m if $c = 5000\frac{\text{m}}{\text{s}}$). Two simulations with 10^5 realizations were run with different noise levels, aiming to verify that the approximation in (2.18) only holds for low level noise. For both simulations the

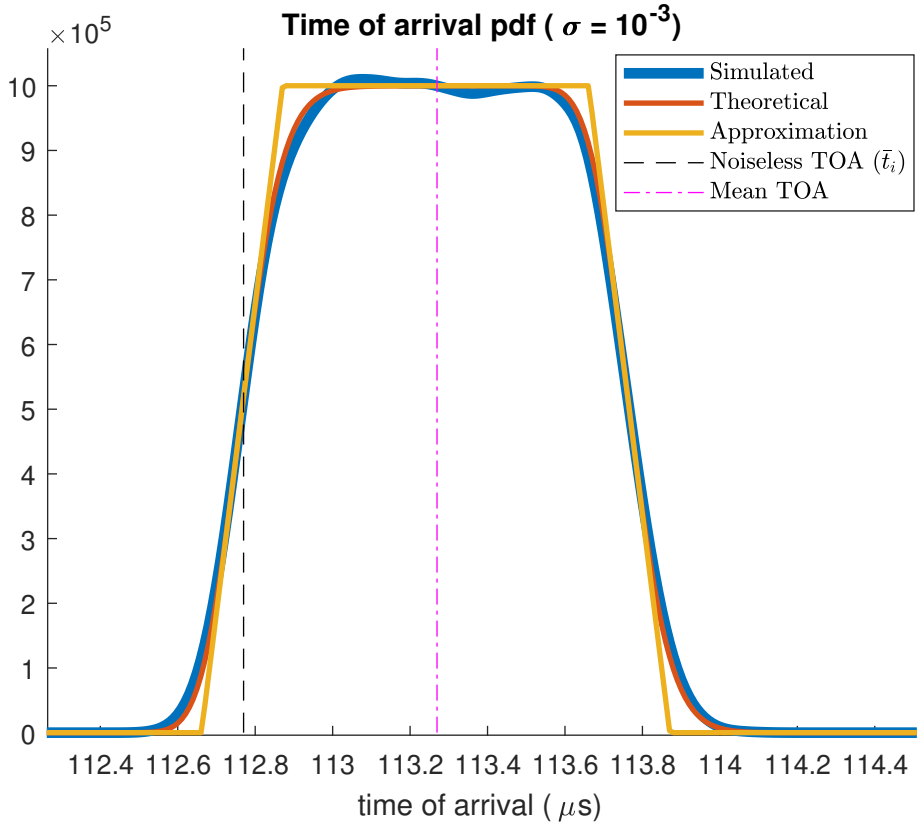

Figure 9: Time of arrival (TOA) pdf with low noise level and sampling interval $T_s = 1\mu$s.

noise $w[n]$ is Gaussian distributed with zero mean, and its standard deviation is 10^{-3} in the first simulation and 5×10^{-3} in the second.

Figures 9 and 10 show the comparison between the distribution of the times of arrival obtained in the simulation, the theoretical time of arrival pdf (2.11) and the approximate one (2.18). These figures also show the value of $\bar{t}_i$, the time of arrival that would be estimated if there was no noise.

The simulated time of arrival distribution is not Gaussian shaped and coincides with the theoretical one. In both cases the noiseless time of arrival (that is, the TOA that would be measured if the waveform were not corrupted by noise) does not coincide with the time of arrival expected value. We conclude that the presence of a zero-mean noise modifies the time of arrival expected value. In the scenario where the noise variance is low (figure 9), the approximate pdf from (2.18) is a good estimate of the theoretical one. However, when the noise variance is high (figure 10), the approximate pdf only fits the main lobe of the theoretical one. When the noise level is high, the threshold can be triggered in different oscillation periods, creating secondary lobes in the time of arrival pdf spaced by half of the oscillation period (in this case, $\frac{1}{2f_0} = 3.33\mu$s).

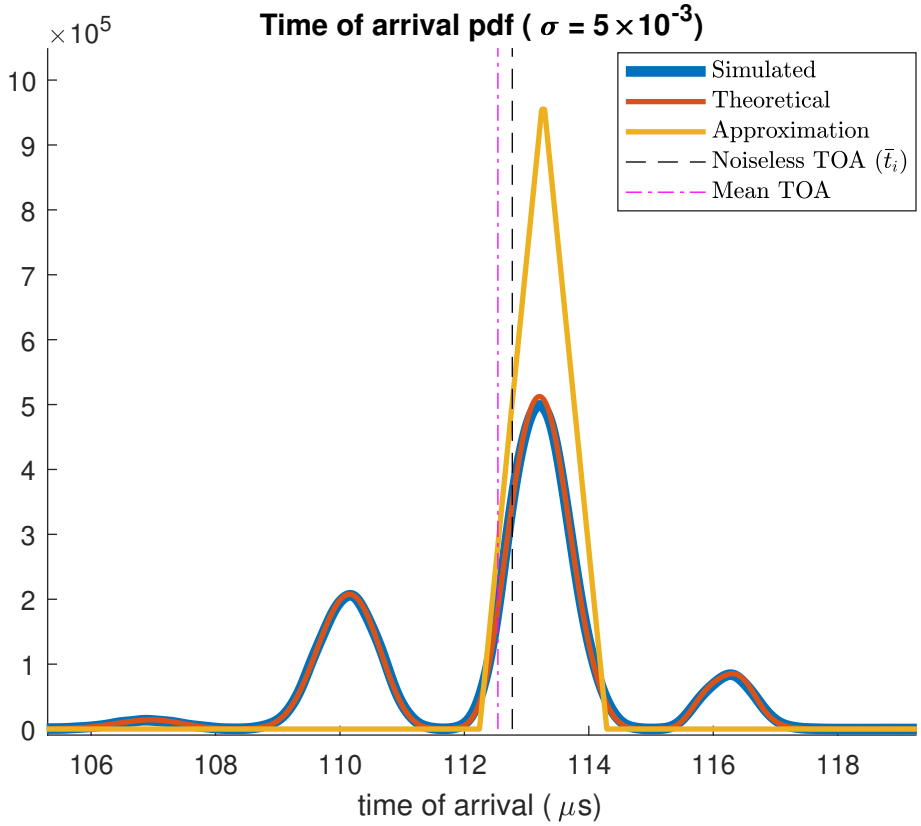

Figure 10: Time of arrival (TOA) pdf with high noise level and sampling interval $T_s = 1\mu$s. The lobes are caused by the oscillation of the waveform, and the distance between adjacent lobes is $\frac{1}{2f_0} = 3.33\mu$s.

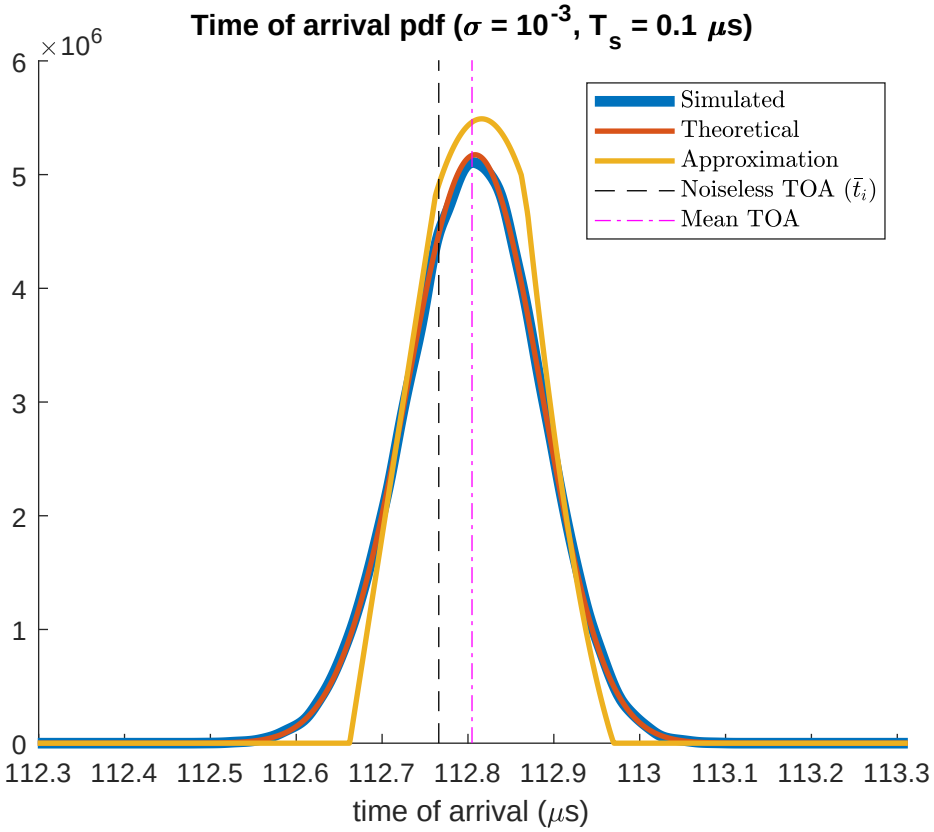

Figure 11: Time of arrival (TOA) pdf with high noise level and sampling interval $T_s = 0.1\mu$s.

For small noise (Figure 9), most of the TOA uncertainty seems to be due to sampling because the "width" of the pdf is slightly larger than 1μs, the sampling period. In order to confirm this insight, the simulation for low noise level was repeated using a sampling rate of 10 MHz instead of 1 MHz. and we show the results of the simulation for high sampling rate in Figure 11. As suspected, the variance of the pdf was reduced when sampling rate was increased. Moreover, the shape of the TOA pdf is closer to a Gaussian distribution for high sampling rate than for lower sampling rate, and the bias caused by the noise (which is the difference between the mean TOA and the noiseless TOA) is lower for high sampling rate.

2.3.2 TDOA bias

Another simulation was performed aiming to verify if the TDOA bias theoretical upper and lower bounds described in (2.23) really limit the bias, as well as assess the performance of the proposed TDOA bias estimator performance. Two sensors were placed in the x-axis at $x = 0$m and $x = 1$m, and the source position was swept from $x = 0.01$m to $x = 0.99$m along the x-axis. The attenuation coefficient was chosen as $\alpha = 2$ m^{-1}, and the noise is

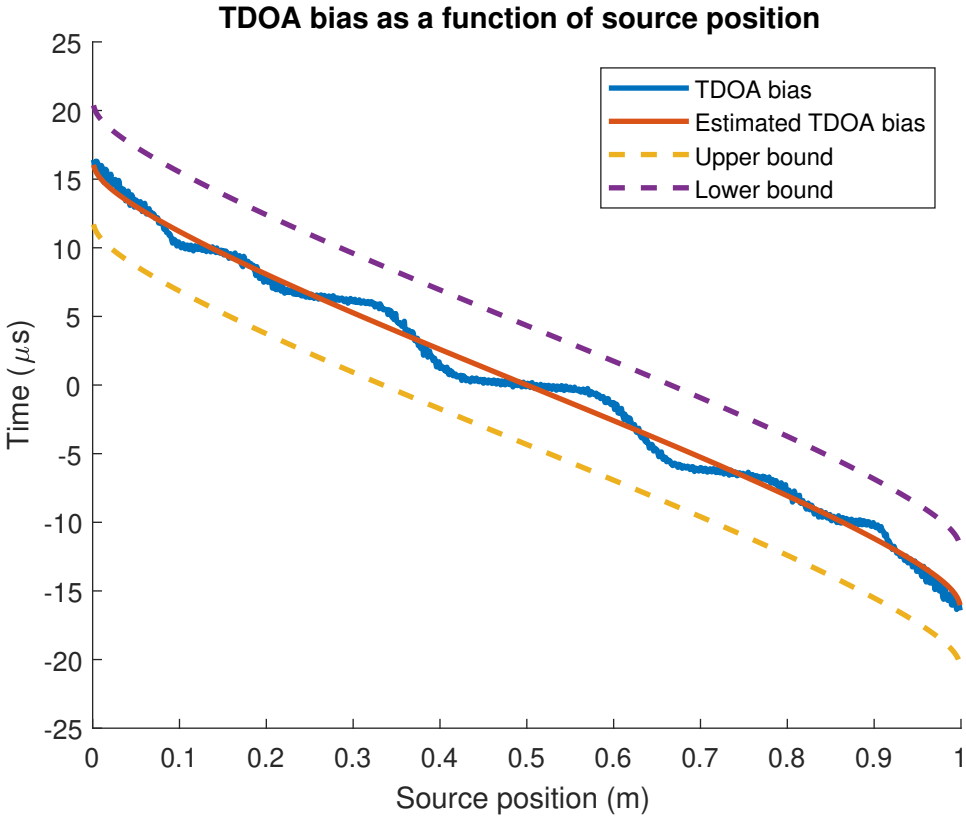

Figure 12: Simulated and estimated time difference of arrival and its theoretical bounds for different source positions

Gaussian-distributed with standard deviation $\sigma = 10^{-3}$. The rest of the parameters are the same as in the previous simulation.

Figure 12 shows these simulation results. The TDOA bias obtained in the simulation respects the theoretical bounds deduced in (2.23). Moreover, the theoretical bias in this scenario is $T+\frac{1}{2f_0}+\Delta\epsilon_{\text{thr}} = 4.33\mu s+\Delta\epsilon_{\text{thr}}$, but the obtained bias is much larger than $4.33\mu s$ in general, showing that most of the bias is due to $\Delta\epsilon_{\text{thr}}$, i.e. caused by the different signal amplitudes received by each sensor on account of the difference of attenuation. That is why the TDOA bias estimator fits well the obtained TDOA bias curve. Another interesting observation is that the bias is minimum at $x = 0.5$m, when the wave propagation path length is the same for both sensors, resulting in no attenuation difference.

2.4 Debiasing

In the end, our objective is to create better source position estimators, which can also be done by making more precise TDOA estimations. Therefore, since we have a bias model, it would be helpful to remove the bias of the TDOA estimates without changing

their variance, but both our exact and approximate bias models require the knowledge of the source position. This problem can be worked around if our source position estimate is the minimum of a cost function $J(x, y; \mathbf{u}) = g(x, y, \mathbf{u})$, where $\mathbf{u}$ is the vector of TDOA measurements. Let $\mathbf{b}(x, y) = \Delta\epsilon_{\text{thr}}$ be the bias model when the source position is (x, y). Then minimizing the cost function

$$J_{\text{debiased}}(x, y; \mathbf{u}) = J(x, y; \mathbf{u} - \mathbf{b}(x, y)) \tag{2.25}$$

offers a debiased source position estimator if the model $\mathbf{b}(x, y)$ is correct, although there will still be a small bias due to the variance of TOA estimates (caused by nonlinearities of the position estimator) and to the fact that $\Delta\epsilon_{\text{thr}}$ is only an approximation to the expected value of the TDOA estimates.

2.4.1 Debiasing TDOAs for the constant velocity model

As explained in the last section, the expression for $\Delta\epsilon_{thr}$ is given by (2.24) if the constant velocity model is taken into account. Note that if we had $\frac{K}{Aa_2} = \frac{K}{Aa_1}$, $\Delta\epsilon_{thr}$ would be zero for any envelope $m(t)$ (thus the TDOA bias would be approximately zero).

Assume it is possible to recalculate TOAs in real time. We denote $r_1[n], \cdots, r_N[n]$ as the received hits (that is, the already segmented signals containing the wave captured by each sensor. See Section 1.1.1 from Chapter 1 for more information about how hits are segmented) and $s_1[n], \cdots, s_N[n]$ the non-attenuated hits (such that $r_\ell[n] = a_\ell s_\ell[n]$). Define the modified hits

$$\tilde{r}_k[n] = \frac{\frac{1}{N}\sum_{\ell=1}^{N} E_\ell}{E_k} r_k[n], \qquad E_\ell = \frac{1}{M}\sqrt{\frac{1}{N}\sum_n r_k^2[n]} \tag{2.26}$$

where E_ℓ is the RMSE of the hit, that can be measured using either the whole hit, or a truncated version of the hit to avoid picking noise and reflections, and M is the length of the truncated hit. Using truncated hits is interesting if hits contain reflected waves because the energy of the reflections do not depend on the attenuation factors a_ℓ. Remember that a_ℓ is not known because it depends on the source position, which is unknown. Since $r_\ell[n] = a_\ell s_\ell[n]$, E_ℓ can be written as

$$E_\ell = a_\ell \sqrt{\frac{1}{N}\sum_n s_\ell[n]^2}. \tag{2.27}$$

Since $s_1[n]$, $s_2[n]$, $\cdots$, $s_L[n]$ are all a displaced version of $s[n]$, they have the same RMSE,

that is denoted here as E_0. Hence, $E_\ell = a_\ell E_0$, thus

$$\tilde{r}_k[n] = \frac{\frac{1}{N}\sum_{\ell=1}^{N} a_\ell E_0}{a_k E_0} r_k[n] = \frac{\frac{1}{N}\sum_{\ell=1}^{N} a_\ell}{a_k} r_k[n]. \tag{2.28}$$

Substituting $r_k[n] = a_k s_k[n]$ in (2.28), we obtain

$$\tilde{r}_k[n] = s_k[n] \frac{1}{N} \sum_{\ell=1}^{N} a_\ell \tag{2.29}$$

This way, we obtained modified signals $\tilde{r}_1[n], \tilde{r}_2[n], \cdots, \tilde{r}_N[n]$ that are delayed versions of each other without the knowledge of the attenuation factors $a_1, \cdots, a_N$. If the threshold is obtained using these modified signals, we would have $\Delta\epsilon_{\text{thr}} = 0$ because there is no difference in attenuation between signals, thus the TDOA bias would be approximately zero. Note that even though the waveform is required to compute the modified hits, the operations needed to calculate them have very low complexity, and can be easily implemented in real time. Hence, the waveform does not need to be stored to generate debiased TOAs.

Note that applying the fixed threshold method to obtain TOAs from the modified hits is equivalent to applying a different threshold to each original hit that depends on its energy: Defining $\beta_k = \frac{\sum_{\ell=1}^{N} E_\ell}{E_k}$ such that $\tilde{r}_k[n] = \beta_k r_k[n]$, the TOA estimated by comparing $\tilde{r}_k[n]$ with a fixed threshold $\tilde{K}$, which is different from the original threshold K, is

$$\min_n\{n : \ |\tilde{r}_i[n]| \geq K\} = \min_n\{n : \ \beta_k |r_i[n]| \geq K\} = \min_n\{n : \ |r_i[n]| \geq \frac{K}{\beta_k}\}. \tag{2.30}$$

It is important to emphasize that our debiasing method only works in structures where waves propagate according to the constant velocity model, and it will not be effective if hits contain reflections. In this case, hits must be windowed to avoid adding the energy of reflections into the energy of the hit.

Our proposed debiasing method is tested in Section 4.4.2.4 from Chapter 4.

2.5 Generalizing TOA pdf for non-white noise

In very noisy acoustic emission tests, bandpass filters can be applied to increase the SNR and increase the accuracy of hit detection and TOA estimation methods. If the noisy waveform is filtered, the resulting signal becomes corrupted by a non-white noise. Furthermore, nonlinear denoising procedures as sparsity-based denoising (using whether a wavelet dictionary or a learned dictionary) also yield non-white noise. For this reason, in

this section we generalized the expression of TOA pdf derived in this chapter to non-white noise. However, in order to avoid very large expressions, we consider the initial sampling instant is $t_0 = 0$. Generalizing the obtained results to any $t_0 \neq 0$ is straightforward.

Denote the signal sampled by sensor k by

$$r_k[n] = s_k[n] + w_k[n], \tag{2.31}$$

where $s_k[n]$ is the delayed and attenuated wave and $w_k[n]$ is the noise. Define the vector $\mathbf{w}[n]$ as

$$\mathbf{w}[n] = \begin{bmatrix} w_k[1] & w_k[2] & \cdots & w_k[n] \end{bmatrix}^T. \tag{2.32}$$

and the interval $\mathcal{I}_m$ as

$$\mathcal{I}_m =]-\infty, K - |s_k[m]|]. \tag{2.33}$$

We omit the index k representing the sensor from $\mathbf{w}[n]$ and $\mathcal{I}_m$ to simplify the notation, since the TOAs measured by different sensors are independent.

The fixed threshold method estimates the TOA as the first instant where the signal crosses the threshold. Thus, denoting as $p[n]$ the probability of the estimated TOA being the instant n, we have

$$p[n] = \mathbb{P}\{|r_k[m]| < K \ \forall m < n \text{ and } |r_k[n]| \geq K\}. \tag{2.34}$$

Assuming the noise is low enough so that it cannot trigger the threshold (i.e. $\mathbb{P}\{|w_k[m]| \geq K\} \approx 0 \ \forall m$), the sign of $r_k[m]$ is determined by $s_k[m]$, thus

$$\begin{aligned} |r_k[m]| = |s_k[m] + w_k[m]| &\approx (s_k[m] + w_k[m])\text{sgn}(s_k[m]) \\ &= |s_k[m]| + w_k[m]\,\text{sgn}(s_k[m]). \end{aligned} \tag{2.35}$$

Recalling that we assumed that the noise pdf is even (thus $\mathbb{P}\{w_k[m] \in \mathcal{A}\} = \mathbb{P}\{-w_k[m] \in \mathcal{A}\}$ for any set $\mathcal{A}$), from (2.35) we obtain

$$\mathbb{P}\{|r_k[m]| < K\} = \mathbb{P}\{w_k[m]\,\text{sgn}(s_k[m]) < K - |s_k[m]|\} = \mathbb{P}\{w_k[m] < K - |s_k[m]|\}. \tag{2.36}$$

Denoting the joint pdf of $\mathbf{w}[n]$ as $f_{\mathbf{w}[n]}(\mathbf{w})$, we can write $p[n]$ as a multiple integral:

$$\begin{aligned} p[n] &= \int_{\mathcal{I}_0 \times \cdots \times \mathcal{I}_{n-1} \times \mathcal{I}_n^c} f_{\mathbf{w}[n]}(w_0, w_1, \cdots, w_n)\, \mathrm{d}w_0 \cdots\, \mathrm{d}w_n \\ &= \int_{-\infty}^{+\infty} \int_{\mathcal{I}_0 \times \cdots \times \mathcal{I}_{n-1}} f_{\mathbf{w}[n]}(w_0, w_1, \cdots, w_n)\, \mathrm{d}w_0 \cdots\, \mathrm{d}w_n \\ &\qquad - \int_{\mathcal{I}_0 \times \cdots \times \mathcal{I}_{n-1} \times \mathcal{I}_n} f_{\mathbf{w}[n]}(w_0, w_1, \cdots, w_n)\, \mathrm{d}w_0 \cdots\, \mathrm{d}w_{n-1}. \quad (2.37) \end{aligned}$$

Denoting the cumulative distribution of $\mathbf{w}[n]$ as $F_{\mathbf{w}[n]}(\mathbf{w})$ and the upper bounds of $\mathcal{I}_1, \cdots, \mathcal{I}_n$ as $q_1, \cdots, q_n$, we obtain from (2.37) the following expression for $p[n]$:

$$p[n] = F_{\mathbf{w}[n-1]}(q_0, q_1, \cdots, q_{n-1}) - F_{\mathbf{w}[n]}(q_0, q_1, \cdots, q_n), \qquad q_i = K - |s_k[i]|. \quad (2.38)$$

2.5.1 TOA pmf for white noise

If the noise is white, (2.38) must be equivalent to the expression of the TOA pmf (2.8) derived before. In this case, the cumulative distribution $F_{\mathbf{w}[n]}(\mathbf{w}[n])$ can be written as:

$$F_{\mathbf{w}[n]}(\mathbf{w}[n]) = \prod_{\ell=0}^{n} F_W(w[\ell]). \quad (2.39)$$

Substituting (2.39) in the expression of $p[n]$ (2.38), we obtain

$$p[n] = (1 - F_W(K - |s_k[n]|)) \prod_{\ell=0}^{n-1} F_W(K - |s_k[\ell]|), \quad (2.40)$$

which is the same equation as (2.8).

2.6 Approximating TOA pdf as Gaussian Mixture Distribution

Along this chapter, we have shown that TOA is not Gaussian-distributed as many authors consider. However, Figure 11 indicates that under low noise level and high sampling rate, the TOA pdf may be approximated as a Gaussian distribution. Moreover, Figure 10 indicates that if the noise level is high, the TOA pdf may be approximated as a mixture of Gaussian distributions. In Chapter 4 we assume that the TOA pmf (given by (2.40)) is approximately a Gaussian distribution or a Gaussian Mixture to derive a nearly-optimal source position estimator. Hence, in this section we verify if these hypotheses are true for high sampling rate.

We ran a simulation in similar conditions as in Figures 9 and 10, but we considered that the initial sampling instant is $t_0 = 0$ (so that TOA distribution is a probability mass function) and we used $T_s = 0.1\mu$s (high sampling rate).

Figures 13 and 14 contain the TOA pmf and CDF for a hit with high and low SNR respectively. For each hit, the pmf $p[n]$ is converted into a pdf $p(t)$ by adding a uniformly-distributed uncertainty $\mathcal{U}(-T_s/2, T_s/2)$ to the TOAs (this is equivalent to assuming that $t_0 \sim \mathcal{U}(-T_s/2, T_s/2)$), resulting in a pdf given by the convolution of $p[n]$ and a uniform distribution:

$$p(t) = \left(\sum_{n=-\infty}^{+\infty} p[n]\delta(t - nT_s) \right) * \frac{1}{T_s}\mathbf{1}_{[-\frac{T_s}{2},\frac{T_s}{2}]}(t) = \frac{1}{T_s} \sum_{n=-\infty}^{+\infty} p[n]\mathbf{1}_{[nT_s-\frac{T_s}{2},nT_s+\frac{T_s}{2}]}(t)$$
$$= \frac{1}{T_s} p[\text{round}(t/T_s)], \quad (2.41)$$

where round(t/Ts) is the nearest integer to t/Ts. Then, a Gaussian distribution is fitted to $p(t)$ for the hit with high SNR, and a Gaussian mixture with two components is fitted to $p(t)$ for the hit with low SNR. The CDF of the fitted distribution was plotted along with the TOA cdf, and in order to allow the comparison between the fitted pdf $p_{\text{fitted}}(t)$ and $p[n]$, we plotted $T_s p_{\text{fitted}}(t)$ along with $p[n]$.

We conclude from Figures 13 and 14 that TOA pmf and cdf are well fitted by a Gaussian Distribution or by a Mixture of Gaussian Distributions depending on the SNR. This approximation is explored in Chapter 4 to derive the expression for the optimal TOA-based estimator assuming that the TOAs follow a Gaussian Mixture Distribution.

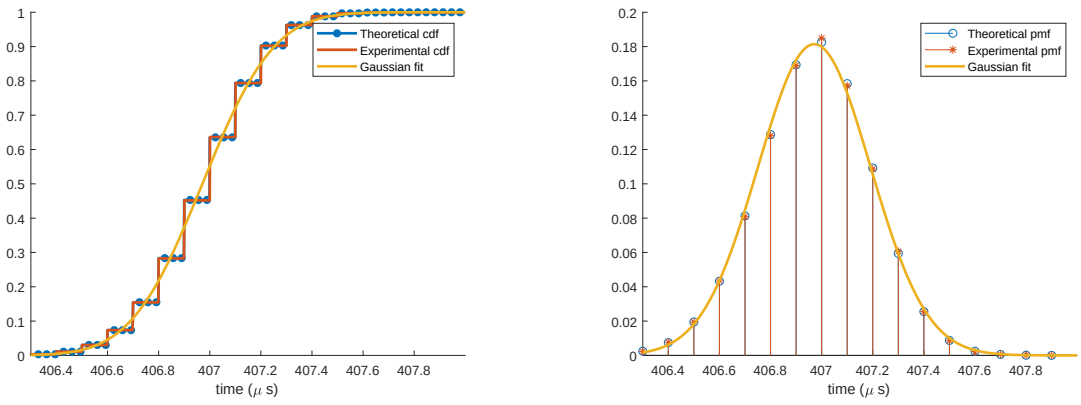

(a) cdf (b) pmf

Figure 13: TOA pmf and cdf for low noise level compared with the fitted Gaussian distribution.

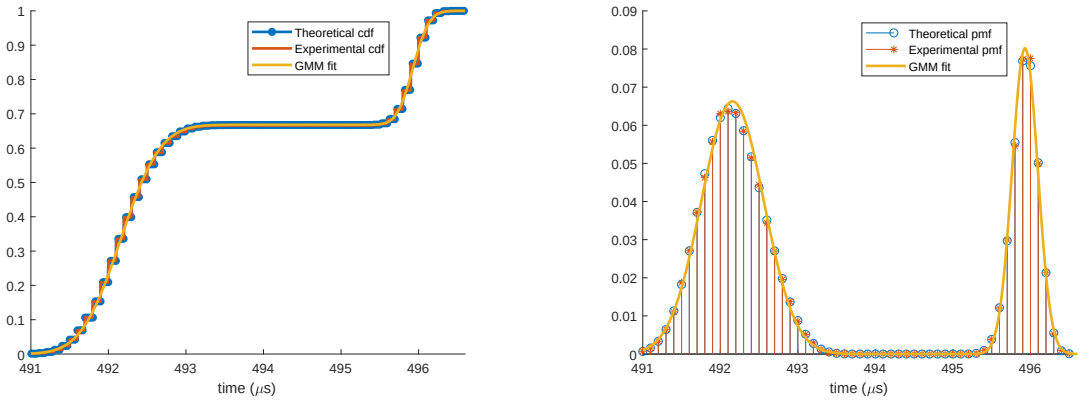

(a) cdf (b) pmf

Figure 14: TOA pmf and cdf for high noise level compared with the fitted Gaussian mixture distribution. GMM stands for Gaussian Mixture Model.

Concluding remarks

In this chapter, we derived the expression for the TOA pdf and showed that it is not Gaussian-distributed as many authors consider. We showed that it can only be approximated as a Gaussian distribution if the sampling rate is high and the noise level is small, but for higher noise levels the TOA pdf can be modeled by a mixture of Gaussian distributions. We also derived an approximate but simplified expression for the TOA pdf in the case where the noise level is small. The advantage of this simplified expression is that it depends on the waveform and its derivative calculated at a single instant instead of depending on the whole waveform as the exact TOA pdf.

Furthermore, we developed a model for the TDOA bias (which leads to bias in the source position estimate) as well as upper and lower bounds, and we concluded that the TDOA bias is mainly caused by the difference of attenuation between the two hits. We also presented a procedure to reduce TDOA bias in structures where the Constant Velocity Model holds. If the hits contain reflections of the wave emitted by the source, they must be windowed before applying our debiasing method to avoid mixing the energy of the reflections with the energy of the hits.

3 SOURCE LOCALIZATION USING TOA MEASUREMENTS

If the wave velocity at the medium is known and at least three sensors are used, localization algorithms can estimate the fault position in a surface based on the time difference of arrival (TDOA) estimates, which is defined as the difference between the estimated times of arrival at two different sensors. [8, 18, 45–49]. However, localization methods usually provide estimated positions that may have large variance and bias. For this reason, several authors have been working in new localization methods [16, 17, 19, 20, 41, 43].

This chapter explores several source localization methods that determine the source position using the measured Times of Arrival (TOAs) instead of the waveforms, which are used only to estimate TOAs. The TOAs can be measured using the fixed threshold algorithm, for example, but other methods can also be used [25,30,31]. It is worth pointing out that we do not consider the problem where two sources are active simultaneously, that is, we assume that each hit received by a sensor corresponds to only one event.

When only three TOAs are used to estimate the position of the source, the system of constitutive equations that relate TOAs with the source position has only one solution, whose closed-form expression is derived in this chapter. However, when more than three sensors are used in localization, this system becomes overdetermined, and in general no exact solution exists. In this case, the solution is often estimated by minimizing a cost function. The performance of the localization algorithm depends on the choice of the cost function under the presence of uncertainties over the measured TOAs and the wave velocity in the medium. The most popular cost functions are investigated in this chapter and their performance on anisotropic medium is compared.

In this chapter, we present two common cost functions for TOA-based localization, and we generalize them for anisotropic models. One of our contributions is to show that one of these cost functions, which depends on the source position and instant of emission, can be written only in terms of the source position. We also derive the expression for

the analytical solution of the 2D localization problem using a different approach than the derivations in [50, 51]. Furthermore, we compare the TOA estimation method based on Akaike Information Criterion with the Fixed Threshold Method in several scenarios. Finally, we compare the performance of different TOA-based localization methods in an anisotropic plate.

3.1 Popular Cost Functions

In order to determine the source position based on measured TOAs $t_1, t_2, \cdots, t_N$, we have to solve the system of equations (1.3), which is overdetermined when more than three sensors are used and there are no co-linear sensors. For this reason, cost functions are often used to obtain an approximate solution for this system. We present two cost functions that are often used in acoustic emission to estimate a source position based on TOA measurements [26, 28, 52, 53], although there are other cost functions presented in the literature as [8, 53, 54].

Consider the direction-dependent anisotropic propagation model presented in Chapter 1. The cost function $J_{\text{TDOA}}(x, y)$ uses the estimated TOAs to compute TDOAs. Let the TOAs $t_1, t_2, \cdots, t_N$ be such that $t_1 \leq t_2 \leq \cdots \leq t_N$. Each TDOA Δt_i is defined as

$$\Delta t_i = t_i - t_1, \qquad i = 2, 3, \cdots, N, \tag{3.1}$$

and the cost function relates the estimated TDOA to the known sensor positions and a tentative source position (x, y) as

$$J_{\text{TDOA}}(x, y) = \sum_{k=2}^{N} \left[(t_k - t_1) - \frac{1}{c_k(x, y)} \sqrt{(x - x_k)^2 + (y - y_k)^2} + \frac{1}{c_1(x, y)} \sqrt{(x - x_1)^2 + (y - y_1)^2} \right]^2, \tag{3.2}$$

where (x_k, y_k) is the position of the k-th sensor and $c_k(x, y)$ is wave velocity assuming it propagates from the point (x, y) to (x_k, y_k).

The cost function $J_{\text{TOA}}(x, y)$ uses the estimated TOAs directly in its expression, given by

$$J_{\text{TOA}}(x, y, t) = \sum_{k=1}^{N} \left[c_k(x, y)(t_k - t) - \sqrt{(x - x_k)^2 + (y - y_k)^2} \right]^2. \tag{3.3}$$

Although J_{TOA} is a function of three variables (x, y and t) instead of two as J_{TDOA}

(which is a function of x and y), it is possible to write the variable t as a function of x and y assuming (x, y, t) is a local minima of J_{TOA}, that is, $\nabla J_{\text{TOA}}(x, y, t) = \mathbf{0}$, transforming J_{TOA} into a two-variable function. Reducing the number of variables of a function we want to minimize is interesting because it decreases the computational cost of the minimization algorithm. Equate the derivative of (3.3) with respect to t to zero:

$$\frac{\partial J_{\text{TOA}}}{\partial t}(x, y, t) = 2\sum_{k=1}^{N} c_k(x, y)(\sqrt{(x - x_k)^2 + (y - y_k)^2} + c_k(x, y)(t - t_k)) = 0. \tag{3.4}$$

t can be isolated from this equation, yielding

$$t = \frac{\sum_{k=1}^{N} t_k c_k^2(x, y) - \sum_{k=1}^{N} c_k(x, y)\sqrt{(x - x_k)^2 + (y - y_k)^2}}{\sum_{k=1}^{N} c_k^2(x, y)}. \tag{3.5}$$

$J_{\text{TOA}}(x, y)$ can be rewritten by substituting (3.5) into (3.3):

$$J_{\text{TOA}}(x, y) = \sum_{k=1}^{N} \left[c_k(x, y) \left(t_k - \frac{\sum_{i=1}^{N} t_i c_i^2(x, y) - \sum_{i=1}^{N} c_i(x, y)\sqrt{(x - x_i)^2 + (y - y_i)^2}}{\sum_{i=1}^{N} c_i^2(x, y)} \right) \right.$$
$$\left. ... - \sqrt{(x - x_k)^2 - (y - y_k)^2} \right]^2. \tag{3.6}$$

In the isotropic case (where $c_k = c \quad \forall k$), the expression of the optimal t is much simpler, and so is $J_{\text{TOA}}(x, y)$:

$$t = \frac{1}{N}\sum_{k=1}^{N} t_k - \frac{1}{N}\sum_{k=1}^{N} \frac{\sqrt{(x - x_k)^2 + (y - y_k)^2}}{c}, \tag{3.7}$$

$$J_{\text{TOA}}(x, y) = \sum_{k=1}^{N} \left[c(t_k - \frac{1}{N}\sum_{i=1}^{N} t_i) + \frac{1}{N}\sum_{i=1}^{N} \sqrt{(x - x_i)^2 + (y - y_i)^2} \right.$$
$$\left. - \sqrt{(x - x_k)^2 - (y - y_k)^2} \right]^2 \tag{3.8}$$

Note that even though $J_{\text{TOA}}(x, y)$ and $J_{\text{TOA}}(x, y, t)$ share the same local minima (thus they produce the same estimated source position when minimized), they are different functions. Another important observation is that both $J_{\text{TOA}}(x, y)$ and $J_{\text{TDOA}}(x, y)$ may have more than one local minimum, so it is important to choose carefully the initialization point conditions of the minimization algorithm we are using. In this work, we use $J_{\text{TOA}}(x, y)$ instead of $J_{\text{TOA}}(x, y, t)$ in this work because $J_{\text{TOA}}(x, y)$ has less variables than $J_{\text{TOA}}(x, y, t)$, thus minimizing $J_{\text{TOA}}(x, y)$ requires less computational complexity.

3.1.1 Role of TDOAs in Localization

Even though J_{TOA} has TOAs in its expression (unlike $J_{\text{TDOA}}(x, y)$, which has only TDOAs), it is possible to write it only in terms of TDOAs. This can be done by placing t_k inside the fraction in (3.6):

$$J_{\text{TOA}}(x,y) = \sum_{k=1}^{N} \left[c_k(x,y) \left(\frac{\sum_{i=1}^{N}(t_k - t_i)c_i^2(x,y) + \sum_{i=1}^{N} c_i(x,y)\sqrt{(x-x_i)^2+(y-y_i)^2}}{\sum_{i=1}^{N} c_i^2(x,y)} \right) - \sqrt{(x-x_k)^2-(y-y_k)^2} \right]^2 \tag{3.9}$$

In the isotropic case, (3.9) becomes

$$J_{\text{TOA}}(x,y) = \sum_{k=1}^{N} \left[\frac{c}{N} \sum_{i=1}^{N}(t_k - t_i) + \frac{1}{N} \sum_{i=1}^{N} \sqrt{(x-x_i)^2+(y-y_i)^2} - \sqrt{(x-x_k)^2-(y-y_k)^2} \right]^2 . \tag{3.10}$$

In both cases, the cost function $J_{\text{TOA}}(x, y)$ depends only on the TDOAs $t_i - t_k$ for $1 \leq i, k \leq N$. Hence, a measurement error of TOAs that does not affect TDOAs (that is, an error that is constant for all TOAs) will not impact the position estimate if $J_{\text{TOA}}(x, y)$ or $J_{\text{TDOA}}(x, y)$ is used (as J_{TDOA} also depends only on TDOAs).

This is intuitive because constant errors in TOAs are completely absorbed by the instant of emission estimate t. In other words, if the estimated source coordinates is $(\hat{x}, \hat{y}, \hat{t})$ for TOAs $t_1, t_2, \cdots, t_N$, then the estimated source coordinates is $(\hat{x}, \hat{y}, \hat{t} + \epsilon)$ for TOAs $t_1 + \epsilon, t_2 + \epsilon, \cdots, t_N + \epsilon$, where ϵ is a constant, leaving the estimated position $(\hat{x}, \hat{y})$ unchanged.

It is worth noting that in most Acoustic Emission applications, the exact instant t the source emits a wave is not important, thus the constant TOA bias (which only affects t) is irrelevant. This is the reason why we modeled TDOA bias in Chapter 2 instead of only TOA bias.

3.2 Closed-Form Solution in Isotropic Media

Isotropic TOA-based source localization methods use cost functions to find the source position (in most cases, estimating the exact instant the source was emitted is not relevant). The choice of a cost function impacts on the accuracy when more than three sensors are used in the isotropic case. However, when only three sensors are used, all cost functions share a global minimum, since there is an exact solution for the system of equations (1.3), as we show next. In this case, solving the system of equations is much less computationally demanding than minimizing a cost function.

The objective of this section is to derive a closed-form expression for the estimated position in 2D isotropic media. This closed-form expression is a well-known result in literature that is employed for example in [50, 51].

3.2.1 1D case

3.2.1.1 Analytical solution

Before tackling the 2D problem, we focus on the unidimensional source localization problem because it is much easier to understand. In this problem, we want to determine the position of a source along a line that connects two sensors, which are positioned at $x = 0$ and $x = L$. If the wave was emitted at an instant t and propagates with velocity c, we can determine the source position x using the measured TOAs t_1 and t_2, equating the distance propagated by the wave with the distance between the source position and the sensor:

$$\begin{cases} c(t_1 - t) = |x| \\ c(t_2 - t) = |L - x| \end{cases} \tag{3.11}$$

In order to solve (3.11), we get rid of the absolute values by assuming x belongs to one of the intervals $]-\infty, 0]$, $[0, L]$ or $]L, \infty[$ and finding the solution for each interval.

First, let us find the solution assuming $0 \leq x \leq L$. In this case, solving (3.11) is straightforward since $|x| = x$ and $|L - x| = L - x$, hence

$$x = \frac{L - c(t_2 - t_1)}{2} \tag{3.12}$$

and

$$t = \frac{t_1 + t_2}{2} - \frac{L}{2c}. \tag{3.13}$$

On the other hand, assuming $x < 0$, (3.11) becomes

$$\begin{cases} c(t_1 - t) = -x, \\ c(t_2 - t) = L - x, \end{cases} \Leftrightarrow \quad \begin{cases} ct - x = ct_1, \\ ct - x = ct_2 - L, \end{cases} \tag{3.14}$$

which is an impossible system of equations for any t_1, t_2 unless $ct_1 = ct_2 - L$, in which case the system will be undetermined (since the TDOA is equal to L/c for sources localized in any point $x < 0$). An analogous situation occurs if $x > L$. Thus, we conclude that the solution of the localization problem lies in the interval $0 < x < L$, regardless of the measured TOAs. Hence, if the actual source position does not belong to $[0, L]$, it is not possible to accurately estimate it.

3.2.1.2 Localizing a source at a negative position

We have concluded that it is not possible to find a solution to (3.11) in the region $x < 0$ or $x > L$, thus we must always assume that $x \in [0, L]$ in the 1D localization problem with only 2 sensors, even if the actual source position is $x^* < 0$ and TOAs are noiseless. Let us find the solution for (3.11) considering that TOAs are generated by a source located at $x = x^* < 0$ that emits a wave at the instant $t = t^*$. In this case, the measured TOAs may be modeled as

$$t_1 = -\frac{x^*}{c} + t^* + \epsilon_1, \tag{3.15}$$

$$t_2 = \frac{L - x^*}{c} + t^* + \epsilon_2, \tag{3.16}$$

where ϵ_1 and ϵ_2 are small perturbations due to noise and imperfections of the TOA estimation algorithm. The measured TDOA does not depend on the source position x^*:

$$t_2 - t_1 = \frac{L}{c} + \epsilon_2 - \epsilon_1, \tag{3.17}$$

and neither does the estimated source position, obtained by substituting the TDOA is (3.12):

$$x = c\frac{\epsilon_1 + \epsilon_2}{2}. \tag{3.18}$$

Thus, the estimated source position depends only on the perturbations of the TOA measurements, and it would be zero if $\epsilon_1 = \epsilon_2 = 0$.

3.2.1.3 Negative position obtained by minimizing a cost function

What would happen if we were using a cost function minimization to estimate x that produces a negative estimate for x? For example, let us see what happens when we use J_{TOA}, which is defined as

$$J(x,t) = \Big[c(t_1 - t) - |x|\Big]^2 + \Big[c(t_2 - t) - |L - x|\Big]^2. \tag{3.19}$$

If $x < 0$, $J(x,t)$ reduces to

$$\Big[c(t_1 - t) + x\Big]^2 + \Big[c(t_2 - t) + x - L\Big]^2. \tag{3.20}$$

Despite the lack of analytical solution for negative values of x, the minimization algorithm always finds a value of x and t where the gradient of $J(x,t)$ is zero. Still assuming $x < 0$, we have

$$\begin{aligned} \frac{\partial J}{\partial t} &= -2(c(t_1 - t) + x) - 2c(c(t_2 - t) + x - L) = 0 \\ &\Rightarrow ct - x = \frac{ct_1 + ct_2 - L}{2}. \end{aligned} \tag{3.21}$$

$$\begin{aligned} \frac{\partial J}{\partial x} &= 2(c(t_1 - t) + x) + 2(c(t_2 - t) + x - L) = 0 \\ &\Rightarrow ct - x = \frac{ct_1 + ct_2 - L}{2}. \end{aligned} \tag{3.22}$$

Hence, $\nabla J(x,y) = 0$ for any (x,t) that satisfies (3.21). The estimated source position will be different if different initial conditions are used in the minimization algorithm. Furthermore, from (3.22) we have $(t_1 - t) = -\frac{1}{c}x - \frac{1}{2}(t_2 - t_1 - \frac{L}{c})$, thus the solutions found by the method may satisfy $t > t_1$ if $t_2 - t_1 - \frac{L}{c} > -\frac{2x}{c}$. This would mean that the sensor received the signal before the instant the source was emitted, which is an impossible situation.

We conclude that it is necessary to verify the solutions of the optimization problems for consistency, as there are source positions that cannot be a solution for the localization problem.

3.2.2 2D Case

Now we solve the two-dimensional case using a polar coordinate system centered in the first sensor position. The k-th sensor lies at a distance of ρ_k from the first one and at an angle θ_k, with $\rho_1 = 0$ and $\theta_1 = 0$, and the coordinates of the source position — which are our unknown variables — are (ρ, θ). For the k-th sensor, the constitutive equations

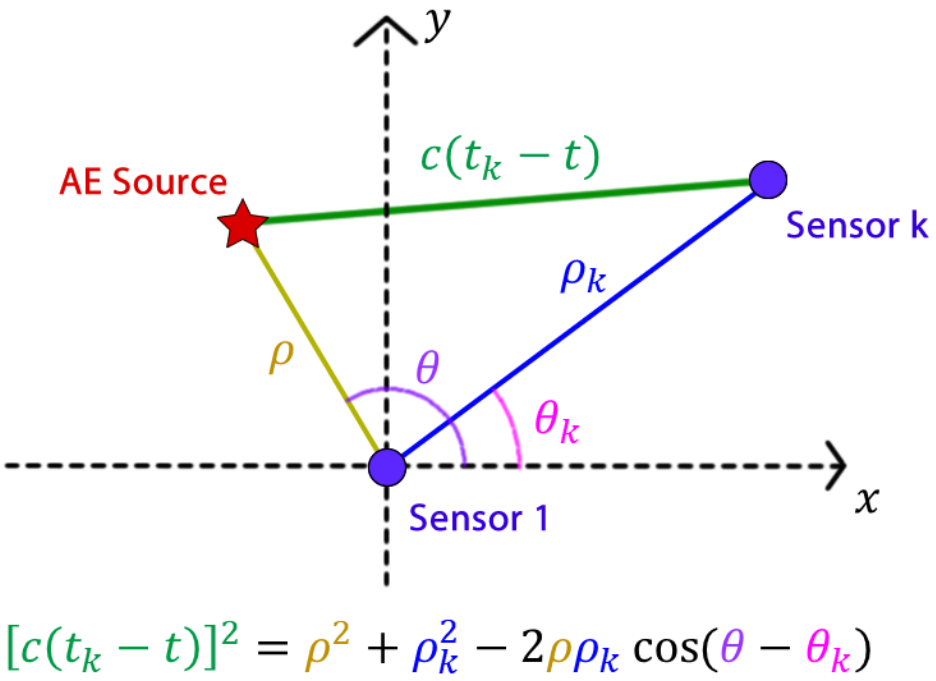

Figure 15: Illustration of equation (3.23). The star represents an acoustic emission source (as a growing crack) and the circles represent the sensors.

are obtained by equating the distance the wave travelled and the distance between the sensor and the source position, as in the 1D case. As illustrated in Figure 15, the distance between the k-th sensor and the source position can be calculated using the law of cosines:

$$c(t_k - t) = \sqrt{\rho_k^2 + \rho^2 - 2\rho\rho_k \cos(\theta - \theta_k)}, \qquad k = 1, 2, 3. \tag{3.23}$$

Note that this equation is simpler for the first sensor, since $\rho_1 = 0$:

$$c(t_1 - t) = \rho. \tag{3.24}$$

Let $\Delta t_k = t_k - t_1$ be the Time Difference of Arrival (TDOA) between the hit received by the k-th sensor and the hit received by the first one. Subtracting (3.24) from (3.23), we have:

$$c\Delta t_k = \sqrt{\rho_k^2 + \rho^2 - 2\rho\rho_k \cos(\theta - \theta_k)} - \rho. \tag{3.25}$$

Isolating ρ using the above equation, we obtain

$$\rho = \frac{\rho_k^2 - c^2\Delta t_k^2}{2c\Delta t_k + 2\rho_k \cos(\theta - \theta_k)}. \tag{3.26}$$

Since this equation holds for $k = 2$ and $k = 3$, in the case of three sensors there is a single

solution satisfying

$$\rho = \frac{\rho_2^2 - c^2\Delta t_2^2}{2c\Delta t_2 + 2\rho_2\cos(\theta - \theta_2)} = \frac{\rho_3^2 - c^2\Delta t_3^2}{2c\Delta t_3 + 2\rho_3\cos(\theta - \theta_3)}.$$

Defining the auxiliary variables a_k and b_k as in (3.27) and (3.28), we can rewrite the equation to obtain (3.29):

$$a_k = \frac{\rho_k}{\rho_k^2 - c^2\Delta t_k^2}, \tag{3.27}$$

$$b_k = \frac{c\Delta t_k}{\rho_k^2 - c^2\Delta t_k^2}, \tag{3.28}$$

$$b_3 - b_2 = a_2\cos(\theta - \theta_2) - a_3\cos(\theta - \theta_3). \tag{3.29}$$

(3.29) is a simple trigonometric equation that can be solved expanding the cosines and performing laborous but straightforward algebraic manipulations. Solving it yields the four solutions summarized in the equation below, where the two $\pm$ are independent operators.

$$\begin{aligned}\theta = \pm\arccos&\left(\frac{b_3 - b_2}{\sqrt{a_2^2 + a_3^2 - 2a_2a_3\cos(\theta_2 - \theta_3)}}\right)\\ \pm\arccos&\left(\frac{a_2\cos(\theta_2) - a_3\cos(\theta_3)}{\sqrt{a_2^2 + a_3^2 - 2a_2a_3\cos(\theta_2 - \theta_3)}}\right).\end{aligned} \tag{3.30}$$

ρ can be easily obtained through the substitution of (3.30) into (3.26) using $k = 2$ or $k = 3$, and t can be obtained using (3.24):

$$t = t_1 - \frac{\rho}{c}. \tag{3.31}$$

Some of the four solutions are spurious. We must ignore the solutions with nonzero imaginary part and those whose source emission instant is larger than at least one TOA. Note that more than one solution that satisfies the constitutive equations (3.23) may exist.

3.2.3 Geometry of the solution space

In order to understand which source positions do not yield a single solution, we generated noiseless TOAs at three sensors located at $(-\frac{1}{2}, 0), (\frac{1}{2}, 0)$ and $(0, 1)$ for several source positions. The number of non-spurious solutions for each position is shown in Figure 16, which shows us that there is a region in which there are two solutions around each sensor.

These regions, shown in yellow and similar to parabolas, do not necessarily intersect, thus even sources located very far away from the sensors can yield single solutions. Moreover, the figure also shows that there can be double solutions even when the source is located inside the triangle formed by the sensor in the case where the source is very close to a sensor.

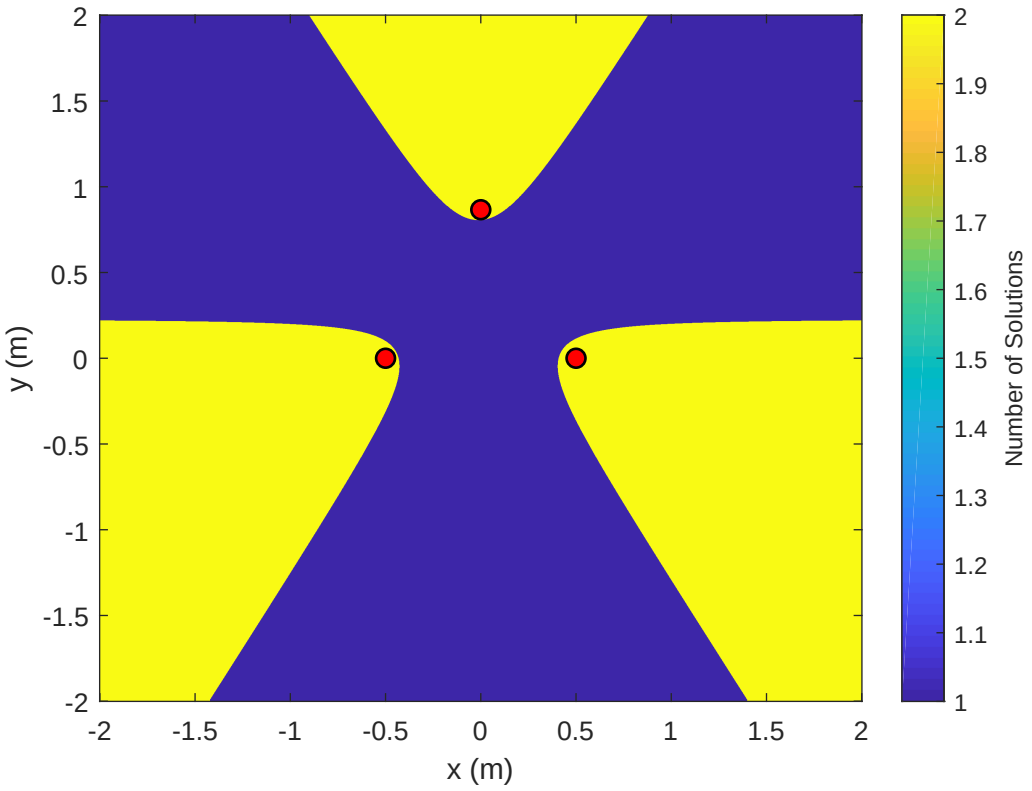

Figure 16: Geometry of the multiple solutions. Yellow indicates a double solution, and blue means a single solution. The sensors are represented as three red circles.

A question that arises is if picking the wrong solution (in the case where two solutions exists), the existence of double solutions affects the localization performance significantly. The performance will be severely degraded if the picked solution is distant from the correct one. For this reason, we repeated the last simulation, but for each source position we calculated the distance between the twin solutions in the case where two solutions exist. The result is shown in Figure 17, where distances higher than 100 cm are limited to 100 cm to ease visualization.

From Figure 17, we conclude that picking the wrong solution does cause a relevant localization error for most source positions where a double solution exists. This error can be higher than 100 cm for sources located inside the triangle formed by the sensors for position that are very close to a sensor. The double solutions coincide at the three lines

that connect the sensors, but their distance grows as the source position distances itself from these lines.

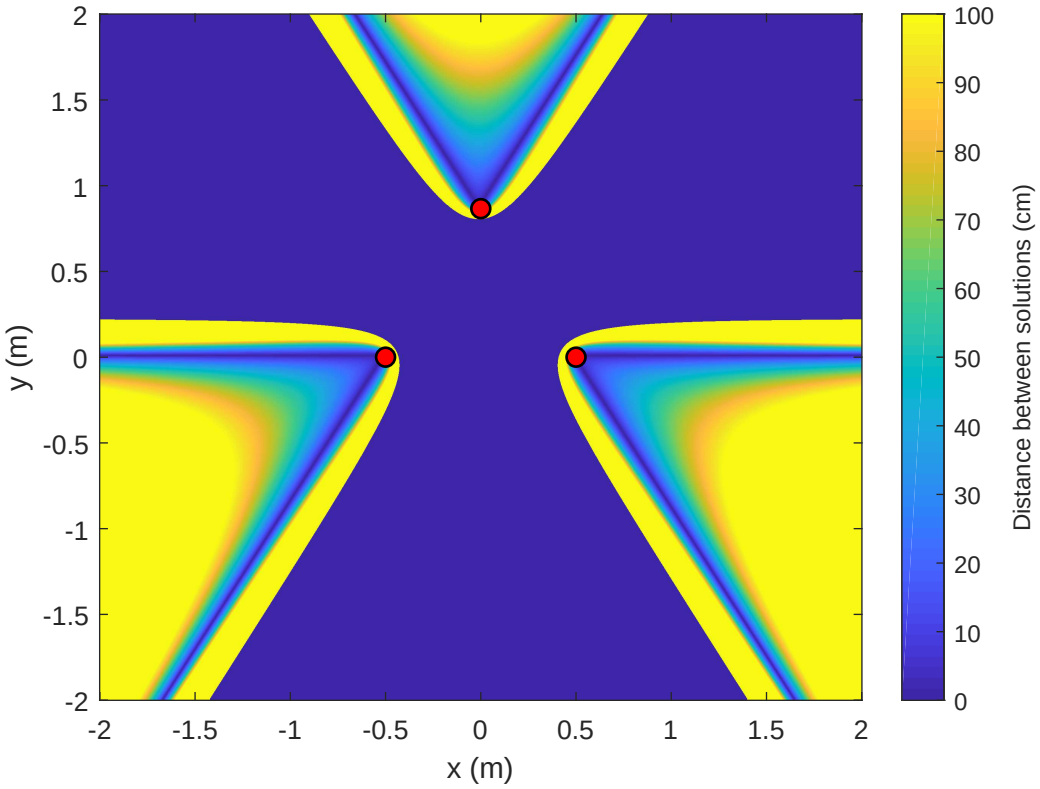

Figure 17: Distance between multiple solutions (cm) in terms of the source position. Distances higher than 100 cm are limited to 100 cm to ease visualization.

Another question that may arise is if the number of solutions is sensitive to noise. Naturally, the answer to this question depends on the source position. For this reason, we ran a simulation in the same conditions as before, except that TOAs measured by sensors are now subjected to a small zero-mean Gaussian noise of standard deviation $\sigma = 1\mu$s. For each source position, we calculated the mean number of solutions using 200 noisy TOA realizations. We show the average number of solutions for each source position in Figure 18.

For noisy TOAs, there are unstable regions around the three lines that connect the sensors. Even a small noise of standard deviation $\sigma = 1\mu$s may generate TOAs for which the localization problem has no exact solution, that is, it is not possible to find a source position that generates those TOAs. Note from Figure 16 that sources in the unstable regions cannot generate TOAs for which the localization problem has no solution for noiseless TOAs, as in this case the actual source position always satisfies the system of equations (3.23).

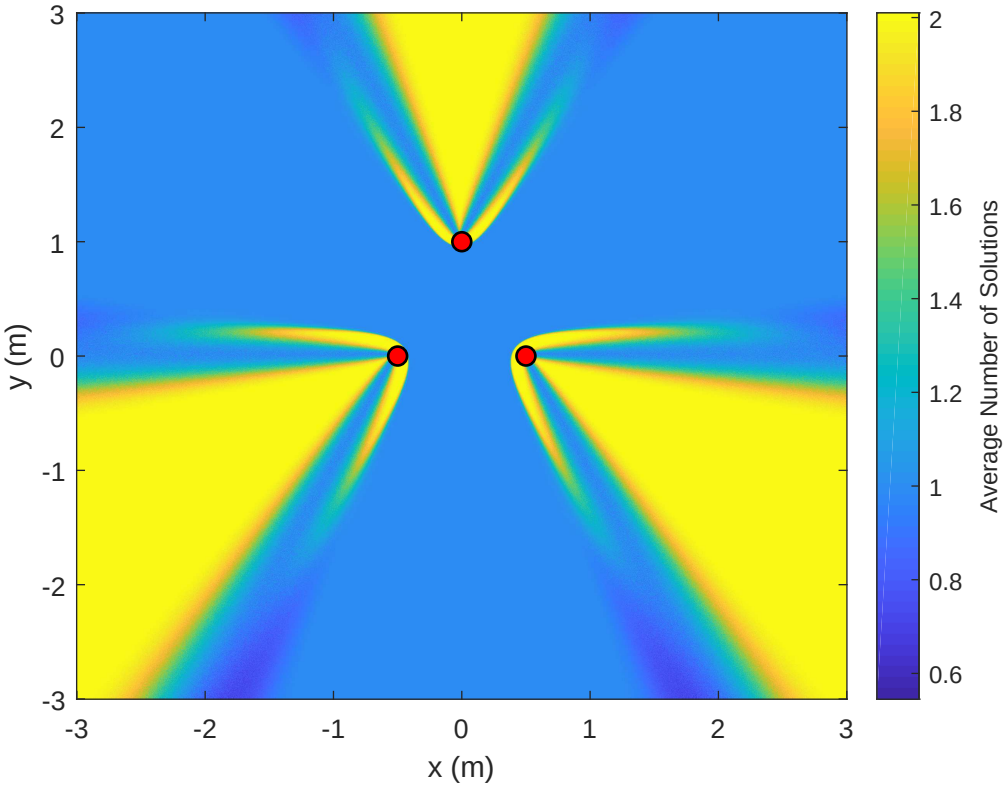

Figure 18: Average number of multiple solutions for noisy TOAs. The sensors are represented as three red circles.

It is worth noting that if TOAs from four or more sensors are available and a cost function minimization is used to locate the source, the secondary solutions disappear in most cases because the fundamental system of equations (1.3) becomes overdetermined in general, and in this case the system does not admit any exact solution.

3.3 TOA Estimation based on the Akaike Information Criterion (AIC)

The Akaike Information Criterion (AIC) [23] is a method to assess the quality of a statistical estimator or model using a set of samples. Even though it was developed in 1973, it was only applied to TOA estimation in practical problems much later [24, 25]. In this section, we deduce the TOA estimation method based on AIC presented in [24, 25] and compare it to the fixed threshold method, showing that AIC has several advantages with respect to the fixed threshold method (as lack of TOA bias and good performance in noisy scenarios), and we also point its limitations.

3.3.1 Derivation of the AIC-based TOA estimator

Suppose we want to have a model for the likelihood function $f(\mathbf{x};\boldsymbol{\theta})$ of a vector of samples $\mathbf{x}$ that depends on an $p \times 1$ vector of estimated parameters $\boldsymbol{\theta}$. The AIC for this model is [23]

$$\mathrm{AIC} = 2p - 2\max_{\boldsymbol{\theta}}\{\ln(f(\mathbf{x};\boldsymbol{\theta}))\}. \tag{3.32}$$

Ideally, better models should have lower AICs — If the model fits well the data, its maximum likelihood $\max_{\boldsymbol{\theta}}\{\ln(f(\mathbf{x};\boldsymbol{\theta}))\}$ will be large, yielding a low value for AIC. On the other hand, in order to prevent low AIC for overfitted models, the number of parameters of the model is penalized by the term p.

It is also possible to use AIC to choose a model from a set of possible models by picking the one with the smallest AIC value. This is how the AIC is used to estimate the time of arrival from a signal. Let us model the signal $x[n]$ received by a sensor as a white stochastic process whose samples are Gaussian random variables with mean $\mu[n]$ and variance $\sigma^2[n]$ in the interval $N_1 \leq n \leq N_2$, where

$$\mu[n] = \begin{cases} \mu_1, & N_1 \leq n < n^* \\ \mu_2, & n^* \leq n \leq N_2 \end{cases} \tag{3.33}$$

and

$$\sigma^2[n] = \begin{cases} \sigma_1^2, & N_1 \leq n < n^* \\ \sigma_2^2, & n^* \leq n \leq N_2 \end{cases} . \tag{3.34}$$

The bounds N_1 and N_2 are known, and we consider that there is an instant n^* between N_1 and N_2 where the variance suddenly changes. Ideally, the estimated TOA must be the instant n^*, as the sudden change of mean and variance means that the wave has reached the sensor. Our objective is to choose the parameters of this model $(\sigma_1, \sigma_2, \mu_1,\ \mu_2)$ in terms of n^* that maximize the likelihood function. Then, we pick n^* that maximizes the likelihood function. Thus, the estimated TOA will be $t_i = n^*T + t_0$, where T is the sampling period and t_0 is the instant of the first sample at $n = 0$.

Recalling that $x[n]$ is corrupted by a white Gaussian noise, the likelihood function is

$$f(\mathbf{x};\sigma_1,\sigma_2,\mu_1,\mu_2) = \prod_{k=N_1}^{n^*-1} \frac{1}{\sigma_1\sqrt{2\pi}} e^{-\frac{1}{2\sigma_1^2}(x[k]-\mu_1)^2} \prod_{k=n^*}^{N_2} \frac{1}{\sigma_2\sqrt{2\pi}} e^{-\frac{1}{2\sigma_2^2}(x[k]-\mu_2)^2}, \tag{3.35}$$

which is equivalent to maximize the log-likelihood function

$$\ln f(\mathbf{x};\sigma_1,\sigma_2,\mu_1,\mu_2) = -(n^*-N_1)\ln\sigma_1 - \frac{1}{2\sigma_1^2}\sum_{k=N_1}^{n^*-N_1}(x[k]-\mu_1)^2$$
$$-(N_2-n^*+1)\ln\sigma_2 - \frac{1}{2\sigma_2^2}\sum_{k=n^*}^{N_2}(x[k]-\mu_2)^2 - (N_2-N_1)\ln\left(\sqrt{2\pi}\right). \quad (3.36)$$

Equating the partial derivatives of $\ln f(\mathbf{x}|\sigma_1,\sigma_2,\mu_1,\mu_2)$ with respect to σ_1, σ_2, μ_1 and μ_2 to zero, we obtain the maximum likelihood estimates for the parameters:

$$\hat{\mu}_1 = \frac{1}{n^*-N_1}\sum_{k=N_1}^{n^*-1}x[k], \quad (3.37)$$

$$\hat{\mu}_2 = \frac{1}{N_2-n^*+1}\sum_{k=n^*}^{N_2}x[k], \quad (3.38)$$

$$\hat{\sigma}_1 = \frac{1}{n^*-N_1-1}\sum_{k=N_1}^{n^*-1}(x[k]-\hat{\mu}_1)^2, \quad (3.39)$$

$$\hat{\sigma}_2 = \frac{1}{N_2-n^*}\sum_{k=n^*}^{N_2}(x[k]-\hat{\mu}_2)^2. \quad (3.40)$$

Note that $\hat{\sigma}_1$ and $\hat{\sigma}_2$ are the unbiased estimators of the variance of $x[n]$ for $N_1 \leq n < n^*$ and $n^* \leq n \leq N_2$, respectively. Substituting the parameter estimates into (3.36), we obtain the expression for the maximum log-likelihood:

$$\ln f(\mathbf{x};\hat{\sigma}_1,\hat{\sigma}_2,\hat{\mu}_1,\hat{\mu}_2) =$$
$$-(N_2-N_1)\sqrt{2\pi} - (n^*-N_1)\ln\hat{\sigma}_1 - \frac{n^*-N_1-1}{2} - (N_2-n^*+1)\ln\hat{\sigma}_2 - \frac{N_2-n^*}{2} =$$
$$(N_2-N_1)\sqrt{2\pi} - (n^*-N_1)\ln\hat{\sigma}_1 - (N_2-n^*+1)\ln\hat{\sigma}_2 - \frac{N_2-N_1-1}{2} \quad (3.41)$$

In order to calculate the AIC, the log-likelihood expression must be substituted in (3.32), where $p = 4$ parameters are used:

$$AIC = 8 + 2\left((N_2-N_1)\sqrt{2\pi} + (n^*-N_1)\ln\hat{\sigma}_1 + (N_2-n^*+1)\ln\hat{\sigma}_2 + \frac{N_2-N_1-1}{2}\right). \quad (3.42)$$

Now, we must calculate the AIC for several values of n^* and pick n^* that yields the minimum AIC. Hence, the terms of (3.42) that do not depend on n^* can be disregarded, as well as the multiplication factor 2. After disregarding these terms, we obtain the

expression for the AIC as a function of n:

$$\mathrm{AIC}[n] = (n - N_1)\ln\hat{\sigma}_1 + (N_2 - n + 1)\ln\hat{\sigma}_2, \tag{3.43}$$

and n^* is estimated as (recall that $\hat{\sigma}_1$ and $\hat{\sigma}_2$ depend on n)

$$n^* = \arg\min_n \mathrm{AIC}[n]. \tag{3.44}$$

3.3.2 Discussion about the AIC

AIC has two huge advantages when compared to the fixed threshold methods: The first one is that it does not depend on the choice of any parameter (except for choosing the time interval $[N_1, N_2]$ that will be used to estimate TOAs), while choosing a bad threshold for the fixed threshold method may cause hits with small amplitude to be discarded or may lead to bad TOA estimates [25]. The second advantage is that TOAs estimated by AIC are not subjected to bias caused by the difference of amplitude between hits, unlike TOAs obtained by the fixed threshold method (as explained in chapter 2). This happens because the value of n that minimizes (3.43) does not depend on the sinal amplitude: If $\mathrm{AIC}_x[n]$ is the AIC of the signal $x[n]$, the AIC of $y[n] = kx[n]$ (where k is a constant) is

$$\begin{aligned}\mathrm{AIC}_y[n] &= (n - N_1)\ln(k^2\sigma_1) + (N_2 - n + 1)\ln(k^2\sigma_2) \\ &= (n - N_1)\ln\sigma_1 + (N - n + 1)\ln\sigma_2 + (N_2 - N_1 + 1)\ln(k^2) \\ &= \mathrm{AIC}_x[n] + (N_2 - N_1 + 1)\ln(k^2). \end{aligned} \tag{3.45}$$

As the term $(N_2 - N_1 + 1)\ln(k^2)$ does not depend on n, we have

$$\arg\min_n \mathrm{AIC}_x[n] = \arg\min_n \mathrm{AIC}_y[n]. \tag{3.46}$$

On the other hand, AIC has much more computational complexity than the fixed threshold method, which makes it harder for real time implementation. If it is desired to estimate TOAs using AIC offline (i.e. not in real time), the waveforms must be stored, leading to the problem of data storage in long acoustic emission tests. Another problem of AIC is that it is highly dependent on the format of the waveform, as hits whose power is not concentrated in the initial samples may cause AIC to pick TOAs incorrectly. A third issue is that AIC assumes that the noise is iid and Gaussian-distributed, thus correlated and non-Gaussian noise may degrade AIC's performance.

Figures 19 and 20 show the TOA estimation using AIC for two different waveforms

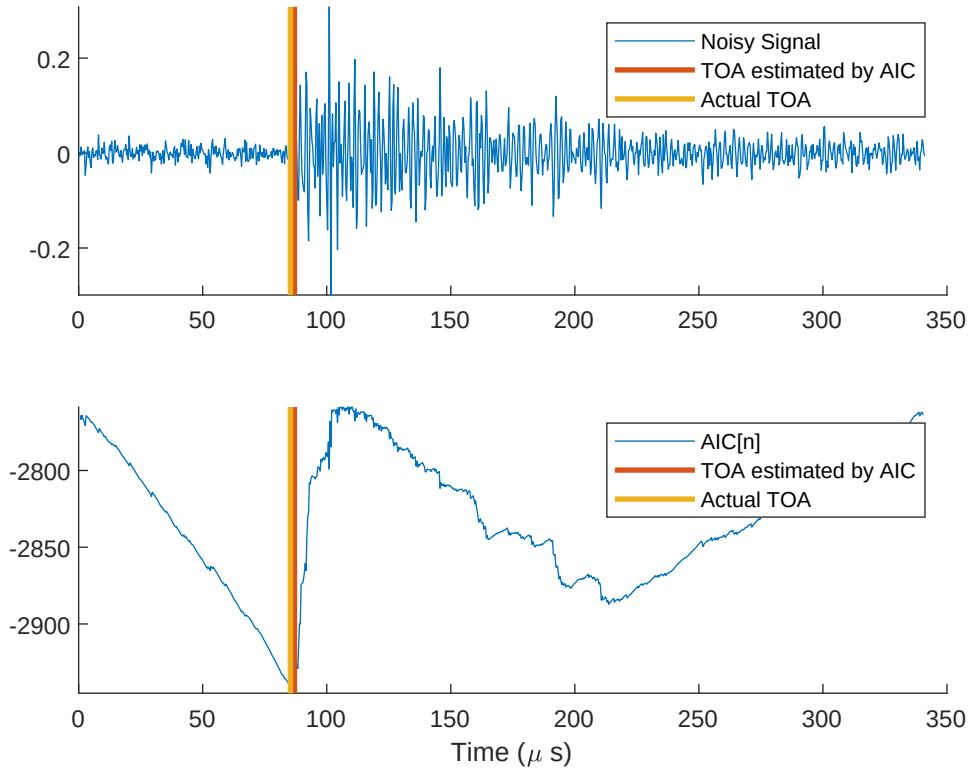

Figure 19: Example of a correct TOA estimation using AIC.

collected during a tensile test of an aircraft at Embraer. In Figure 19, the minimum of AIC$[n]$ is very close to the actual time of arrival of the hit. Note that there is a local minimum at $n = 214$, when the wave begins to vanish, but the minimum at $n = 87$ is much lower than the one at $n = 214$. However, in Figure 20, the minimum at the end of the hit is lower than the minimum at its beginning because the energy of this hit is not concentrated at its beginning as in Figure 19. Thus, in this case AIC estimates the TOA as the end of the wave instead of its first samples. For this reason, AIC is very dependent on the waveform, and may not work on waveforms with high duration, or hits whose energy is not concentrated in the first samples.

It is worth noting that the AIC estimates the TOA based on the waveform samples in the interval $[N_1, N_2]$. This interval must be chosen correctly in order to AIC function properly, and even though it must contain the source signal, N_2 must not be too large because AIC may pick the TOA as the last samples of the signal of interest, at the point where the signal variance falls to zero. Moreover, if N_2 is too large, AIC may compute reflections of the hit, which may lead to less precise TOA estimates if the energy of the reflections is not negligible.

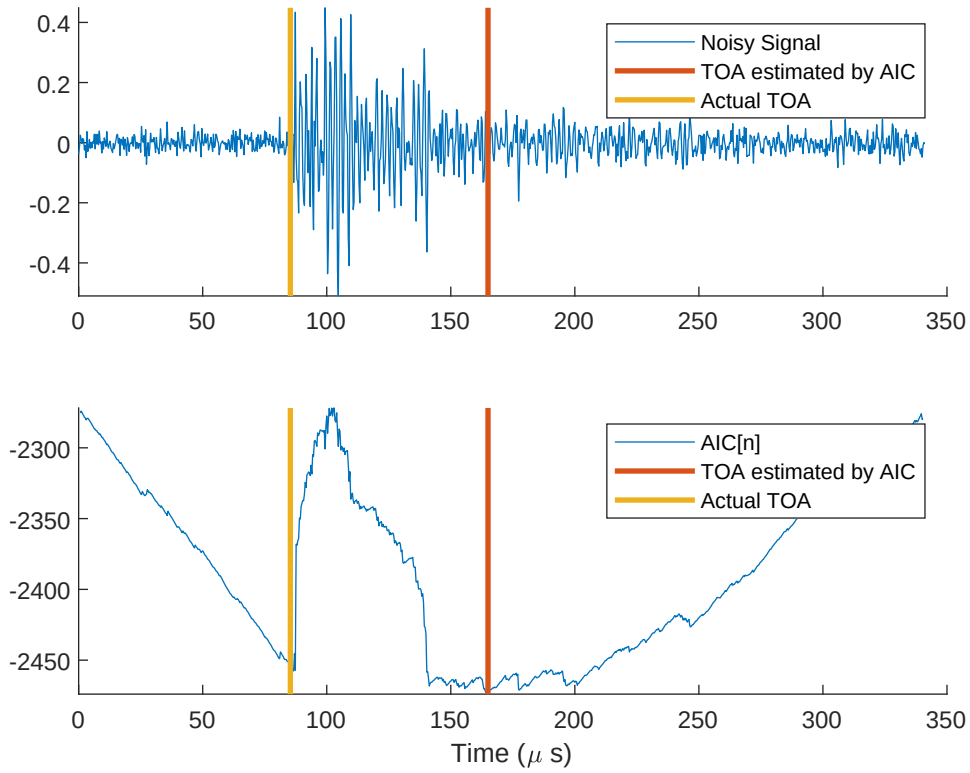

Figure 20: Example of a wrong TOA estimation using AIC. In this case, AIC estimates the TOA as the instant where the high energy components of the wave vanish.

3.3.3 Comparison of AIC and Fixed Threshold

We added white Gaussian noise to the waveform from Figure 19 (the case where minimizing AIC[n] works) for SNRs from 0 dB to 70 db. Then, we delayed one of the waveforms, and for each SNR we performed TOA estimation using AIC and fixed threshold with three different threshold levels ($K = 0.01$, $K = 0.03$ and $K = 0.05$), and we compared the obtained TDOAs in Figure 21. It is more interesting to compare estimated TDOAs than TOAs because the TOA errors that are not present in TDOAs do not affect localization, as explained in Section 3.1.1. The AIC picker was implemented using $N_1 = 0$, and N_2 was chosen as the instant where the absolute value of the signal is maximum.

We also did another simulation identical the previous one, except that the delayed waveform is multiplied by $\frac{1}{2}$ to take into account the attenuation due to wave propagation, and we plotted the results in Figure 22. Finally, we did a third simulation in the same conditions of the others considering the attenuation factor $\frac{1}{2}$, but we performed the bias correction proposed in Chapter 2, that is, we applied the fixed threshold method to the modified signals defined in (2.26). The third simulation is shown in Figure 23.

First of all, note that the AIC TDOA estimate is the same for all simulations, confirming that TOAs obtained by minimizing AIC do not depend on the amplitude of the waveform, as discussed in 3.3.2. Furthermore, the mean error curves for the fixed threshold algorithm are much smoother than the AIC curves, which presents a slope between SNR = 30 dB and SNR = 60 dB that is intrinsic to the waveform. This happens because the performance of AIC is much more dependent on the waveform than the fixed threshold method.

For very high SNR (above 60 dB), AIC finds the actual TDOA in all cases. For both the first simulation — where no attenuation is taken into account (Figure 21) — and the third one (Figure 23), in which our bias correction method is applied, the fixed threshold method also estimates TOAs perfectly, but in the second simulation there is a bias in TDOA measurements for $K = 0.03$ and $K = 0.05$. Moreover, the fixed threshold method achieves zero TDOA error at much lower SNRs than AIC in the first and third simulation, even though AIC's mean error for SNR > 10 dB is very small (approximately 1 sample, or 1μs).

On the other hand, AIC's mean error is much lower than the worst fixed threshold $K = 0.01$ for intermediate SNR levels (between 10 dB and 25 dB), and falls to approximately 1 sample earlier than all other estimators, except for $K = 0.05$ using debiased TOAs, whose mean error falls at the same point as AIC.

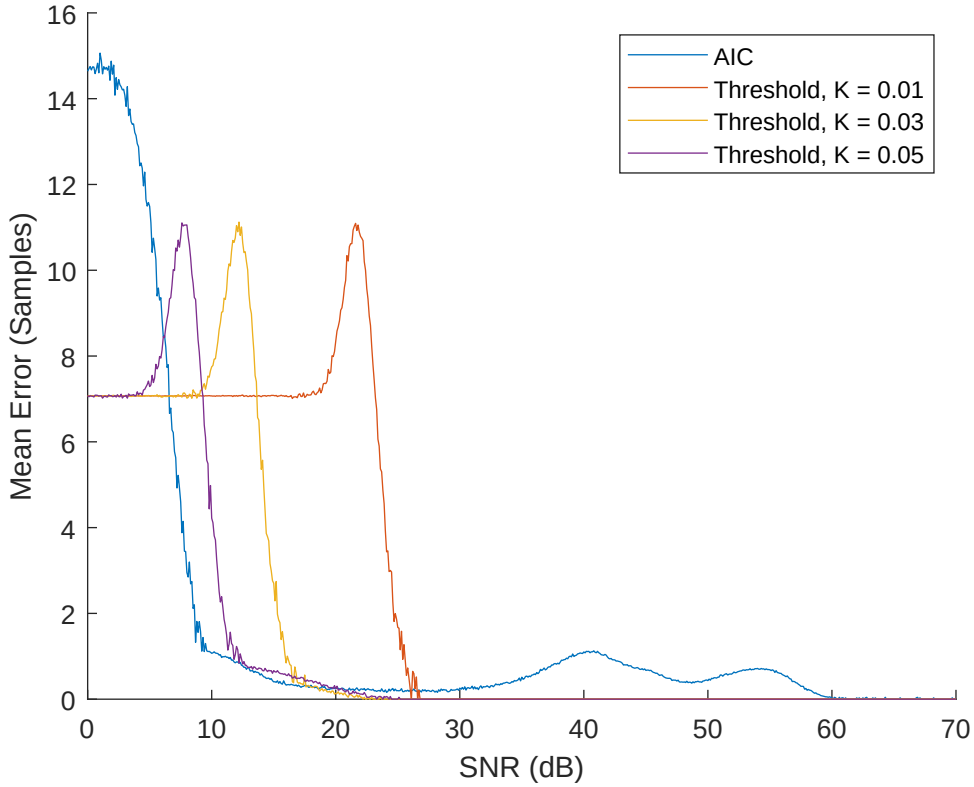

Figure 21: Performance of TDOA estimation for different methods. For each SNR, TOAs are obtained from two noisy hits, and then TDOA is calculated. Attenuation is not considered in this case, thus the second hit is a delayed version of the first one.

For the waveform used in this simulations, using the fixed threshold method with $K = 0.05$ and debiased TOAs yields better performance than AIC. However, it is not possible to choose the best threshold for each waveform, as it must assume a fixed value, and $K = 0.05$ may present worse performance for other waveforms. Depending on the choice of the threshold, AIC can achieve much smaller error for average SNRs, even if debiased TOAs are used. Furthermore, using AIC does not lead to TDOA bias, which may be one of the reasons why AIC is being widely used [7, 24, 25, 55].

Hence, even though AIC may have worse performance than the best fixed threshold, it does not depend on choosing the right threshold, while the fixed threshold method may present worse performance for non-optimal thresholds. The two disadvantages of AIC with respect to the fixed threshold method are that it has much more computational complexity, and it may not work for waveforms whose energy is not concentrated in the first samples.

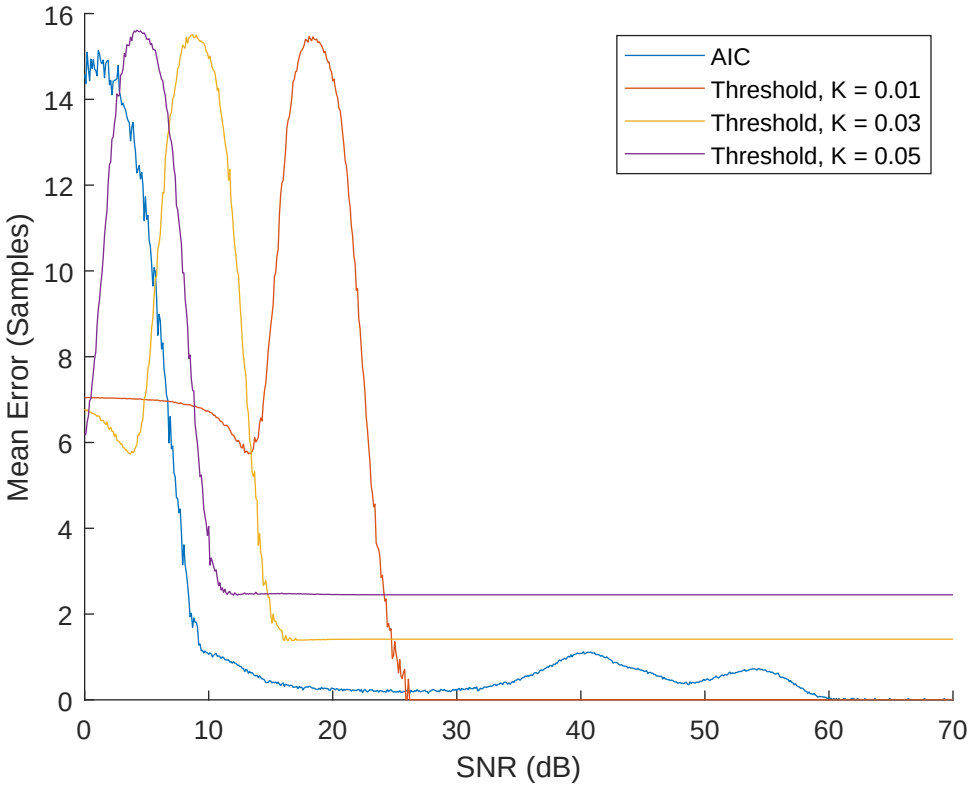

Figure 22: Performance of TDOA estimation for different methods. For each SNR, TOAs are obtained from two noisy hits, and then TDOA is calculated. The second hit is a delayed and attenuated version of the first one.

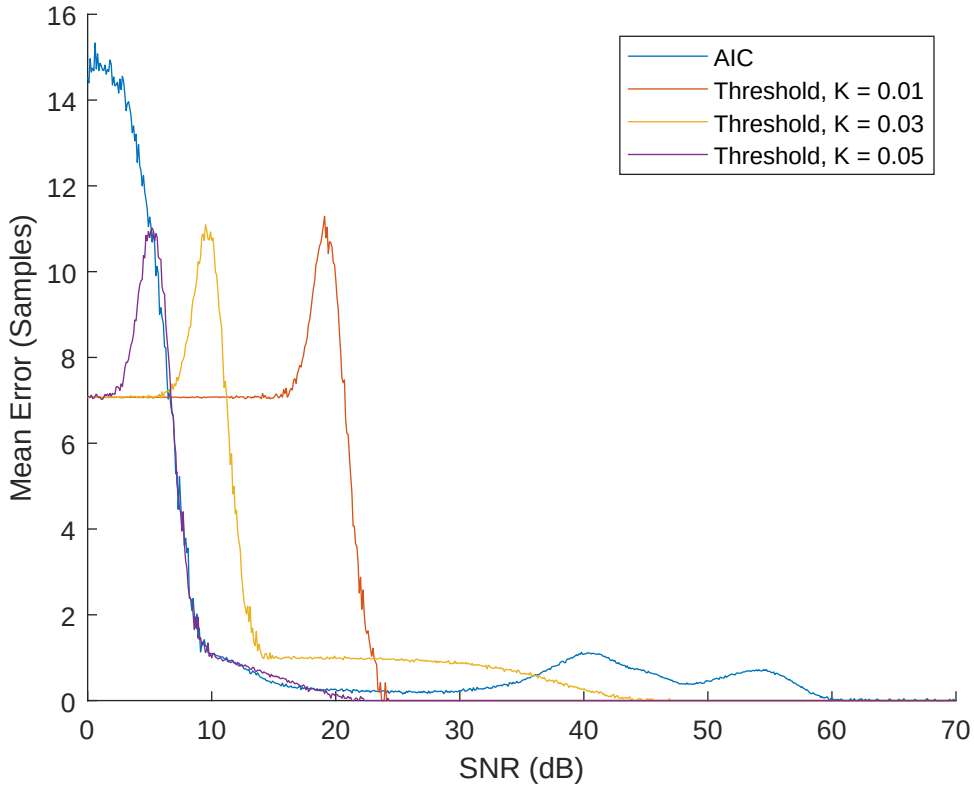

Figure 23: Performance of TDOA estimation for different methods. For each SNR, TOAs are obtained from two noisy hits, and then TDOA is calculated. The second hit is a delayed and attenuated version of the first one. TOAs obtained by the fixed threshold method are debiased using the algorithm proposed in Chapter 2.

3.4 Localization using the Elliptical Anisotropic Model

Using data from an AST test performed at Embraer on an anisotropic plate, we estimate the parameters of the Elliptical Anisotropic Model presented in Section 1.1.2, which is used in the anisotropic version of the cost function $J_{\text{TOA}}(x, y)$ (3.3) to localize artificial sources generated through a pencil-lead break test performed in the same structure. In AST tests, each sensor pulses one at a time, emitting a wave that is sampled by the others. The obtained TOAs are then used to obtain the parameters of the model.

The objective of this section is to compare the isotropic and anisotropic versions of the cost functions J_{TOA} and J_{TDOA} using TOAs obtained by the fixed threshold method, but we also compare them with the isotropic J_{TOA} using debiased TOAs and TOAs estimated by the AIC method. In this pencil-lead break test, seven sensors are used to monitor the structure, but only three sensors are used to localize each source (that is, only the hits wit three smallest TOAs are used), thus J_{TOA} and J_{TDOA} are equivalent.

3.4.1 Learning the Model

In order to use the anisotropic model in source localization algorithms, its parameters must be estimated. This can be done by performing an acoustic emission test where the source position is known (such as a pencil lead break test or an AST test). In AST tests, the instant t the wave was emitted is known, thus a velocity c_i is estimated for each sensor i as

$$c_i = \frac{d_i}{t_i - t}, \tag{3.47}$$

where d_i is the distance between the sensor and the source (whose position is known). The velocity c_i represents the a noisy measurement of the velocity in the direction of the line that connects the i-th sensor to the source position.

The estimated velocity $\hat{c}(\theta)$ at angle θ is modeled as an ellipse that depends on the parameters a, b and β according to (1.8):

$$\hat{c}(\theta) = \frac{ab}{\sqrt{a^2 \sin^2(\theta - \beta) + b^2 \cos^2(\theta - \beta)}}. \tag{3.48}$$

The parameters a, b and β are estimated using a least squares approach:

$$(a, b, \beta) = \arg \min_{(a,b,\beta)} \sum_{i=1}^{N} \left(c_i - \frac{ab}{\sqrt{a^2 \sin^2(\theta_i - \beta) + b^2 \cos^2(\theta_i - \beta)}} \right)^2. \tag{3.49}$$

3.4.1.1 Pencil-lead breaks on anisotropic plate

Ten pencil-lead breaks were performed on five different positions on an anisotropic plate-like structure. We localized each event using both isotropic and anisotropic $J_{\mathrm{TOA}}(x, y)$ (3.3) using TOAs obtained by the fixed threshold method and the isotropic J_{TOA} using TOAs obtained by our TOA debiasing method proposed in Chapter 2 and by the AIC-based TOA estimation method. In order to avoid computing reflections in the debiasing method, only the samples $n^* - 100$ to $n^* + 100$ were used to calculate the energy of the hits, where n^* is the instant the hit crosses the fixed threshold. The AIC method was implemented using $N_1 = n^* - 256$ (which is $256\mu s$ before the threshold crossing because the sampling period is 1 μs) and N_2 as the instant where the absolute value of the signal is maximum (recall that AIC estimates n in the interval $[N_1, N_2]$ to compute the TOA $t_i = nT_s$).

The estimated source positions along with the sensors and the actual pencil lead break coordinates are presented in Figure 24. The scale of this figure and the exact position of the sensors in this test are not provided, as requested by Embraer.

We did not use anisotropic J_{TOA} with AIC or debiased TOAs in this test because the anisotropic parameters were obtained through an AST test whose waveforms are not available.

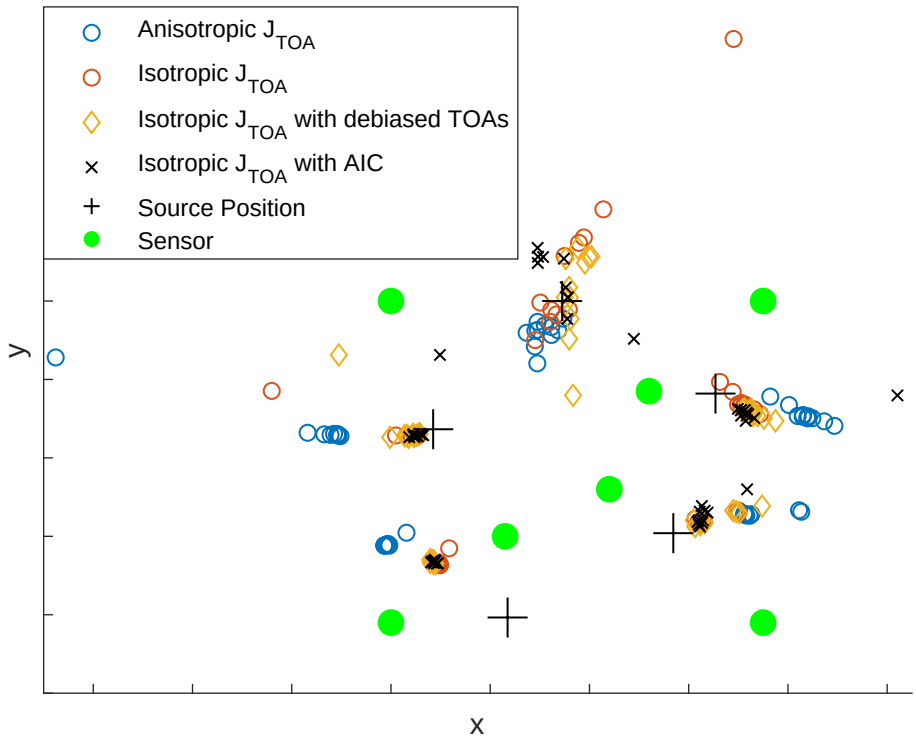

Figure 24: Comparison between both isotropic and anisotropic J_{TOA} using TOAs obtained by the fixed threshold method and isotropic J_{TOA} using TOAs obtained by AIC and TOAs obtained by our TOA debiasing method in anisotropic plate.

Isotropic J_{TOA} presents high error in the upper region of the plate, while anisotropic J_{TOA} concentrates the events close to the break points. For the other points, the performance of isotropic J_{TOA} was the same or worse than its anisotropic version, probably due to uncertainties in the anisotropy parameters. On the other hand, isotropic J_{TOA} with AIC produces better estimates than the other methods in all cases. This is because AIC does not present TOA bias as the fixed threshold method, yielding a smaller localization bias even if a cost function with an imprecise wave velocity is used.

We observed that hits generated by the same pencil-lead break are not approximately multiple from each other in this test, thus the Constant Velocity Model does not hold for this structure. That is why our debiasing method did not present a consistently better performance than J_{TOA} with TOAs obtained by the fixed threshold method because the constant velocity model is not a good approximation for this structure. However, it successfully debiased the estimated positions located in the upper right corner of the figure, achieving better accuracy than isotropic J_{TOA} with original TOAs in this case.

3.4.2 Isotropic Localization in Anisotropic Plate

In order to further compare the performance of isotropic J_{TOA} and J_{TDOA} in an anisotropic plate, we simulated an acoustic emission test using an elliptical anisotropy model where the maximum wave speed is $4000\frac{m}{s}$ at 45^{o} and the minimum one is $2000\frac{m}{s}$ (at -45^{o}). TOAs were estimated using the fixed threshold method, and the sensor were positioned at $(0,0), (0,1), (1,0)$ and $(1,1)$. We simulate a source in several positions and we localized it using the isotropic versions of both cost functions with $c = 3000\frac{m}{s}$ — the average between the maximum and the minimum velocities.

The result is shown in Figure 25, where each source position is connected by lines to its estimates. The estimated positions produced by J_{TOA} are much closer to the actual source positions than the ones obtained by J_{TDOA} in most cases, indicating that J_{TOA} is more robust to uncertainties in the wave velocity.

In Figure 26, the anisotropic versions of J_{TOA} and J_{TDOA} were used with the correct anisotropy parameters. Both anisotropic cost functions had similar accuracy, but they performed better than their isotropic versions.

Note that even though J_{TOA} performed better than J_{TDOA} in most cases, J_{TDOA} produces more accurate results than J_{TOA} for some source positions. This is expected because the performance of the cost functions depends on the source position and the geometry of the sensors.

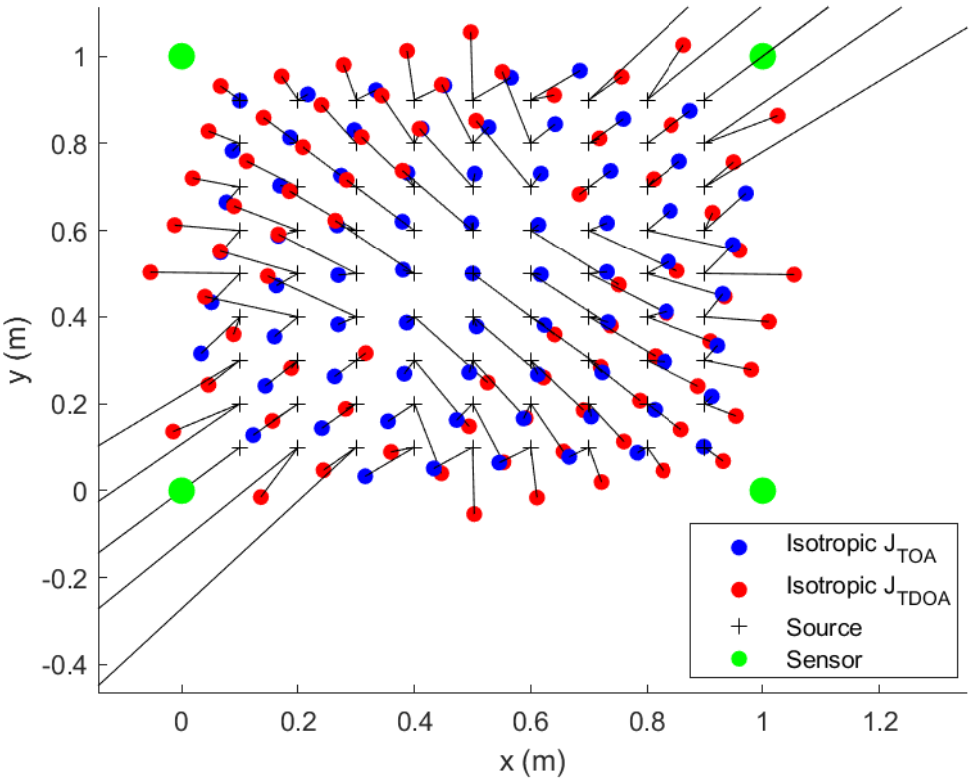

Figure 25: Localization using isotropic cost functions in anisotropic plate.

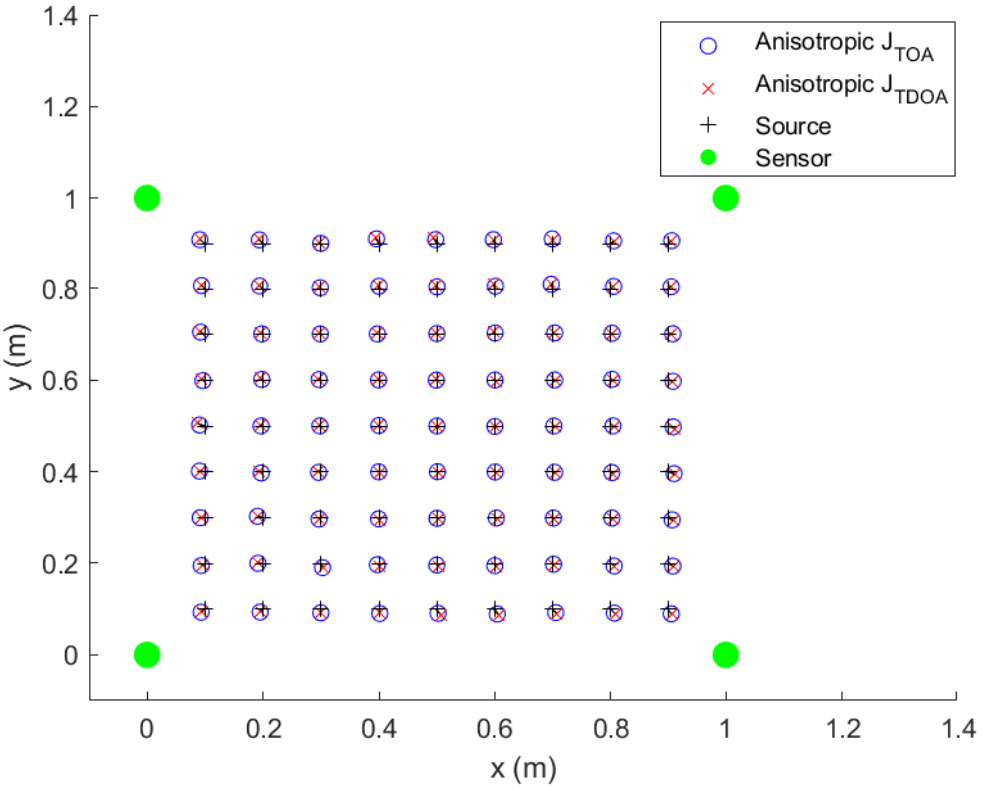

Figure 26: Localization using anisotropic cost functions in anisotropic plate.

Concluding remarks

In this chapter, we introduced the cost functions $J_{\mathrm{TOA}}(x, y, t)$ and $J_{\mathrm{TDOA}}(x, y)$ considering an anisotropic structure, and we showed that the variable t in $J_{\mathrm{TOA}}(x, y, t)$ can be written in terms of x and y, yielding the cost function $J_{TOA}(x, y)$. We derived the closed-form solution for anisotropic media considering that three sensors are used, and we showed that it is possible to generate the same TOAs at two different source position, which means that the localization problem may have two solutions depending on the source position and on the geometry of the sensors.

We presented the TOA estimator based on AIC, which has better performance than the fixed threshold method in most cases at the cost of more computational complexity. AIC produces unbiased TOAs and is robust to noise, but it may pick TOAs incorrectly if the energy of the waveform is not concentrated in the first samples.

Finally, we compared the anisotropic cost functions using TOAs extracted from AIC, the fixed threshold algorithm and TOAs generated by with our TOA debiasing technique using data from a pencil lead break in an anisotropic plate. In general, isotropic J_{TOA} using TOAs obtained from AIC presented better results than the other methods. This is because AIC reduces the TOA bias more successfully than our debiasing technique, since in this structure the Constant Velocity Model is not a good approximation due to the large number of reflections. We also simulated sources at several positions in an anisotropic plate and localized them using isotropic and anisotropic cost functions, and we concluded that for anisotropic plates, isotropic J_{TOA} yields more accurate estimates than isotropic J_{TDOA} in general for anisotropic plates, and the anisotropic cost functions perform much better than their isotropic versions.

4 OPTIMAL SOURCE POSITION ESTIMATOR USING TOAS

Previously, we introduced the cost functions J_{TOA} and J_{TDOA} and showed that J_{TOA} seems to be more robust than J_{TDOA}. In this chapter, we unify the cost functions J_{TOA} and J_{TDOA} into a generic cost function, and we derive an expression for the optimal cost function (that is, the one that yields the minimum mean-square localization error among all possible TOA-based estimators) when the TOAs follow a Gaussian or mixture of Gaussians distribution.

Using this generic cost function, we prove that J_{TOA} is the optimal cost function when the noise is independent and identically distributed (iid) in time and across sensors. For the sake of simplicity, we assume that the velocities used in the cost functions are the actual ones.

Although in Chapter 2 we showed that TOA is not Gaussian-distributed when it is estimated using the fixed threshold algorithm, the Gaussian distribution with a mean not necessarily zero is a good approximation when the noise level is low and the sampling frequency is high.

In order to determine the optimal estimator, the Fisher Information Matrix must be calculated and compared to the inverse of the covariance matrix of our position estimator (see Section 4.2). The Fisher Information Matrix for the acoustic emission localization problem using Gaussian TOA or TDOA measurements was calculated in [50] in the case where only three sensors are used to localize the source — In this case, no cost functions are needed because the localization problem has a closed-form solution. In this work, we calculate the Fisher Information Matrix for $N > 3$ sensors and we also find the optimal estimator, that is, the one whose covariance matrix is the inverse of the Fisher Information Matrix.

4.1 Generalizing the cost functions

It is possible to generalize the cost functions J_{TOA} and J_{TDOA} and write them as a generic cost function that uses TDOA's instead of TOAs considering the wave propagates through an isotropic medium with velocity c. Let $\tau_i = \frac{1}{c}\sqrt{(x-x_i)^2+(y-y_i)^2}$ be the time the signal emitted by a source at (x, y) position takes to reach the i-th sensor, placed at position (x_i, y_i). Denoting t_i as the time of arrival measured by the i-th sensor, the expressions of $J_{TOA}(x, y, t)$ and $J_{TDOA}(x, y)$ are

$$J_{TOA}(x,y) = \sum_{i=1}^{N}(t_i - t(x,y) - \tau_i)^2, \qquad t(x,y) = \frac{1}{N}\sum_{i=1}^{N} t_i - \frac{1}{N}\sum_{i=1}^{N}\tau_i. \tag{4.1}$$

and

$$J_{TDOA}(x,y) = \sum_{i=1}^{N}(t_i - t_1 - \tau_i + \tau_1)^2, \tag{4.2}$$

where $t(x, y)$ is the instant the wave was emitted, which is already written in terms of (x, y) as explained in Section 3.1. Define $\mathbf{u}$ as the measured TOA vectors and $\mathbf{v}$ as the TOA that would ideally be measured if the source position was (x, y):

$$\mathbf{u} = [t_1, t_2, \cdots, t_N]^T \quad \text{and} \quad \mathbf{v} = [\tau_1 + t(x,y), \tau_2 + t(x,y), \cdots, \tau_N + t(x,y)]^T. \tag{4.3}$$

Vector $\mathbf{v}$ is deterministic and depends on (x, y), while $\mathbf{u}$ is a random vector that does not depend on the tentative source position (x, y). These vectors can be used to rewrite the cost functions $J_{\text{TDOA}}(x, y)$ and $J_{\text{TOA}}(x, y)$:

$$J_{\text{TOA}}(x,y) = \sum_{i=1}^{N}(u_i - v_i)^2 = (\mathbf{u}-\mathbf{v})^T(\mathbf{u}-\mathbf{v}) \tag{4.4}$$

and

$$J_{TDOA}(x,y) = \sum_{i=1}^{N}(u_i - v_i - u_1 + v_1)^2 = \|\mathbf{A}(\mathbf{u}-\mathbf{v})\|_2^2 = (\mathbf{u}-\mathbf{v})^T\mathbf{G}(\mathbf{u}-\mathbf{v}), \tag{4.5}$$

where u_i and v_i are the i-th components of $\mathbf{u}$ and $\mathbf{v}$, $\mathbf{A}$ is a $N \times N$ matrix defined by

$$\mathbf{A} = \mathbf{I} - \mathbf{1}\mathbf{e}_1^T = \begin{bmatrix} 0 & 0 & 0 & \cdots & 0 \\ -1 & 1 & 0 & \cdots & 0 \\ -1 & 0 & 1 & \cdots & 0 \\ \vdots & \vdots & \vdots & \ddots & \vdots \\ -1 & 0 & 0 & \cdots & 1 \end{bmatrix} \tag{4.6}$$

and $\mathbf{G} = \mathbf{A}^T\mathbf{A} = \mathbf{I} - \mathbf{1}\mathbf{e}_1^T - \mathbf{e}_1\mathbf{1}^T + N\mathbf{e}_1\mathbf{e}_1^T$. We use the notation $\mathbf{1}$ to denote a vector whose elements are all equation to 1, and $\mathbf{e}_k$ the denote a vector whose elements are all zero, except for the k-th element, which is equal to 1.

Hence, we define the generalized cost function

$$J(x, y) = (\mathbf{u} - \mathbf{v})^T\mathbf{G}(\mathbf{u} - \mathbf{v}), \tag{4.7}$$

where $\mathbf{G}$ is any $N \times N$ symmetrical positive semi-definite matrix with rank ≥ 2. This generalized cost function describes both J_{TDOA} and J_{TOA}: If $\mathbf{G} = \mathbf{I}$, $J(x, y) = J_{\text{TOA}}(x, y)$, and if $\mathbf{G} = \mathbf{I} - \mathbf{1}\mathbf{e}_1^T - \mathbf{e}_1\mathbf{1}^T + N\mathbf{e}_1\mathbf{e}_1^T$, $J(x, y) = J_{\text{TDOA}}(x, y)$.

There is an interesting interpretation for this generalized cost function: Consider the system of N equations $\mathbf{u} = \mathbf{v}(x, y)$, which is similar to the system of constitutive equations (1.3) presented in Chapter 1, except that the variable t is written in terms of (x, y). If we choose an equivalent system of equations where each equation is a linear combination of the equations of the original system, we would have $\mathbf{A}\mathbf{u} = \mathbf{A}\mathbf{v}(x, y)$, where the rows of $\mathbf{A}$ are the coefficients used in each linear combination. The least squares solution corresponding to this system of equations is the minimum of

$$J(x, y) = (\mathbf{A}\mathbf{u} - \mathbf{A}\mathbf{v})^T(\mathbf{A}\mathbf{u} - \mathbf{A}\mathbf{v}) = (\mathbf{u} - \mathbf{v})^T\mathbf{A}^T\mathbf{A}(\mathbf{u} - \mathbf{v}) = (\mathbf{u} - \mathbf{v})^T\mathbf{G}(\mathbf{u} - \mathbf{v}), \tag{4.8}$$

where $\mathbf{G} = \mathbf{A}^T\mathbf{A}$. This way, if $\mathbf{A} = \mathbf{I}$, we obtain J_{TOA}, and we obtain J_{TDOA} if $\mathbf{A} = \mathbf{I} - \mathbf{1}\mathbf{e}_1^T$.

4.1.1 Biased TOA measurements

In Chapter (2) we showed that TOA and TDOA measurements are actually biased and we derived a model for this bias. It is possible to incorporate the bias model in the generalized cost function (4.7) to localize the source using debiased TOAs.

Let $\mathbf{x} = \begin{bmatrix} x \\ y \end{bmatrix}$ be the vector form of (x, y) and suppose we have a TOA bias model $\mathbf{b}(\mathbf{x})$ such that

$$\mathbb{E}\{u_i\} = b_i(\mathbf{x}) + \tau_i + t, \tag{4.9}$$

that is,

$$\mathbf{b} = \mathbb{E}\{\mathbf{u}\} - \tau - t\mathbf{1}. \tag{4.10}$$

Here, we consider that $\mathbf{b}(\mathbf{x})$ is any bias model, so it does not have to be exactly the one developed in Chapter 2. The bias model $\mathbf{b}(\mathbf{x})$ can be used to generalize $J(x, y)$ even

further. Defining

$$v_i = b_i(\mathbf{x}) + \tau_i + t, \tag{4.11}$$

we have $\mathbb{E}\{\mathbf{u}\} = \mathbf{v}$. The generalized cost function with debiased TOAs has a similar expression to (4.7), but the definition of $\mathbf{v}$ follows (4.11) instead of (4.3):

$$J(\mathbf{x}, t) = (\mathbf{u} - \mathbf{v})^T \mathbf{G} (\mathbf{u} - \mathbf{v}), \qquad \mathbf{v} = \mathbb{E}\{\mathbf{u}\} = \mathbf{b}(\mathbf{x}) + \tau(\mathbf{x}) + t\mathbf{1}. \tag{4.12}$$

As done before with J_{TOA}, the variable t in $J(\mathbf{x}, t)$ can be expressed in terms of x, y by setting $\frac{\partial J(\mathbf{x},t)}{\partial t} = 0$:

$$\frac{\partial J(\mathbf{x}, t)}{\partial t} = -2\mathbf{1}^T \mathbf{G} (\mathbf{u} - (\mathbf{b}(\mathbf{x}) + \tau(\mathbf{x}) + t\mathbf{1})) = 0, \tag{4.13}$$

thus

$$t(x, y) = \frac{\mathbf{1}^T \mathbf{G} (\mathbf{u} - (\mathbf{b}(\mathbf{x}) + \tau(\mathbf{x})))}{\mathbf{1}^T \mathbf{G} \mathbf{1}}. \tag{4.14}$$

Hence, the generalized cost function written only in terms of x and y is

$$J(\mathbf{x}) = (\mathbf{u} - \mathbf{v})^T \mathbf{G} (\mathbf{u} - \mathbf{v}), \qquad \mathbf{v} = \mathbb{E}\{\mathbf{u}\} = \mathbf{b}(\mathbf{x}) + \tau(\mathbf{x}) + t(x, y)\mathbf{1}, \tag{4.15}$$

where $t(x, y)$ is given by (4.14).

The original cost functions $J_{TOA}(x, y)$ and $J_{TDOA}(x, y)$ are obtained from (4.15) by setting $\mathbf{b}(\mathbf{x}) = \mathbf{0}$. Note that for the Constant Velocity Model, using a bias function $\mathbf{b}(\mathbf{x})$ is not necessary because it is possible to debias TOAs using our debiasing method described in Chapter 2.

4.1.2 The Maximum Likelihood Estimator for Gaussian Mixture Models

It is possible to generalize (4.7) even further by viewing it as a particular case of the Maximum Likelihood Estimator (MLE) when TOAs are distributed according to a Gaussian Mixture Model. In order to avoid large expressions, we employ the notation $\mathcal{N}(\mathbf{u}; \mathbf{v}, \mathbf{C})$ to denote a multivariate Gaussian function with mean $\mathbf{v}$ and covariance matrix $\mathbf{C}$ calculated at point $\mathbf{u}$:

$$\mathcal{N}(\mathbf{u}; \mathbf{v}, \mathbf{C}) = \frac{1}{\sqrt{(2\pi)^N \det \mathbf{C}}} e^{-\frac{1}{2}(\mathbf{u}-\mathbf{v})^T \mathbf{C}^{-1} (\mathbf{u}-\mathbf{v})}. \tag{4.16}$$

Consider that TOAs follow a mixture of M Gaussian distributions (that is, a Gaussian Mixture Model — GMM) with weights $w_1, \cdots, w_M$, covariance matrices $\mathbf{C}_1, \cdots, \mathbf{C}_M$ and

means $\mathbf{v}_1, \cdots, \mathbf{v}_M$ given by (4.11):

$$f(\mathbf{u}; x, y, t) = \sum_{m=1}^{M} w_m \mathcal{N}(\mathbf{u}; \mathbf{v}_m, \mathbf{C}_m), \qquad \mathbf{v}_m = \mathbf{b}_m + \tau(x, y) + t\mathbf{1}, \tag{4.17}$$

where

$$\tau(x, y) = \begin{bmatrix} \tau_1(x, y) \\ \tau_2(x, y) \\ \vdots \\ \tau_M(x, y) \end{bmatrix}. \tag{4.18}$$

We assume that the mixture components do not overlap, that is, we assume that for each $\mathbf{u}$ there are $M-1$ mixture components that are approximately zero when calculated at the point $\mathbf{u}$, thus $f(\mathbf{u}; x, y, t)$ can be approximated by only one mixture component:

$$f(\mathbf{u}; x, y, t) \approx \mathcal{N}(\mathbf{u}; \mathbf{v}_m, \mathbf{C}_m), \qquad \text{for some } m. \tag{4.19}$$

Let $\mathcal{S}_1, \mathcal{S}_2, \cdots, \mathcal{S}_M$ be a partition on $\mathbb{R}^N$ such that the m-th mixture component is different than zero for $\mathbf{u} \in \mathcal{S}_m$ and approximately zero for $\mathbf{u} \notin \mathcal{S}_m$ (that is, each Gaussian mixture component lies in a single set $\mathcal{S}_m$):

$$\mathcal{N}(\mathbf{u}; \mathbf{v}_k, \mathbf{C}_k) \approx 0 \quad \text{for } \mathbf{u} \in \mathcal{S}_\ell, \quad \ell \neq k, \tag{4.20}$$

Figure 27 shown an illustration of $f(\mathbf{u}; x, y, t)$ for only one sensor and the intervals $\mathcal{S}_1, \cdots, \mathcal{S}_M$.

The definition of the partition $\mathcal{S}_1, \cdots, \mathcal{S}_M$ allows us to rewrite (4.19) defining m explicitly:

$$f(\mathbf{u}; x, y, t) \approx \mathcal{N}(\mathbf{u}; \mathbf{v}_m, \mathbf{C}_m), \qquad m = \{k | \mathbf{u} \in \mathcal{S}_k\}. \tag{4.21}$$

The hypothesis of disjoint Gaussian distributions eases the calculation of the parameters of the GMM. Under this hypothesis, $w_m = \mathbb{P}\{\mathbf{u} \in \mathcal{S}_m\}$ is the probability of $\mathbf{u}$ be in the interval $\mathcal{S}_m$, $\mathbf{b}_m = \mathbb{E}\{\mathbf{u} - t\mathbf{1} - \tau(x, y) | \mathbf{u} \in \mathcal{S}_m\}$ is the TOA bias given that $\mathbf{u} \in \mathcal{S}_m$, $\mathbf{C}_m = \text{cov}(\mathbf{u} | \mathbf{u} \in \mathcal{S}_m)$ is the covariance matrix of $\mathbf{u}$ given that it belongs to $\mathcal{S}_m$ and $\mathbf{v}_m = \mathbb{E}\{\mathbf{u} | \mathbf{u} \in \mathcal{S}_m\}$.

The maximum likelihood estimator for x, y and t is obtained by maximizing (4.21), or equivalently, its logarithm:

$$\ln\left(f(\mathbf{u}; x, y, t)\right) = \left(\ln(w_m) - \ln(\sqrt{(2\pi)^N |\mathbf{C}_m|}) - \frac{1}{2}(\mathbf{u} - \mathbf{v}_m)^T \mathbf{C}_m^{-1} (\mathbf{u} - \mathbf{v}_m)\right). \tag{4.22}$$

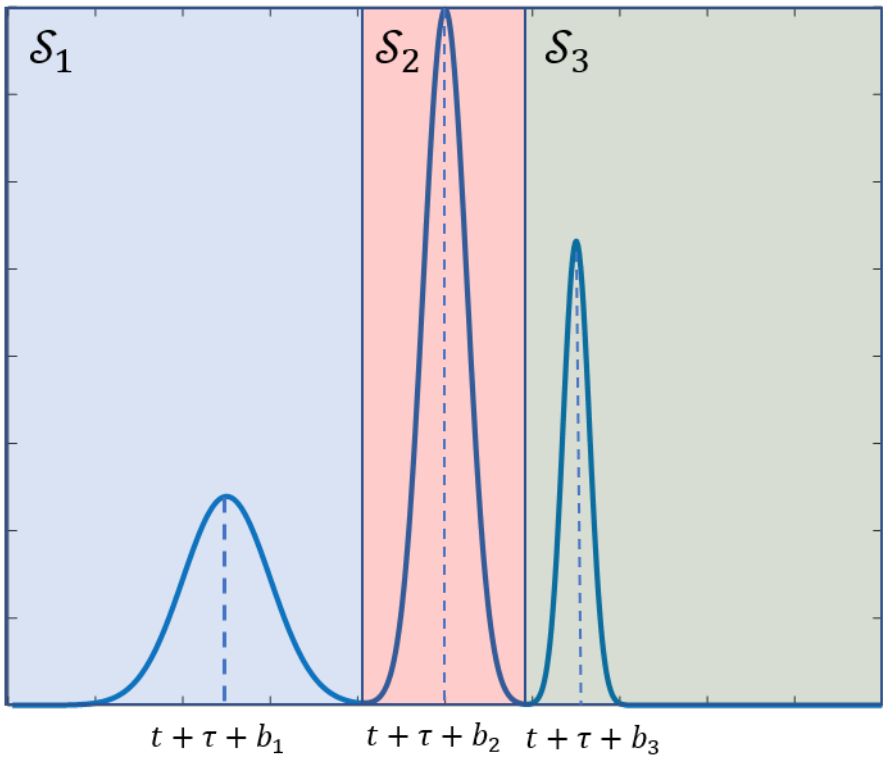

Figure 27: Illustration of $f(\mathbf{u}; x, y, t)$ for only one sensor.

Hence, the cost function that yields the maximum likelihood estimator when minimized is

$$J_{\text{MLE}}(x,y,t) = \min_k \left(-\ln(w_k) + \ln(\sqrt{(2\pi)^N |\mathbf{C}_k|}) + \frac{1}{2}(\mathbf{u}-\mathbf{v}_k)^T \mathbf{C}_k^{-1}(\mathbf{u}-\mathbf{v}_k) \right),$$
$$\mathbf{v}_k = \tau(x,y) + \mathbf{b}_k + t\mathbf{1}. \quad (4.23)$$

The estimate produced by $J_{\text{MLE}}(x,y,t)$ coincides with (4.7) if there is only one component in the mixture (that is, TOAs are Gaussian-distributed) and $\mathbf{G} = \mathbf{C}_k^{-1}$.

4.2 Optimal Estimator and the Cramér-Rao Lower Bound

Suppose we want to estimate a vector of deterministic parameters $\boldsymbol{\theta}$ using a vector of measurements $\mathbf{u}$ whose pdf $f_{\mathbf{u}}(\mathbf{u};\boldsymbol{\theta})$ depends on $\boldsymbol{\theta}$. It is possible to show that the covariance matrix $\mathbf{C}_{\hat{\boldsymbol{\theta}}}$ of any unbiased estimator $\hat{\boldsymbol{\theta}}(\mathbf{u})$ is bounded by the the Cramér-Rao

Lower Bound inequality [56]:

$$\mathbf{C}_{\hat{\boldsymbol{\theta}}} \succeq \mathcal{I}(\boldsymbol{\theta})^{-1}, \tag{4.24}$$

where $\succeq$ is defined as

$$\mathbf{A} \succeq \mathbf{B} \Leftrightarrow (\mathbf{A} - \mathbf{B}) \text{ is positive semi-definite.} \tag{4.25}$$

$\mathcal{I}(\boldsymbol{\theta})$ is the Fisher Information Matrix, defined by

$$[\mathcal{I}(\boldsymbol{\theta})]_{i,j} = -\mathbb{E}\left\{ \frac{\partial^2}{\partial\theta_i \partial\theta_j} \ln(f_{\mathbf{u}}(\mathbf{u};\boldsymbol{\theta})) \;\middle|\; \boldsymbol{\theta} \right\}. \tag{4.26}$$

Note that the Fisher Information Matrix does not depend on the estimator we are using.

Equation (4.24) means that if λ is the k-th largest eigenvalue of $\mathbf{C}_{\hat{\boldsymbol{\theta}}}$ and $\mathbf{b}$ is the k-th smallest eigenvalue of $\mathcal{I}(\boldsymbol{\theta})$, then $\lambda \geq \frac{1}{\mathbf{b}}$. In other words, the eigenvalues of the covariance matrix of any estimator cannot be smaller than a fixed value that depends only on the pdf of the measurement vector. An unbiased estimator is optimal if the eigenvalues of its covariance matrix reach their bounds, i.e. $\mathbf{C}_{\hat{\boldsymbol{\theta}}} = \mathcal{I}(\boldsymbol{\theta})^{-1}$.

4.3 Deriving the Optimal Source Position Estimator

Define the cost functions for $k = 1, 2, \cdots, M$:

$$J_k(x, y, t) = \frac{1}{2}(\mathbf{u} - \mathbf{v}_k)^T \mathbf{C}_k^{-1}(\mathbf{u} - \mathbf{v}_k), \qquad \mathbf{v}_k = \tau(x, y) + \mathbf{b}_k + t(x, y)\mathbf{1}, \tag{4.27}$$

where

$$t(x, y) = \frac{1}{N}\mathbf{1}^T\mathbf{u} - \frac{1}{N}\mathbf{1}^T(\mathbf{b}_k + \tau). \tag{4.28}$$

Each one of these M cost functions is a version of (4.15) using a different value for $\mathbf{C}$ and $\mathbf{b}$ that is associated to a component of the Gaussian Mixture (recall that M is the number of disjoint intervals $\mathcal{S}_1, \cdots, \mathcal{S}_M$, that is, the number of mixture components).

Let us define the cost function

$$J(x, y) = J_m(x, y), \qquad m = \{k : \mathbf{u} \in \mathcal{S}_k\}. \tag{4.29}$$

In this section, we show that that minimizing (4.29) yields a nearly-optimal unbiased estimate for the source position. In order to prove the optimality of (4.29), we assume that m is correctly picked, but we show how to pick m using the signals received by the sensors in Section 4.3.3.

Note that the Maximum Likelihood Estimator can be written in a form similar to (4.29), but using a different value for m:

$$J_{\text{MLE}}(x,y) \;=\; J_m(x,y), \qquad m \;=\; \arg\min_k \left(-\ln(w_k) + \ln(\sqrt{(2\pi)^N |\mathbf{C}_k|}) + J_k(x,y) \right). \tag{4.30}$$

Hence, (4.29) may coincide with the MLE if they use the same value for m, but they are different estimators in general. However, their estimates always coincide if the noise level is low enough so that the number of components in the Gaussian mixture is $M = 1$, as in this case both estimators always pick $m = 1$.

Since we want to determine if the estimator $\hat{\mathbf{x}} = \arg\min_{\mathbf{x}} J(\mathbf{x})$ is optimal (where $J(x,y)$ is given by (4.29)), we need to calculate its covariance matrix and also the Fisher Information Matrix.

4.3.1 Obtaining the Fisher Information Matrix

Let us denote the actual source position as $\mathbf{x}^*$ and its instant of emission as t^*. As derived before, the log-likelihood function $\mathcal{L}(\mathbf{x}^*, t^*) = \log(f(\mathbf{u}; \mathbf{x}^*, t^*))$ is

$$\mathcal{L}(\mathbf{x}^*, t^*) = \ln\left(\frac{w_m}{\sqrt{|2\pi \mathbf{C}_m|}} \right) - \frac{1}{2}(\mathbf{u} - \tau - \mathbf{b}_m - t^*\mathbf{1})^T \mathbf{C}_m^{-1} (\mathbf{u} - \tau - \mathbf{b}_m - t^*\mathbf{1}). \tag{4.31}$$

Defining $\bar{\tau}_m = \tau + \mathbf{b}_m$, the first and second derivatives of $\mathcal{L}(\mathbf{x}^*, t^*)$ are

$$\mathcal{L}_x = \bar{\tau}_{m,x}^T \mathbf{C}_m^{-1} (\mathbf{u} - \bar{\tau}_m - t^*\mathbf{1}), \tag{4.32}$$

$$\mathcal{L}_y = \bar{\tau}_{m,y}^T \mathbf{C}_m^{-1} (\mathbf{u} - \bar{\tau}_m - t^*\mathbf{1}), \tag{4.33}$$

$$\mathcal{L}_t = \mathbf{1}^T \mathbf{C}_m^{-1} (\mathbf{u} - \bar{\tau}_m - t^*\mathbf{1}), \tag{4.34}$$

$$\mathcal{L}_{xx} = \bar{\tau}_{m,xx}^T \mathbf{C}_m^{-1} (\mathbf{u} - \bar{\tau}_m - t^*\mathbf{1}) - \bar{\tau}_{m,x}^T \mathbf{C}^{-1} \bar{\tau}_{m,x}, \tag{4.35}$$

$$\mathcal{L}_{yy} = \bar{\tau}_{m,yy}^T \mathbf{C}_m^{-1} (\mathbf{u} - \bar{\tau}_m - t^*\mathbf{1}) - \bar{\tau}_{m,y}^T \mathbf{C}^{-1} \bar{\tau}_{m,y}, \tag{4.36}$$

$$\mathcal{L}_{tt} = -\mathbf{1}^T \mathbf{C}_m^{-1} \mathbf{1}, \tag{4.37}$$

$$\mathcal{L}_{xy} = \bar{\tau}_{m,xy}^T \mathbf{C}_m^{-1} (\mathbf{u} - \bar{\tau}_m - t^*\mathbf{1}) - \bar{\tau}_{m,x}^T \mathbf{C}^{-1} \bar{\tau}_{m,y}, \tag{4.38}$$

$$\mathcal{L}_{xt} = -\mathbf{1}^T \mathbf{C}_m^{-1} \bar{\tau}_{m,x}, \tag{4.39}$$

$$\mathcal{L}_{yt} = -\mathbf{1}^T \mathbf{C}_m^{-1} \bar{\tau}_{m,y}. \tag{4.40}$$

The Fisher Information Matrix is given by

$$\mathcal{I}(\mathbf{x}^*, t^*) = -\mathbb{E}\left\{\begin{bmatrix}\mathcal{L}_{xx} & \mathcal{L}_{xy} & \mathcal{L}_{xt}\\ \mathcal{L}_{xy} & \mathcal{L}_{yy} & \mathcal{L}_{yt}\\ \mathcal{L}_{xt} & \mathcal{L}_{yt} & \mathcal{L}_{tt}\end{bmatrix}\right\} = \sum_{k=1}^{M} w_k \mathbb{E}\left\{\begin{bmatrix}\mathcal{L}_{xx} & \mathcal{L}_{xy} & \mathcal{L}_{xt}\\ \mathcal{L}_{xy} & \mathcal{L}_{yy} & \mathcal{L}_{yt}\\ \mathcal{L}_{xt} & \mathcal{L}_{yt} & \mathcal{L}_{tt}\end{bmatrix} \;\middle|\; \mathbf{u} \in \mathcal{S}_k\right\}. \quad (4.41)$$

Each conditional expectation being summed in (4.41) can be computed by assuming $\mathbf{u}$ follows a Gaussian distribution with mean $\mathbf{v}_k = \tau_k + \mathbf{b}_k - t^*\mathbf{1}$ and covariance matrix $\mathbf{C}_k$. Applying each conditional expectation to equations (4.35) to (4.40) and substituting the results in (4.41), we obtain

$$\mathcal{I}(\mathbf{x}^*, t^*) = \sum_{k=1}^{M} w_k \begin{bmatrix}\bar{\tau}_{k,x}^T \mathbf{C}_k^{-1} \bar{\tau}_{k,x} & \bar{\tau}_{k,x}^T \mathbf{C}_k^{-1} \tau_{k,y} & \mathbf{1}^T \mathbf{C}_k^{-1} \bar{\tau}_{k,x}\\ \bar{\tau}_{k,y}^T \mathbf{C}_k^{-1} \bar{\tau}_{k,y} & \bar{\tau}_{k,x}^T \mathbf{C}_k^{-1} \bar{\tau}_{k,y} & \mathbf{1}^T \mathbf{C}_k^{-1} \bar{\tau}_{k,y}\\ \mathbf{1}^T \mathbf{C}_k^{-1} \bar{\tau}_{k,x} & \mathbf{1}^T \mathbf{C}_k^{-1} \bar{\tau}_{k,y} & \mathbf{1}^T \mathbf{C}_k^{-1} \mathbf{1}.\end{bmatrix} \quad (4.42)$$

4.3.2 Covariance Matrix

In order to calculate the covariance matrix of the estimator $(\hat{x}, \hat{y}) = \arg\min_{x,y} J(x, y)$, where $J(x, y)$ is given by (4.29), we will approximate $J(x, y)$ by its second-order Taylor polynomial around the source position $\mathbf{x}^*$, given by

$$J(\mathbf{x}) \approx J(\mathbf{x}^*) + \nabla J(\mathbf{x}^*)(\mathbf{x} - \mathbf{x}^*) + \frac{1}{2}(\mathbf{x} - \mathbf{x}^*)^T \mathbf{H}(\mathbf{x}^*)(\mathbf{x} - \mathbf{x}^*). \quad (4.43)$$

The estimated position $\hat{\mathbf{x}}$ is calculated by setting $\nabla J(\hat{\mathbf{x}}) = 0$. Since $\nabla J(\mathbf{x}) \approx \nabla J(\mathbf{x}^*) + \mathbf{H}(\mathbf{x}^*)(\mathbf{x} - \mathbf{x}^*)$, we have

$$\hat{\mathbf{x}} - \mathbf{x}^* \approx -\mathbf{H}^{-1}(\mathbf{x}^*) \nabla J(\mathbf{x}^*), \quad (4.44)$$

thus

$$(\hat{\mathbf{x}} - \mathbf{x}^*)(\hat{\mathbf{x}} - \mathbf{x}^*)^T \approx \mathbf{H}^{-1}(\mathbf{x}^*) \nabla J(\mathbf{x}^*) \nabla J(\mathbf{x}^*)^T \mathbf{H}^{-1}(\mathbf{x}^*). \quad (4.45)$$

We now use the following approximations:

$$\mathbb{E}\{\hat{\mathbf{x}} - \mathbf{x}^*\} \approx -\mathbb{E}\{\mathbf{H}(\mathbf{x}^*)\}^{-1} \mathbb{E}\{\nabla J(\mathbf{x}^*)\}, \quad (4.46)$$

$$\mathbb{E}\{(\hat{\mathbf{x}} - \mathbf{x}^*)(\hat{\mathbf{x}} - \mathbf{x}^*)^T\} \approx \mathbb{E}\{\mathbf{H}(\mathbf{x}^*)\}^{-1} \mathbb{E}\{\nabla J(\mathbf{x}^*) \nabla J(\mathbf{x}^*)^T\} \mathbb{E}\{\mathbf{H}(\mathbf{x}^*)\}^{-1}. \quad (4.47)$$

These approximations are also used in [54, 57] to derive the optimal estimator for the source localization problem in the scenario where the instant the source emits a signal is known, as in radar applications.

The partial derivatives of $J(x, y)$ are needed to compute the expectation of $\mathbf{H}(\mathbf{x}^*)$ and

$\nabla J(\mathbf{x}^*)\nabla J(\mathbf{x}^*)^T$:

$$\frac{\partial J}{\partial x} = 2\mathbf{v}_{m,x}^T \mathbf{C}_m^{-1}(\mathbf{v}_m - \mathbf{u}), \tag{4.48}$$

$$\frac{\partial J}{\partial y} = 2\mathbf{v}_{m,y}^T \mathbf{C}_m^{-1}(\mathbf{v}_m - \mathbf{u}), \tag{4.49}$$

$$\frac{\partial^2 J}{\partial x^2} = 2\mathbf{v}_{m,xx}^T \mathbf{C}_m^{-1}(\mathbf{v}_m - \mathbf{u}) + 2\mathbf{v}_{m,x}^T \mathbf{C}_m^{-1}\mathbf{v}_{m,x}, \tag{4.50}$$

$$\frac{\partial^2 J}{\partial y^2} = 2\mathbf{v}_{m,yy}^T \mathbf{C}_m^{-1}(\mathbf{v}_m - \mathbf{u}) + 2\mathbf{v}_{m,y}^T \mathbf{C}_m^{-1}\mathbf{v}_{m,y}, \tag{4.51}$$

$$\frac{\partial^2 J}{\partial x \partial y} = 2\mathbf{v}_{m,xy}^T \mathbf{C}_m^{-1}(\mathbf{v}_m - \mathbf{u}) + 2\mathbf{v}_{m,x}^T \mathbf{C}_m^{-1}\mathbf{v}_{m,y}. \tag{4.52}$$

Therefore,

$$\nabla J(\mathbf{x}^*) = 2\begin{bmatrix} \mathbf{v}_{m,x}^T \mathbf{C}_m^{-1}(\mathbf{v}_m - \mathbf{u}) \\ \mathbf{v}_{m,y}^T \mathbf{C}_m^{-1}(\mathbf{v}_m - \mathbf{u}) \end{bmatrix}, \tag{4.53}$$

$$\mathbb{E}\{\nabla J(\mathbf{x}^*)\} = 2\sum_{k=1}^{M} \mathbb{E}\left\{ \begin{bmatrix} \mathbf{v}_{k,x}^T \mathbf{C}_k^{-1}(\mathbf{v}_k - \mathbf{u}) \\ \mathbf{v}_{k,y}^T \mathbf{C}_k^{-1}(\mathbf{v}_k - \mathbf{u}) \end{bmatrix} \;\middle|\; \mathbf{u} \in \mathcal{S}_k \right\}, \tag{4.54}$$

$$\begin{aligned} \mathbb{E}\{\nabla J(\mathbf{x}^*)\nabla J(\mathbf{x}^*)^T\} &= \sum_{k=1}^{M} w_k \mathbb{E}\{\nabla J(\mathbf{x}^*)\nabla J(\mathbf{x}^*)^T \mid \mathbf{u} \in \mathcal{S}_k\} \\ &= 4\sum_{k=1}^{M} w_k \begin{bmatrix} \mathbf{v}_{k,x}^T \mathbf{C}_k^{-1}\mathbf{v}_{k,x} & \mathbf{v}_{k,x}^T \mathbf{C}_k^{-1}\mathbf{v}_{k,y} \\ \mathbf{v}_{k,x}^T \mathbf{C}_k^{-1}\mathbf{v}_{k,y} & \mathbf{v}_{k,y}^T \mathbf{C}_k^{-1}\mathbf{v}_{k,y} \end{bmatrix} \end{aligned} \tag{4.55}$$

and

$$\mathbb{E}\{\mathbf{H}(\mathbf{x}^*)\} = 2\sum_{k=1}^{M} w_k \begin{bmatrix} \mathbf{v}_{k,x}^T \mathbf{C}_k^{-1}\mathbf{v}_{k,x} & \mathbf{v}_{k,x}^T \mathbf{C}_k^{-1}\mathbf{v}_{k,y} \\ \mathbf{v}_{k,x}^T \mathbf{C}_k^{-1}\mathbf{v}_{k,y} & \mathbf{v}_{k,y}^T \mathbf{C}_k^{-1}\mathbf{v}_{k,y} \end{bmatrix}. \tag{4.56}$$

As $\mathbb{E}\{\mathbf{u}|\mathbf{u} \in \mathcal{S}_k\} = \mathbf{v}_k$, we have from (4.53) that $\mathbb{E}\{\nabla J(\mathbf{x}^*)\} = \mathbf{0}$, thus we conclude from (4.46) that the position estimator is approximately unbiased:

$$\mathbb{E}\{\hat{\mathbf{x}} - \mathbf{x}^*\} \approx -\mathbb{E}\{\mathbf{H}(\mathbf{x}^*)\}^{-1}\mathbb{E}\{\nabla J(\mathbf{x}^*)\} = \mathbf{0}, \tag{4.57}$$

In order to shorten the next expressions, let us define the matrix

$$\mathbf{A}_k = \begin{bmatrix} \mathbf{v}_{k,x}^T \mathbf{C}_k^{-1}\mathbf{v}_{k,x} & \mathbf{v}_{k,x}^T \mathbf{C}_k^{-1}\mathbf{v}_{k,y} \\ \mathbf{v}_{k,x}^T \mathbf{C}_k^{-1}\mathbf{v}_{k,y} & \mathbf{v}_{k,y}^T \mathbf{C}_k^{-1}\mathbf{v}_{k,y} \end{bmatrix}, \tag{4.58}$$

such that $\mathbb{E}\{\mathbf{H}(\mathbf{x}^*)\} = 2\sum_{k=1}^{M} w_k \mathbf{A}_k$ and $\mathbb{E}\{\nabla J(\mathbf{x}^*)\nabla J(\mathbf{x}^*)^T\} = 4\sum_{k=1}^{M} w_k \mathbf{A}_k$.

From (4.47), the covariance matrix $\mathbf{C}_\mathbf{x} = \mathbb{E}\{(\hat{\mathbf{x}} - \mathbf{x}^*)(\hat{\mathbf{x}} - \mathbf{x}^*)^T\}$ of the estimated

position is

$$\mathbf{C}_{\mathbf{x}} \approx \left(\sum_{k=1}^{M} w_k \mathbf{A}_k\right)^{-1} \left(\sum_{k=1}^{M} w_k \mathbf{A}_k\right) \left(\sum_{k=1}^{M} w_k \mathbf{A}_k\right)^{-1} = \left(\sum_{k=1}^{M} w_k \mathbf{A}_k\right)^{-1}. \tag{4.59}$$

Since $\mathbf{v}_k = \bar{\tau}_k + t\mathbf{1}$, we have $\mathbf{v}_{k,x} = \bar{\tau}_{k,x}$ and $\mathbf{v}_{k,y} = \bar{\tau}_{k,y}$. Thus, (4.59) can be written as

$$\mathbf{C}_{\mathbf{x}} \approx \left(\sum_{k=1}^{M} w_k \begin{bmatrix} \bar{\tau}_{k,x}^T \mathbf{C}_k^{-1} \bar{\tau}_{k,x} & \bar{\tau}_{k,x}^T \mathbf{C}_k^{-1} \bar{\tau}_{k,y} \\ \bar{\tau}_{k,y}^T \mathbf{C}_k^{-1} \bar{\tau}_{k,y} & \bar{\tau}_{k,x}^T \mathbf{C}_k^{-1} \bar{\tau}_{k,y} \end{bmatrix}\right)^{-1}, \tag{4.60}$$

which is the inverse of the submatrix of the Fisher Information Matrix (4.42) that contains only the spatial components. Hence, (4.29) is the optimal TOA-based source position estimator.

It must be highlighted that we made the following hypotheses to show that this estimator is optimal:

1. The noise variance is not very high, so that the Taylor approximation (4.43) works. This is also necessary to guarantee that the estimator is approximately unbiased.
2. The parameters of the TOA pdf $w_k, \mathbf{b}_k$ and $\mathbf{C}_k$ are known.

Hence, (4.29) may not be optimal if these conditions are not satisfied.

Note that any modified cost function $J_{\text{mod}}(x, y) = kJ(x, y)$ also yields an optimal estimator for any k because multiplying $J(x, y)$ by a constant does not affect its critical points.

4.3.3 Implementation of the Optimal Estimator

In order to show that (4.29) is optimal, we assumed that the parameters of the Gaussian mixture $(\mathbf{b}_1, \cdots, \mathbf{b}_M)$, $(\mathbf{C}_1, \cdots, \mathbf{C}_M)$ and $(w_1, \cdots, w_M)$ are known, and we also assumed that m is such that $\mathbf{u} \in \mathcal{S}_m$, but these parameters must be estimated in practical problems. In this section, we describe a procedure to choose m and to estimate the GMM parameters using the signals received by the sensors. To ease the comprehension our method, we assume that the signals are corrupted by white noise and that the noises at different sensors are independent.

Given the signals $r_1[n], \cdots, r_N[n]$ received by the N sensors, we estimate the TOA pmf for each sensor using the expression derived in Chapter 2, but we substituted the

noiseless waveform by the noisy hit:

$$p[n] = (1 - \Phi[n]) \prod_{k=0}^{n-1} \Phi[k], \qquad \Phi[n] = F_W(K - |r_i[n]|). \tag{4.61}$$

The obtained pdf is not exactly a Gaussian mixture, but we need to extract the GMM parameters from it. Thus, we convert the pmf $p[n]$ to a pdf $p(t) = \frac{1}{T_s} p[\text{round}(t/T_s)]$ and then we fit $p(t)$ into a Gaussian Mixture Model, as done in Section 2.6 from Chapter 2. Then, the means $\mu_{i,1}, \cdots, \mu_{i,M}$, variances $\sigma^2_{i,1}, \cdots, \sigma^2_{i,M}$ and weights $w_{i,1}, \cdots, w_{i,M}$ of each mixture component are extracted for each sensor $i = 1, 2, \cdots, N$.

Now, we have to pick the index m. If there are M_i mixture components at the i-th sensor, there are $M = M_1 M_2 \cdots M_N$ possible values for m. Since we are assuming white noise, we use a simplified notation: Instead of choosing m from M possibilities, we can choose which mixture to use from each sensor individually because TOAs are independent. This way, we have to choose an index m_i for each sensor that ranges from 1 to M_i.

m_i can be picked by extracting the sets $\mathcal{S}_1, \cdots, \mathcal{S}_{M_i}$ from the fitted pdf and finding the set to which m_i belongs. This is equivalent to finding the Gaussian component that most contributes to the fitted pdf:

$$m_i = \arg\max_k \frac{w_k}{\sqrt{2\pi\sigma_k^2}} e^{-\frac{(u_i - \mu_k)}{2\sigma_k^2}}. \tag{4.62}$$

Finally, we must extract the TOA bias for the i-th sensor b_i from the mean of the chosen GMM component μ_{m_i}. Ideally, μ_{m_i} and b_{m_i} would be related by

$$\mu_{m_i} = \tau(x^*, y^*) + t^* + b_{m_i}, \tag{4.63}$$

but we do not know $\tau(x^*, y^*)$ or t^*. We estimate b_i with the naive assumption that $\tau(x^*, y^*) + t^*$ is the first instant where $p[n]$ crosses a very small fixed threshold K_p, that is, the instant where it assumes a non-negligible value. Hence, b_i is estimated as

$$b_i = \mu_{m_i} - \bar{n} T_s, \qquad \bar{n} = \min_n \{n : \ p[n] \geq K_{\text{pdf}}\}. \tag{4.64}$$

Therefore, the source position estimated by our proposed estimator is

$$(\hat{x}, \hat{y}) = \arg\min_{x,y} (\mathbf{u} - \mathbf{v})^T \mathbf{C}^{-1} (\mathbf{u} - \mathbf{v}), \qquad \mathbf{v} = \tau(x, y) + \mathbf{b} + t(x, y)\mathbf{1}, \tag{4.65}$$

where $t(x,y) = \frac{1}{N}\mathbf{1}^T\mathbf{u} - \frac{1}{N}\mathbf{1}^T(\mathbf{b}+\tau)$, $\mathbf{b} = \begin{bmatrix} b_1 \\ \vdots \\ b_N \end{bmatrix}$ and $\mathbf{C} = \text{diag}(\sigma^2_{m_1}, \sigma^2_{m_2}, \cdots, \sigma^2_{m_N})$.

The proposed algorithm is summarized in Algorithm 1.

Note that our method requires the signals sampled by sensors $r_i[n]$ to localize the source, thus it does not use only TOAs as the cost functions J_{TOA} and J_{TDOA}. Storing waveforms may be an issue for long acoustic emission tests that last weeks or months, as the waveforms may require an enormous storage capacity. However, it is possible to use our method without the need to store the whole waveforms because it uses $r_i[n]$ only to calculate $p[n] = (1-\Phi[n])\prod_{k=0}^{n-1}\Phi[k]$, which can be computed recursively: Defining $Q[n] = \prod_{k=0}^{n-1}\Phi[k]$, we have

$$p[n] = (1-\Phi[n])Q[n], \qquad Q[n] = Q[n-1]\Phi[n-1]. \tag{4.66}$$

Since the computational cost of computing $\Phi[n] = F_W(K - |r_i[n]|)$ is small, it is possible to compute $p[n]$ in real time and discard the signals $r_1[n], \cdots, r_N[n]$ instead of storing them. Storing $p[n]$ instead of the signals is much more efficient because $p[n]$ assumes a non-negligible value for only a small number of samples, thus it is possible to store only these non-negligible samples. Therefore, our method does not present the problem of storing a huge number of waveforms in long acoustic emission tests as the methods presented in Chapter 5.

Algorithm 1: The proposed optimal TOA-based source position estimator.

Data: TOAs $u_1, \cdots, u_N$; Very small threshold K_p; Signals sampled by sensors $r_1[n], \cdots, r_N[n]$; Noise cdf $F_W(w)$; Fixed threshold K; Sampling period T_s;

Result: Estimated source position $(\hat{x}, \hat{y})$

for *i=1:N* **do**

Estimate the TOA pmf as

$$p[n] = (1 - \Phi[n]) \prod_{k=0}^{n-1} \Phi[k], \qquad \Phi[k] = F_W(K - |r_i[n]|).$$

Fit a Gaussian Mixture Model to the function $p(t) = \frac{1}{T_s} p[\text{round}(t/T_s)]$, obtaining the means $\mu_{i,1}, \cdots, \mu_{i,M}$, variances $\sigma^2_{i,1}, \cdots, \sigma^2_{i,M}$ and weights $w_{i,1}, \cdots, w_{i,M}$ for each mixture component;

Set m_i as

$$m_i = \arg\max_{\ell} \frac{w_\ell}{\sqrt{2\pi\sigma^2_\ell}} e^{-\frac{(u_i - \mu_\ell)^2}{2\sigma^2_\ell}}.$$

Calculate $\bar{n}$ as the first instant where $p[n]$ crosses a very small threshold K_p and set b_i as

$$b_i = \mu_{m_i} - \bar{n} T_s, \qquad \bar{n} = \min_n \{n : \ p[n] \geq K_p\}.$$

Set $\mathbf{C} = \text{diag}(\sigma^2_{m_1}, \sigma^2_{m_2}, \cdots, \sigma^2_{m_N})$;

The estimated source position $(\hat{x}, \hat{y})$ is

$$(\hat{x}, \hat{y}) = \arg\min_{x,y} (\mathbf{u} - \mathbf{v})^T \mathbf{C}^{-1} (\mathbf{u} - \mathbf{v}), \qquad \mathbf{v} = \tau(x, y) + \mathbf{b} + t(x, y)\mathbf{1},$$

where $t(x, y) = \frac{1}{N} \mathbf{1}^T \mathbf{u} - \frac{1}{N} \mathbf{1}^T (\mathbf{b} + \tau)$.

4.3.4 Special case: Unbiased i.i.d. Gaussian TOAs

Consider that the noise level is small enough so that TOAs can be approximated by a Gaussian distribution, in which case $M = 1$. If TOAs are unbiased and i.i.d. random variables, then their covariance matrix is

$$\mathbf{C}_1 = \sigma^2 \mathbf{I}, \tag{4.67}$$

thus

$$\mathbf{C}_1^{-1} = \frac{1}{\sigma^2} \mathbf{I}. \tag{4.68}$$

In this case, $\mathbf{C}_1^{-1}$ is proportional to $\mathbf{G}$ when $J(x,y) = J_{TOA}(x,y)$. Thus, for small noise, $J_{TOA}(x,y)$ is the optimal cost function when the TOAs are unbiased and independent Gaussian random variables with the same variance, which would happen if all sensors are at approximately the same distance from the source.

4.4 Simulations

In this section, we validate the derivations of this chapter through simulations. First, we generate unbiased iid Gaussian TOAs artificially at different source positions using two different noise variances to verify in which conditions J_{TOA} is the optimal cost function.

Then, we test our method for a fixed source position and different SNRs in three different scenarios: In the first case, we generate artificial TOAs following a Gaussian Mixture Distribution and estimate the source position using the actual GMM parameters in order to validate the optimality of our estimator in the case where TOAs follow a GMM. In the second scenario, we tested our method using noisy hits and parameters estimated from the noisy signals, and in the third case we applied a lowpass filter to the noisy hits before extracting parameters to improve the performance of the optimal estimator. In the three scenarios, our TOA debiasing method described in Chapter 2 was used.

Finally, we compare the performance of the presented localization algorithm using biased TOAs and TOAs debiased with our method to show that debiasing TOAs reduces the MSE.

4.4.1 Gaussian TOAs generated at different source positions

We positioned 4 sensors at the coordinates $(0,0), (0,1), (1,0)$ and $(1,1)$ in order to estimate the position of sources located inside the convex polygon whose vertices are the positions of the sensors (in this case, this polygon is a square). The simulated TOAs were Gaussian random variables with no bias and standard deviation of $1\mu s$. Keeping the y coordinate of the source position fixed and equal to $y = 40$cm, we swept the x coordinate from 0m to 1m. For each position, we calculated the variance of the estimators using 10^5 samples (defining the variance as the trace of the covariance matrix), and then we compared it with the trace of the Fisher information matrix inverse. We also plotted its efficiency as a function of source position, which was calculated as

$$\eta = \frac{\text{tr}\{\mathcal{I}(\mathbf{x}^*)^{-1}\}}{\text{tr}\{\mathbf{C}_\mathbf{x}\}}. \tag{4.69}$$

Note that $\eta = 1$ if the estimator is optimal.

The standard deviation of the estimator and its efficiency are plotted in Figures 28 and 29, respectively, in function of the source position. The variance of the cost function J_{TOA} coincides with the optimal one (denoted by CRLB — Cramér-Rao Lower Bound), and its efficiency is approximately 100% at all source positions (note that the efficiency can slightly surpass 100% for some positions because we are using a finite number of samples to estimate the covariance matrix, and also because the position estimates are not completely unbiased). This is not the case for J_{TDOA}, whose variance is always above the optimal one and whose efficiency is not close to 1 for most source positions.

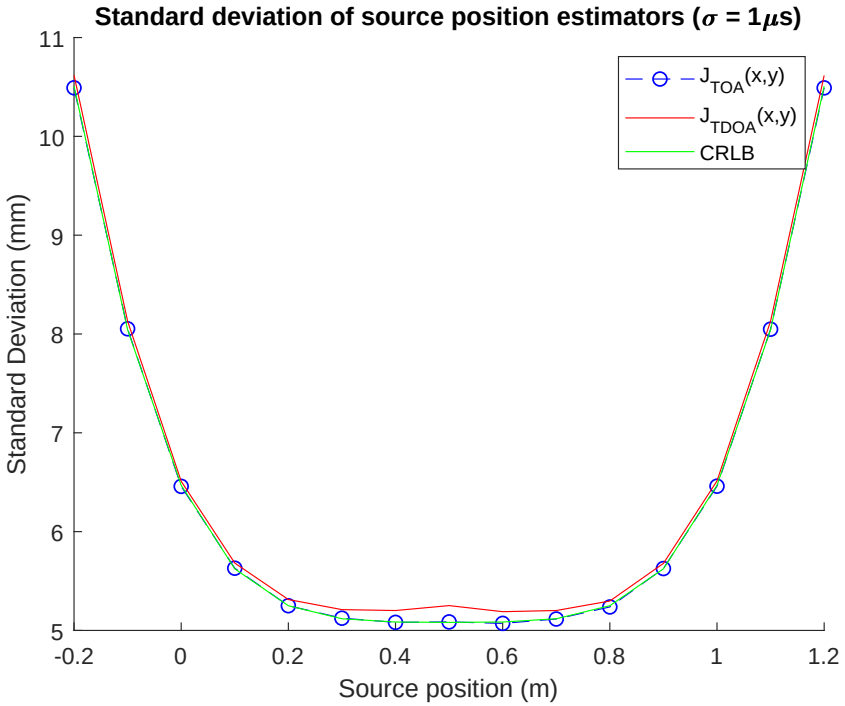

Figure 28: Standard deviation of the source position estimators as a function of source position for $\sigma = 1\mu s$. The horizontal coordinates of the sensors are $x = 0$ and $x = 1$.

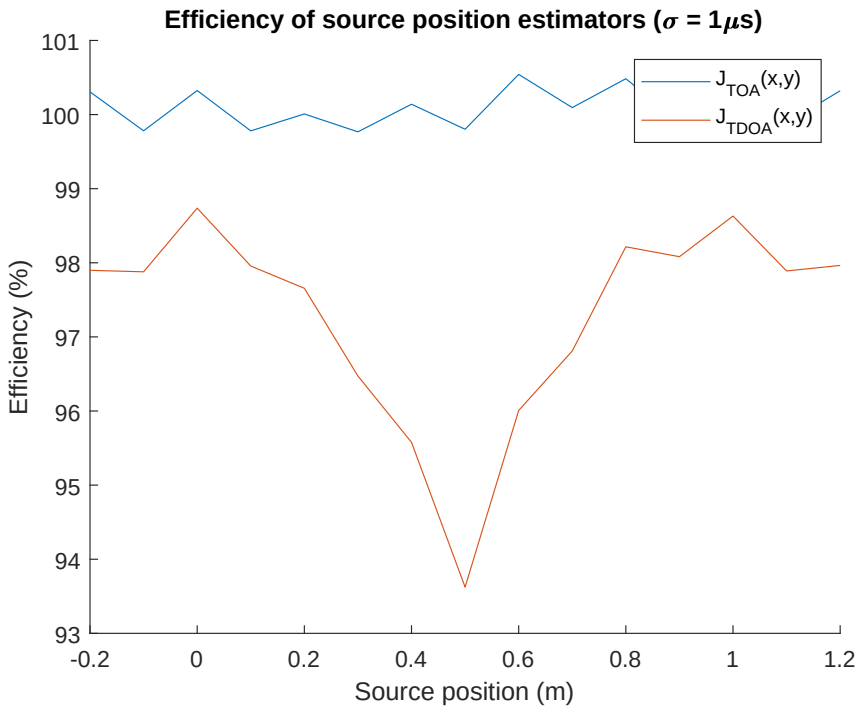

Figure 29: Efficiency of the source position estimators as a function of source position for $\sigma = 1\mu s$. The horizontal coordinates of the sensors are $x = 0$ and $x = 1$.

In the next simulation, we raised the standard deviation to $10\mu s$, and used 10^5 samples to calculate the variance. The results are shown in figures 30 and 31.

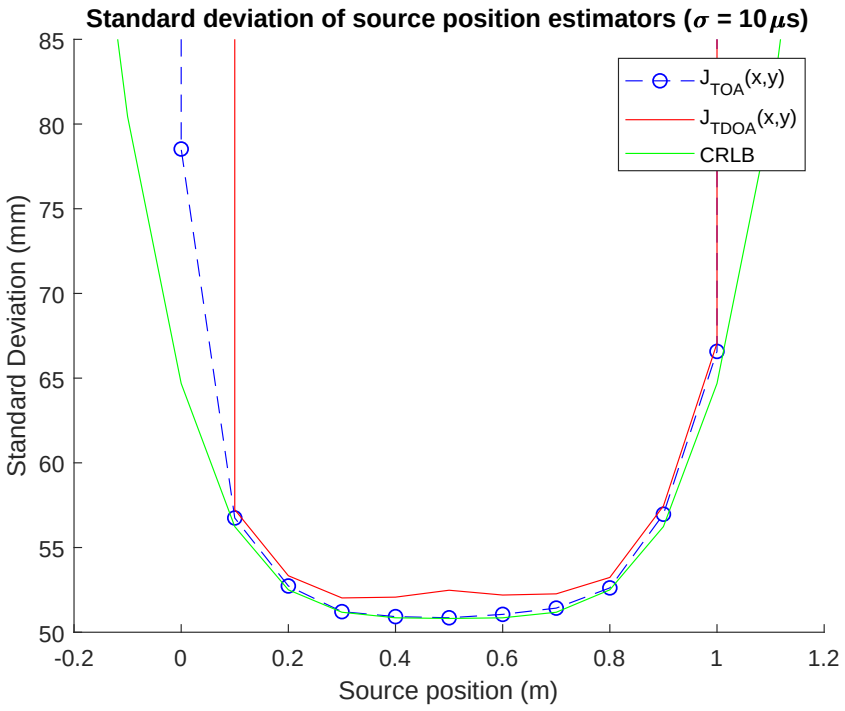

Figure 30: Standard deviation of the source position estimators as a function of source position for $\sigma = 10\mu s$. The horizontal coordinates of the sensors are $x = 0$ and $x = 1$.

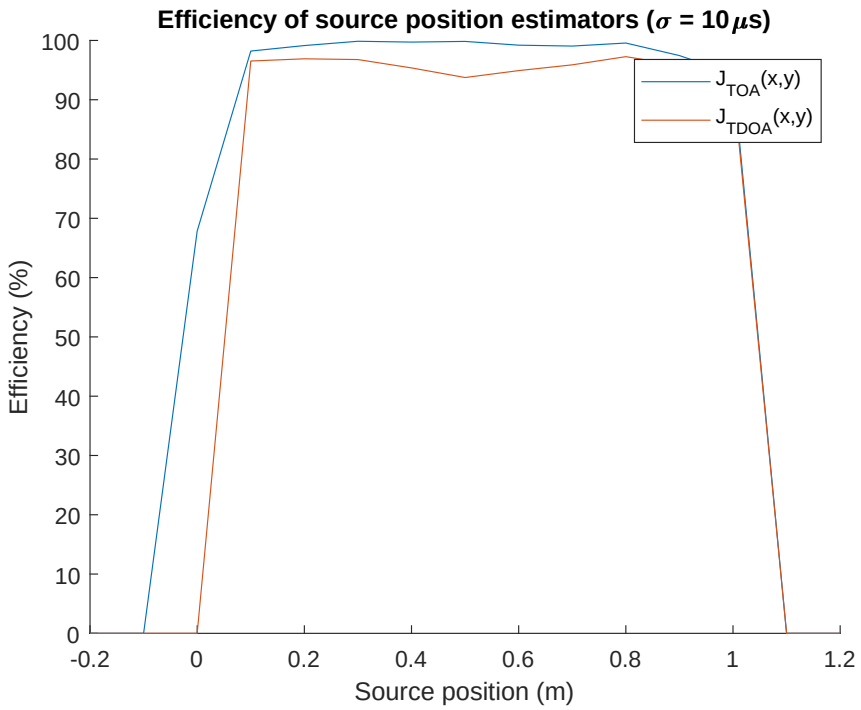

Figure 31: Efficiency of the source position estimators as a function of source position for $\sigma = 10\mu s$. The horizontal coordinates of the sensors are $x = 0$ and $x = 1$.

Figure 31 shows us that J_{TOA} is very close to the optimal one when the source lies inside the region of interest (defined as the convex polygon whose vertexes are the positions of the sensors). However, outside this polygon, J_{TOA} is no longer the optimal cost function because the approximations we did in order to prove the estimator is optimal are not precise in this region. This happens because the approximation $\mathbf{x} \approx \mathbf{x}^* - H^{-1}(\mathbf{x}^*)\nabla J(\mathbf{x}^*)$ does not hold when $\mathbf{x}^*$ is in a region where the concavity of $J(x, y)$ is not approximately constant, and the sensor positions are local maxima of $J(x, y)$. Furthermore, the Hessian oscillates much faster outside the region of interest than inside it, so the approximations (4.46) and (4.47) no longer work.

Moreover, when noisy measurements are used, the estimated position may be in a local but not global minimum of the cost function. Local minima were not considered when we derived the covariance matrix expression, and they would yield a larger MSE than the optimal one and also bias the estimator.

The estimator bias as a function of source position is shown in Figures 32 and 33 for standard deviations $\sigma = 1\mu$s and $\sigma = 10\mu$s, respectively. For $\sigma = 1\mu$s, the bias in the region of interest is approximately 0.02mm, thus it can be neglected. For $\sigma = 10\mu$s, the bias in the region of interest is approximately 1mm while the standard deviation is 5cm, thus the position bias does not interfere much in the MSE at the region of interest (the

bias when the source lies inside the region of interest is negligible). This also shows us that even when unbiased TOAs are used (recall that in this simulation TOAs are unbiased), their variance can still cause a small bias to position estimates since we observed that bias increased with variance. Nevertheless, the bias would be zero if the approximations (4.43) and (4.46) were exact.

For a source outside the region of interest, however, there is a non-negligible bias for both variances because the hypotheses we did to prove that our estimator is unbiased do not hold in this region. In particular, the Hessian of the cost functions are not constant approximately constant for sources located outside the region of interest.

It is important to remark that the sensors are scattered around a region we want to monitor. Although we discussed the performance of our cost function outside the region of interest, the precision of localization algorithms is much more important when the source position is inside the region of interest than when it is outside it. Inside the region of interest, our method presents a very small bias (which is not exactly zero due to the approximations we made) and a variance that is very close to the optimal one.

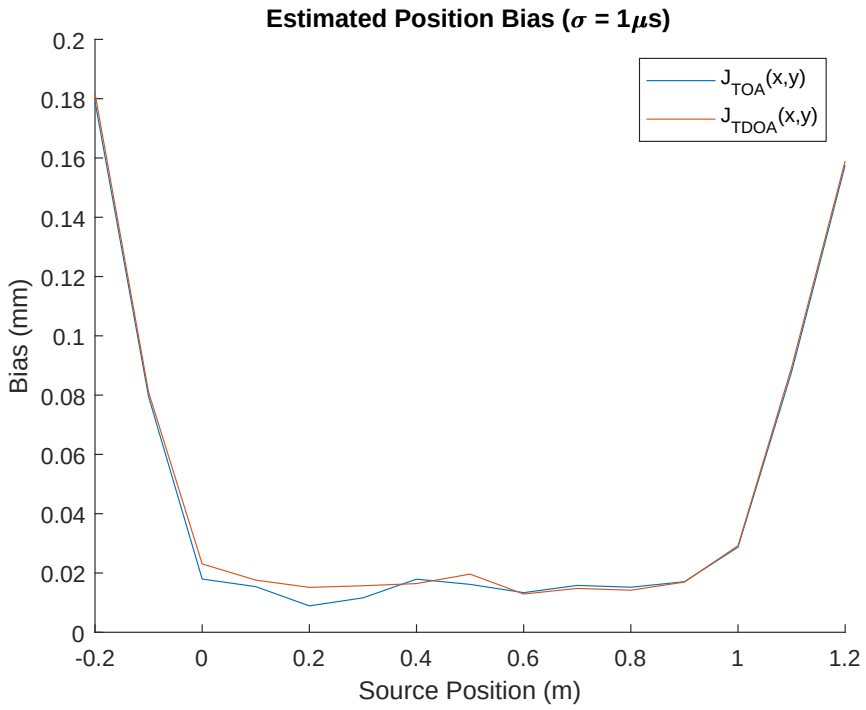

Figure 32: Estimated position bias as a function of source position for $\sigma = 1\mu s$.

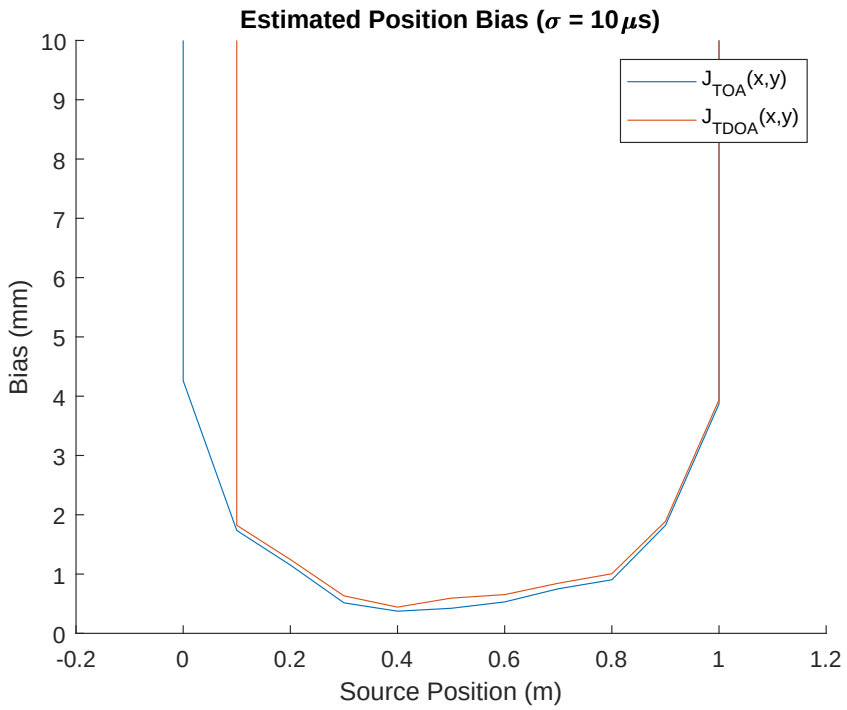

Figure 33: Estimated position bias as a function of source position for $\sigma = 10\mu s$.

4.4.2 Fixed source position and different SNRs

Besides deriving the optimal source position estimator for Gaussian TOAs (which is a good approximation if the noise level is low), we have also generalized it to TOAs that follow a Gaussian Mixture distribution, which is an approximation for high noise level. However, in order to find the optimal estimator, we have assumed two hypotheses:

- The noise level must not be very high, or else the Taylor approximation (4.43) will not work and the estimator will be biased, since $\mathbf{x}$ must not be distant from $\mathbf{x}^*$.
- The TOA pdf is known given the source position, that is, the mean, variance and weight of each Gaussian Mixture component.

If the first hypothesis is not respected, the performance of our estimator may decrease and become even worse than the performance of other cost functions. If the second hypothesis is not true, the derived expression for the CRLB deviates from the true CRLB, thus other estimators may show lower MSE than the derived CRLB. Nevertheless, even if these assumptions are not completely true, our estimator may still show better performance than other methods.

For this reason, we have done four simulations in similar conditions as before, except

that the source position is fixed at $\mathbf{x}^* = (0.3, 0.4)$ and white Gaussian noise with different variances was added to the generated signal. In all simulations, a modulated Hann window was used as equivalent source waveform $s[n]$:

$$s[n] = \sin^2\left(\frac{\pi n}{1000}\right)\sin\left(\frac{2\pi n}{67}\right). \tag{4.70}$$

The sampling rate is 10 MHz, hence the frequency of the carrier is $\frac{10^7}{67} \approx 150$ kHz, the resonance frequency for some Acoustic Emission sensors. The Constant Velocity Model was used to generate hits, thus all hits are attenuated and delayed versions of $s[n]$. However, a constant TOA bias model $\mathbf{b}$ that does not depend on the source position was used by our estimators.

In all simulations, we calculate TOAs using the TOA debiasing technique proposed in Section 2.4 from Chapter 2 with a fixed threshold $K = 0.3$. The Optimal Estimator was implemented using Algorithm 1, and the Maximum Likelihood Estimator used the parameters estimated by this algorithm.

4.4.2.1 Gaussian TOAs and known pdf

In this simulation, we used the noisy hits to obtain auxiliary TOAs through the fixed threshold method. Then, the mean and variance of these auxiliary TOAs were computed and used to generate TOAs following a Gaussian Mixture distribution with known parameters, except for $\tau(x, y)$, which depends on the source position.

The MSE in terms of noise standard deviation for the presented methods is shown in Figures 34 and 35. The MSE of the optimal estimator is very close to the Cramér-Rao Lower Bound, confirming our derivations. Moreover, we conclude from Figure 34 that the Maximum Likelihood Estimator does not coincide with the optimal one if σ is high, but Figure 35 shows that the MLE is optimal for low noise level.

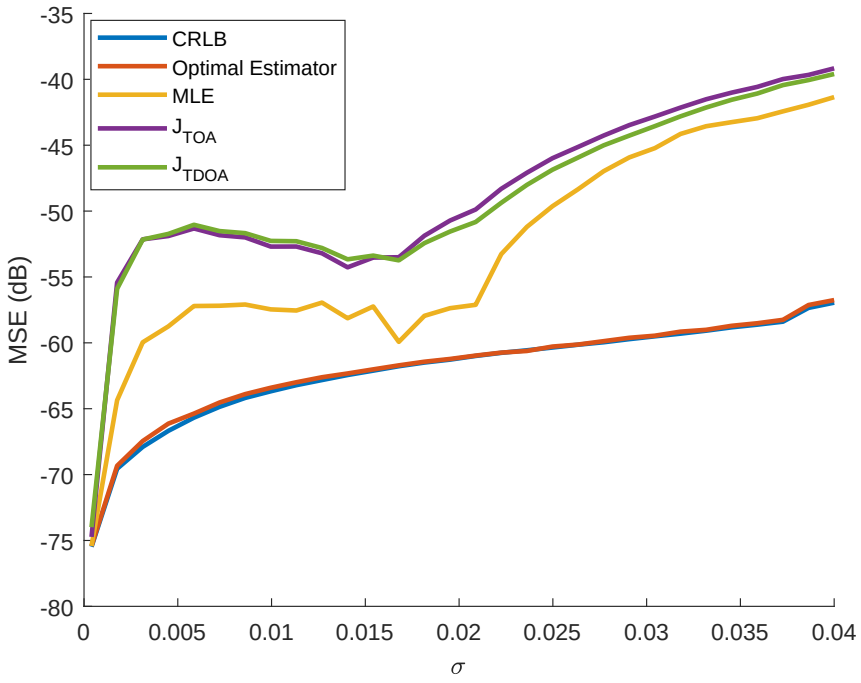

Figure 34: MSE of TOA-based localization methods in terms of noise standard deviation. The parameters of Gaussian Mixtures used by GMM and Optimal Estimator are the actual ones, and TOAs are distributed according to a GMM.

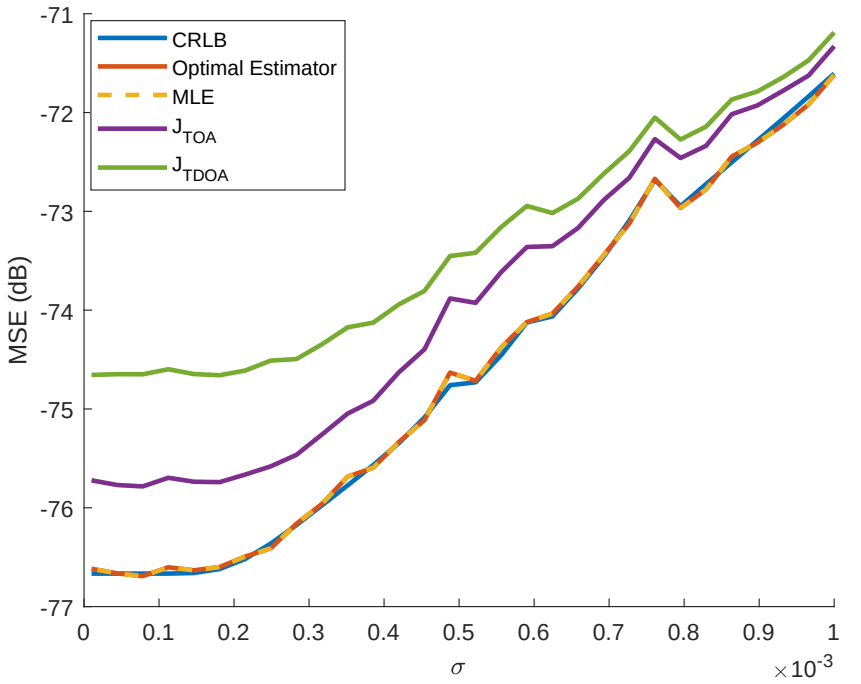

Figure 35: Zoomed version of Figure 34 at small variances.

4.4.2.2 Empirical TOAs and unknown pdf

In this simulation, the actual TOAs obtained from the fixed threshold method are used to localize the source. Hence, TOAs are not exactly Gaussian-distributed in this case. The Cramér-Rao Lower Bound was calculated using the actual Gaussian Mixture parameters as in the last simulation, but the parameters used by the MLE and the Optimal Estimator were estimated from noisy hits using Algorithm 1.

Algorithm 1 requires as input the noise cdf to extract the TOA pmf from noisy hits. The formula to estimate $p[n]$ (2.40) was derived considering that the waveform $r_i[n]$ is noiseless, but as in this case $r_i[n]$ is noisy, we used the cdf of a Gaussian random variable with half the variance of the actual noise as input in Algorithm 1. We have observed empirically that using the cdf of a Gaussian noise with lower variance than the actual variance yields better results than using the actual noise cdf.

Figure 36 shows that if the noise variance is very high, the derived optimal estimator does not perform better than the others, but it does have a significantly better performance for intermediate variances where the TOA pdfs cannot be approximated as single Gaussian distributions.

It can be seen at Figure 37 that the optimal estimator has lower MSE than the other estimators for very low variances, but it may perform worse than them if the variance is not very low, but low enough so that TOAs pdf is nearly Gaussian. This is because the MSE of J_{TOA} and J_{TDOA} fall abruptly when the TOA distribution becomes approximately Gaussian (or a mixture with only one component), while the MLE and the optimal estimator do not because they depend on the noisy parameters of the estimated Gaussian pdf. For smaller variances, the parameters from the pdf approximate well the actual ones, thus the Optimal Estimator becomes again better than J_{TOA} and J_{TDOA}.

Note that the MSE of the estimators fall below the Cramér-Rao Lower Bound if σ is small. This happens because we derived the CRLB for TOAs following a known Gaussian Mixture distribution, but the true distribution is not exactly a mixture of Gaussians. Even if it were, the parameters used in the mixture of Gaussians used by the estimators are estimated, not exact.

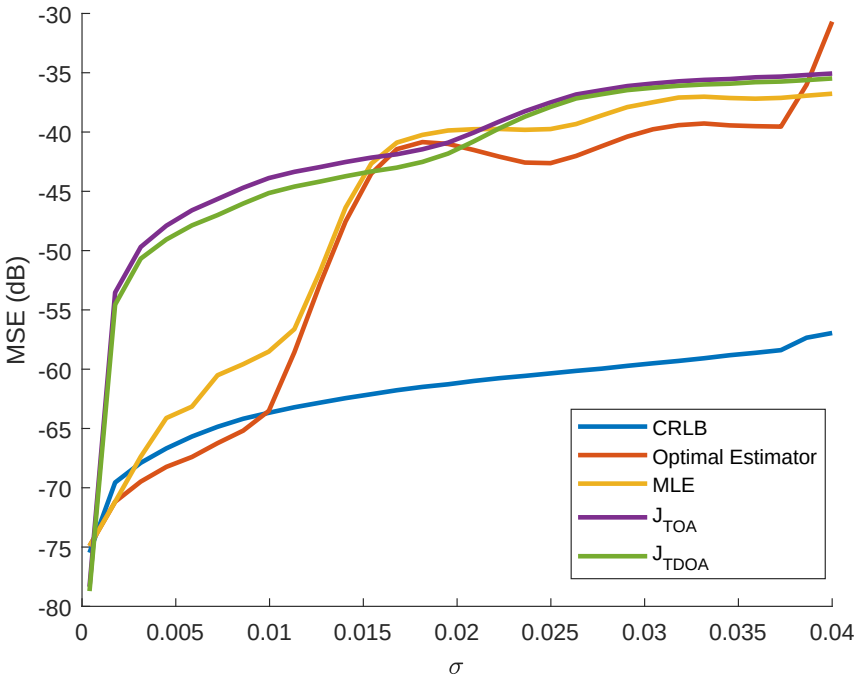

Figure 36: MSE of TOA-based localization methods in terms of noise standard deviation. The parameters of Gaussian Mixtures are obtained from noisy hits.

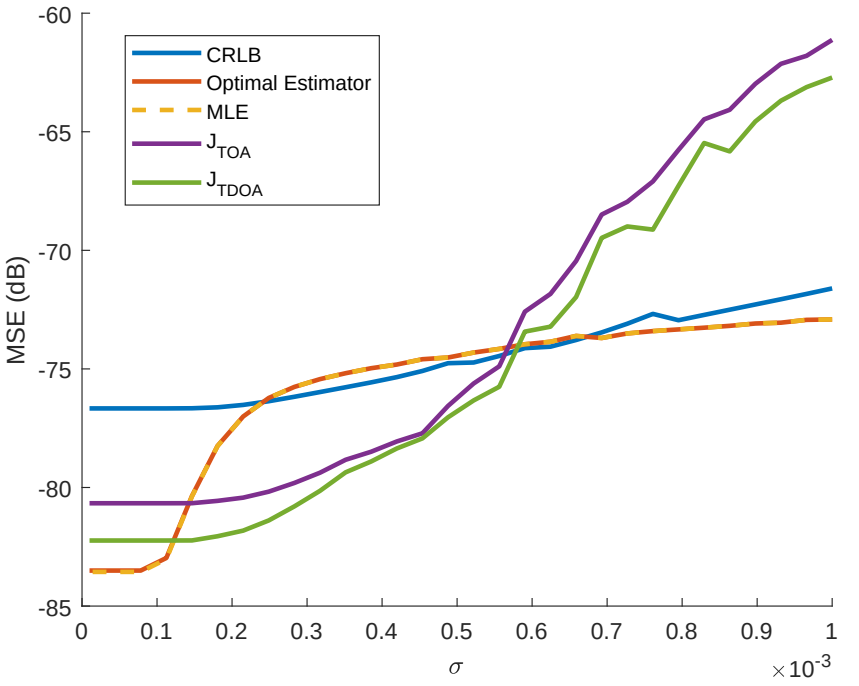

Figure 37: Zoomed version of Figure 36 at small variances.

4.4.2.3 Empirical TOAs obtained from filtered hits and unknown pdf

The main issue of MLE and the optimal estimator is that they depend on the noise pdf, which is not accessible in practice and must be estimated. If the noise variance is high, these parameters can be poorly estimated and cause performance loss in the localization methods, as verified in the last simulation. For this reason, a lowpass filter is applied to hits before calculating the threshold in this simulation. The filter used was a Butterworth filter of order 15 and digital cutoff frequency $\omega_c = 0.1\pi$ (or 1 MHz), but the TOA pmf was calculated assuming white Gaussian noise.

The results are shown in Figures 38 and 39. With the filter, the parameters of the GMM are better estimated, and the optimal estimator has better performance than all other methods even for high variance. The MLE also presents much lower MSE than J_{TOA} and J_{TDOA} for high noise level.

If the noise variance is very low, J_{TOA} and J_{TDOA} perform better than the optimal estimator only in a small interval of σ. Thus, both MLE and the optimal estimator are better options than J_{TOA} and J_{TDOA} in most cases.

Since the noise is assumed white to calculate the TOA pmf (which is used to extract the GMM parameters), the optimal estimator may perform worse using filtered hits than using the original hits for some variances (as for $10^{-3} < \sigma < 5 \times 10^{-3}$), but using filtered hits implies in lower MSE in most cases.

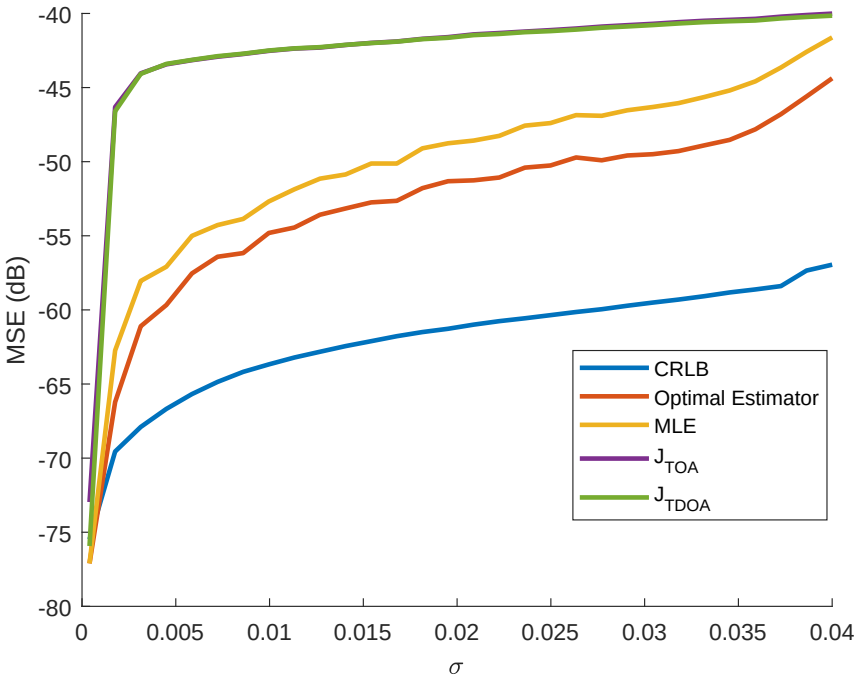

Figure 38: MSE of TOA-based localization methods in terms of noise standard deviation. Both TOAs and the parameters of Gaussian Mixtures are obtained from filtered hits.

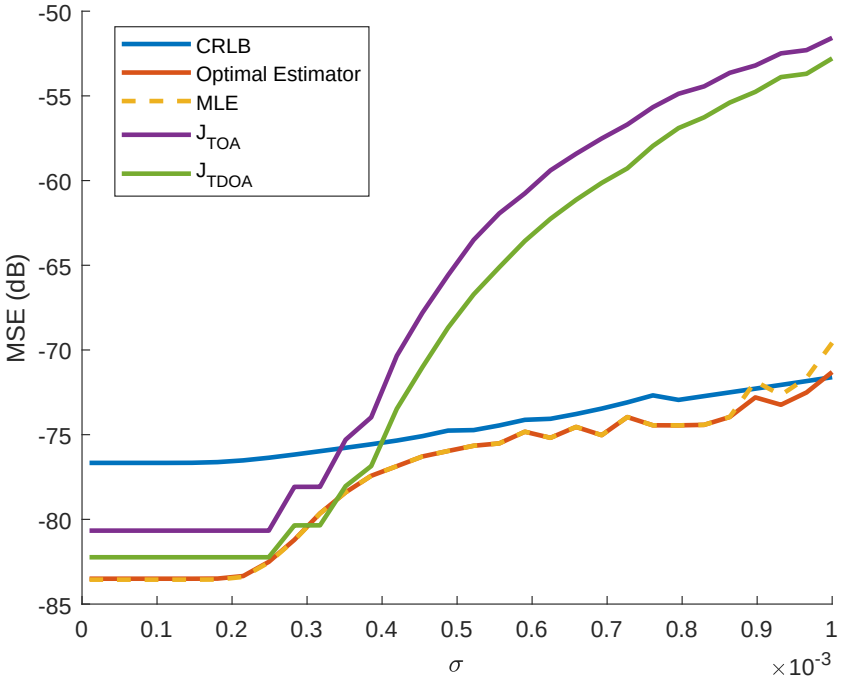

Figure 39: Zoomed version of Figure 38 at small variances.

4.4.2.4 Effect of TOA debiasing

We repeated the simulations in 4.4.2.2 and 4.4.2.3, that is, using empirical TOAs (extracted or not from filtered hits) and unknown pdf. In all previous simulations, TOAs were debiased using the method described in Chapter 2. In this simulation, original TOAs are used by localization methods, whose performance are compared to the same methods using debiased TOAs.

Figure 40 shows the comparison using TOAs extracted from original hits, and in Figure 41 hits are filtered before TOAs extraction. In both cases, it is clear that our debiasing method significantly decreases the MSE of TOA-based localization methods. These figures also show that the optimal estimator only achieves a much better performance than J_{TOA} if TOAs are unbiased, since otherwise the MSEs of these estimators are very close to each other for all values of σ.

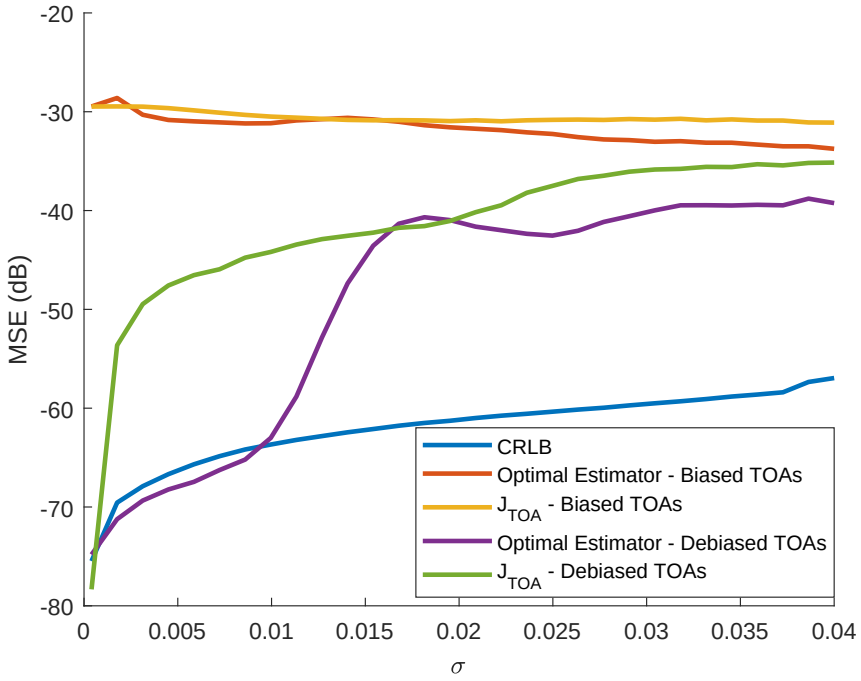

Figure 40: Comparison of localization methods using biased and unbiased TOAs. TOAs are extracted from original hits.

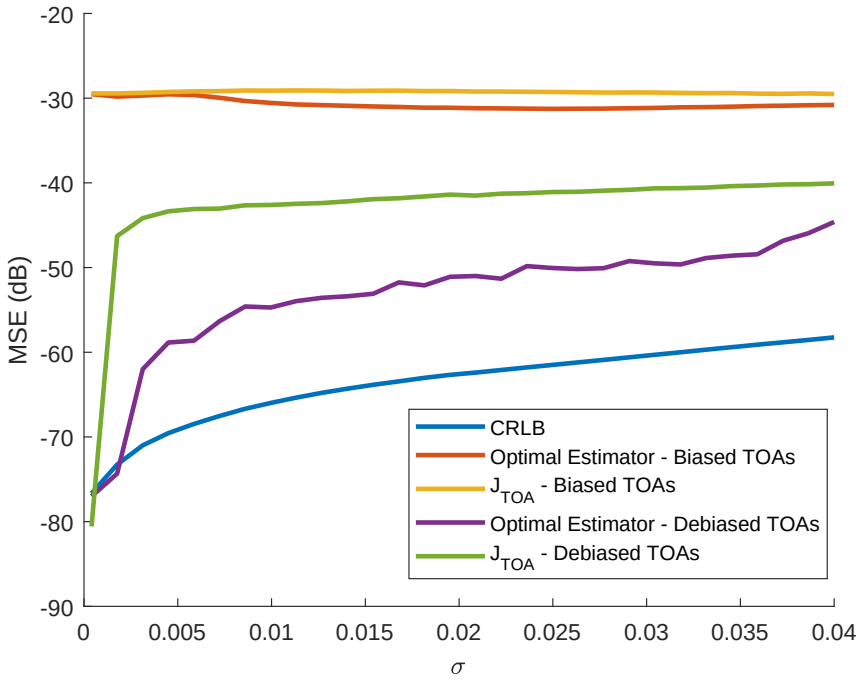

Figure 41: Comparison of localization methods using biased and unbiased TOAs. TOAs are extracted from filtered hits.

Concluding remarks

In this chapter, we derived the optimal source position estimator assuming TOAs follow a mixture of Gaussian distributions, which is approximately true for high sampling rate as explored in Chapter 2. This estimator is only optimal if the noise variance is not very high (so that the Taylor expansion (4.43) is a good approximation), and the parameters of the mixture are known. Even though these parameters are not known in practical applications, they can be estimated from noisy waveforms and used to localize the source, yielding better results than the cost functions $J_{\text{TOA}}(x, y)$ and $J_{\text{TDOA}}(x, y)$ in several scenarios, especially if the noise variance is high and in the case where a low-pass filter is applied to hits before extracting TOAs. In these cases, the optimal estimator has better performance than $J_{\text{TOA}}(x, y)$ even if biased TOAs are used. We also showed that $J_{\text{TOA}}(x, y)$ coincides with the optimal estimator and the maximum likelihood estimator if TOAs are unbiased i.i.d. Gaussian random variables.

It may be difficult to run algorithms that use the waveforms sampled by sensors in long acoustic emission tests because storing the signal may require a huge storage capability. Even though the waveforms are required to estimate the parameters of the mixture, it is possible to calculate $p[n]$ in real time and store $p[n]$ instead of the whole hit, which

is advantageous because $p[n]$ assumes a non-negligible value for only a small number of samples, thus it is possible to store only these samples and discard the rest. This way, the derived optimal estimator avoids the storage problem.

5 WAVEFORM-BASED SOURCE LOCALIZATION

In TOA-based localization methods, the waveforms acquired by the sensors are processed in real time in order to calculate their TOAs. Once TOAs are estimated, the waveforms can be discarded because only the information of TOAs is used to determine the source position. In this chapter, we explore localization techniques that use directly the waveforms instead of the TOAs, bypassing the TOA calculation step.

Waveform-based localization techniques require much more computational complexity than TOA-based methods, which makes them harder to be implemented in real time. If not implemented in real time, the storage of the waveforms is required, unlike TOA-based methods. On the other hand, when waveforms are used to localize the source instead of TOAs, more information is available. For this reason, waveform-based methods as [13–16] in principle should be able to perform better than TOA-based ones. Moreover, some waveform-based methods may be able to localize sources using less than three sensors [14, 58], unlike traditional TOA-based methods.

We develop in this chapter two versions of a localization technique that uses a linear propagation model to estimate the source position using the waveforms sampled by the sensors. While the first version of our method uses a least-squares approach, the second one considers the source signal is sparse in a known dictionary. The redundancy of information carried by acoustic emission signals is exploited using sparse reconstruction methods in [13,59], and the wavelet transform is widely used in acoustic emission [9,60–62] due to the sparsity of acoustic emission signals in wavelet dictionaries. This motivates us to assume that the signal emitted by the source is sparse in a known dictionary to improve our localization method. In this chapter, we use a wavelet dictionary that does not depend on data. However, if training data is available, it is possible to learn a dictionary where the source signal is sparse (or improve the existing one) using Dictionary Learning algorithms, as [63].

Usually, hits from the same source are required by source localization methods, thus

identifying which hits come from the same source is essential for correct localization. We also extend our waveform-based localization technique to hit grouping. For this reason, we also explore hit grouping methods that use the waveform to group hits into events.

5.1 Sparse Reconstruction

Sparse reconstruction is a technique that solves a system of linear equations that does not admit a single exact solution exploiting the a priori information of the sparsity of the solution [64]. In other words, the sparse reconstruction problem aims to obtain an $L \times 1$ sparse vector $\mathbf{s}$ such that $\mathbf{y} \approx \mathbf{D}\mathbf{s}$, where $\mathbf{y}$ is a known $M \times 1$ vector with $M < L$ and $\mathbf{D}$ is a known $M \times L$ matrix. One approach to solve this problem is by minimizing a cost function that penalizes the ℓ_p-norm[1] of $\mathbf{s}$, with $0 \leq p < 2$, as

$$J_\lambda(\mathbf{s};\lambda) = \|\mathbf{y} - \mathbf{D}\mathbf{s}\|_2^2 + \lambda \|\mathbf{s}\|_p . \tag{5.1}$$

In this work, we focus on the case where $p = 0$, but other cost functions or other values for p could also be employed. There are several algorithms in the literature that minimize greedily the cost function $J_\lambda(\mathbf{s};\lambda)$ (that is, algorithms that try to minimize the cost function by solving simpler problems, obtaining an approximation of the global minimum of the function), as Orthogonal Matching Pursuit (OMP) [65] — used in this chapter — and Homotopy ℓ_0-DCD (Hℓ_0-DCD) [66].

We say that two cost functions $J_1(\mathbf{s})$ and $J_2(\mathbf{s})$ are equivalent if the value of $\mathbf{s}$ that minimizes $J_1(\mathbf{s})$ also minimizes $J_2(\mathbf{s})$. It is possible to prove that there is an equivalence between the three of the most common sparse cost functions, as stated in the next proposition. The equivalence between these cost functions is also explored in the literature [67].

It is important to talk about the equivalence of these cost functions because they depend on different parameters whose choice is not straightforward, and for some applications it may be easier to choose the parameters for one of these cost functions than for the others.

Proposition 1. *$\forall \epsilon > 0$ and $\forall K > 0$, $\exists \lambda > 0$ such that the cost function*

$$J_\lambda(\mathbf{s};\lambda) = \|\mathbf{y} - \mathbf{D}\mathbf{s}\|_2^2 + \lambda \|\mathbf{s}\|_0 \tag{5.2}$$

[1] If $0 \leq p < 1$, $\|\mathbf{s}\|_p$ is not convex, and therefore is a *pseudo-norm*, not a true norm. For $p = 0$, $\|\mathbf{s}\|_0$ is defined as the number of nonzero elements of $\mathbf{s}$. It can be shown that $\|\mathbf{s}\|_0 = \lim_{p\to 0} \|\mathbf{s}\|_p$.

is equivalent to

$$J_K(\mathbf{s}; K) = \|\mathbf{y} - \mathbf{D}\mathbf{s}\|_2^2 \quad \text{s.t. } \|\mathbf{s}\|_0 \leq K \tag{5.3}$$

and

$$J_\epsilon(\mathbf{s}; \epsilon) = \|\mathbf{s}\|_0 \quad \text{s.t. } \|\mathbf{y} - \mathbf{D}\mathbf{s}\|_2^2 \leq \epsilon^2 \tag{5.4}$$

Proof. Denote $\mathbf{s}_K^*$ and $\mathbf{s}_\epsilon^*$ the values of $\mathbf{s}$ that minimize $J_K(\mathbf{s}; K)$ and $J_\epsilon(\mathbf{s}; \epsilon)$, respectively. These solutions also minimize the cost functions

$$J'_K(\mathbf{s}) = \|\mathbf{y} - \mathbf{D}\mathbf{s}\|_2^2 \quad \text{s.t. } \|\mathbf{s}\|_0 = \|\mathbf{s}_K^*\|_0$$

and

$$J'_\epsilon(\mathbf{s}) = \|\mathbf{s}\|_0 \quad \text{s.t. } \|\mathbf{y} - \mathbf{D}\mathbf{s}\|_2^2 = \|\mathbf{y} - \mathbf{D}\mathbf{s}_\epsilon^*\|_2^2$$

because $J'_K(\mathbf{s})$ and $J'_\epsilon(\mathbf{s})$ have tighter constraints than $J_K(\mathbf{s})$ and $J_\epsilon(\mathbf{s})$, and the solutions that minimize the less constrained cost functions also satisfy the constraints of $J'_K(\mathbf{s})$ and $J'_\epsilon(\mathbf{s})$.

In order to solve a minimization problem with equality bounds we can use Lagrange multipliers, yielding cost functions $J_{\lambda_K}(\mathbf{s})$ and $J_{\lambda_\epsilon}(\mathbf{s})$ that are minimized by $\mathbf{s}_K^*$ and $\mathbf{s}_\epsilon^*$ for some constants $\lambda_K > 0$ and $\lambda_\epsilon > 0$:

$$J_{\lambda_K}(\mathbf{s}) = \|\mathbf{y} - \mathbf{D}\mathbf{s}\|_2^2 + \lambda_K(\|\mathbf{s}\|_0 - \|\mathbf{s}_K^*\|_0),$$

$$J_{\epsilon_K}(\mathbf{s}) = \|\mathbf{s}\|_0 + \lambda_\epsilon(\|\mathbf{y} - \mathbf{D}\mathbf{s}\|_2^2 - \|\mathbf{y} - \mathbf{D}\mathbf{s}_\epsilon^*\|_2^2).$$

Note that unlike the parameter λ, the Lagrange multipliers λ_K and λ_ϵ cannot be chosen arbitrarily, as they depend on $\mathbf{y}$, $\mathbf{D}$ and λ.

The cost functions $J_{\lambda_K}(\mathbf{s})$ and $J_{\epsilon_K}(\mathbf{s})$ are equivalent to

$$J'_{\lambda_K}(\mathbf{s}) = \|\mathbf{y} - \mathbf{D}\mathbf{s}\|_2^2 + \lambda_K \|\mathbf{s}\|_0$$

and

$$J'_{\epsilon_K}(\mathbf{s}) = \|\mathbf{y} - \mathbf{D}\mathbf{s}\|_2^2 + \frac{1}{\lambda_\epsilon} \|\mathbf{s}\|_0$$

because $J'_{\lambda_K}(\mathbf{s})$ and $J'_{\lambda_\epsilon}(\mathbf{s})$ can be written as $J'_{\lambda_K}(\mathbf{s}) = J_{\lambda_K}(\mathbf{s}) + b_K$ and $J'_{\lambda_\epsilon}(\mathbf{s}) = a_\epsilon J_{\lambda_\epsilon}(\mathbf{s}) + b_\epsilon$, where b_K, a_ϵ and b_ϵ are constants that do not depend on $\mathbf{s}$.

Thus, since $J'_{\lambda_K}(\mathbf{s}) = J_\lambda(\mathbf{s}; \lambda_K)$ and $J'_{\epsilon_K}(\mathbf{s}) = J_\lambda(\mathbf{s}; \frac{1}{\lambda_\epsilon})$ for $\lambda = \lambda_K$ and $\lambda = \frac{1}{\lambda_\epsilon}$ the cost functions $J_K(\mathbf{s}; K)$ and $J_\epsilon(\mathbf{s}; \epsilon)$ are equivalent to $J_\lambda(\mathbf{s}; \lambda)$. □

From this proposition, it is straightforward to conclude that for any $\lambda > 0$, $J_\lambda(\mathbf{s}; \lambda)$ is

equivalent to $J_K(\mathbf{s}; K)$ and $J_\epsilon(\mathbf{s}; \epsilon)$ for some $K > 0$ and $\epsilon > 0$.

5.1.1 Exploring sparsity in Acoustic Emission

In Chapter 2, we defined the equivalent waveform at the source position (denoted in that chapter as $A\psi[n]$) as an auxiliary signal that generates the signals received by the sensors if a propagation model is applied to it. Consider that the equivalent waveform $\mathbf{y}_0 \in \mathbb{R}^M$ at the source position (x_s, y_s) is sparse in a known dictionary $\mathbf{D} \in \mathbb{R}^{M \times L}$ that can either be a fixed dictionary (that does not depend on the data) or a dictionary that was learned from a training set using a Dictionary Learning algorithm as [63, 68–70]:

$$\mathbf{y}_0 = \mathbf{D}\mathbf{s}_0, \qquad \|\mathbf{s}_0\|_0 = K \ll L, \tag{5.5}$$

where $\mathbf{s}_0$ is the sparse representation of $\mathbf{y}_0$ in the dictionary $\mathbf{D}$. Note that $\mathbf{y}_0$ is a collection of M samples of the equivalent source signal.

Also, consider the vectorized signal $\mathbf{y}_i = \begin{bmatrix} r_i[0] & r_i[1] & \cdots & r_i[M-1] \end{bmatrix}^T$ received by sensor i is $\mathbf{y}_0$ transformed by a known $M \times M$ matrix $\mathbf{H}_i(x, y)$ that depends on the source position (x, y):

$$\mathbf{y}_i = \mathbf{H}_i(x, y)\mathbf{y}_0 = \mathbf{H}_i(x, y)\mathbf{D}\mathbf{s}_0, \quad 1 \leq i \leq N, \tag{5.6}$$

where L is the number of sensors. Matrix $\mathbf{H}_i(x, y)$ represents a linear system that models the propagation of the wave from the point (x, y) to the i-th sensor. If the linear system that deforms the wave is time-invariant, $\mathbf{H}_i(x, y)$ is a Toeplitz matrix (because, since the system is time-invariant, all rows of $\mathbf{H}_i(x, y)$ must be a linear-shifted version of its first row).

It is worth noting that the vectors of samples $\mathbf{y}_i$ and equivalent waveforms $\mathbf{y}_0$ are represented using bold characters, and they shall not be confused with the actual source position (x_s, y_s) or the tentative source position (x, y).

In this chapter, we explore algorithms based on sparsity to create a method that recovers $\mathbf{s}_0$ using the measurement vectors $\mathbf{y}_i$ and a known propagation model, but we also derive a least squares approach. We present the methods considering the noiseless case (that is, we assume the model is exact and there is no measurement noise, in which case the results are exact), but the tests are performed considering a noisy scenario and uncertainties over the model.

We assume the measurement vectors $\mathbf{y}_1, \mathbf{y}_2, \cdots, \mathbf{y}_N$ are vectors of synchronized samples for each sensor. Each measurement vector $\mathbf{y}_i$ corresponds to M samples taken from

instant $t = t_0$ to $t = (M-1)T_s + t_0$, where T_s is the sampling interval and t_0 is the instant of the first sample. This way, each $\mathbf{y}_i$ represents the hit obtained by each sensor. In our algorithm, no restrictions about t_0 are made – the sensors can start sampling before or after the wave has reached the first sensor. We also assume that there is only one source emitting a signal during the period comprised by the measurement vectors, thus we do not tackle the problem of source separation.

Denote

$$\mathbf{y} = \begin{bmatrix} \mathbf{y}_1 \\ \mathbf{y}_2 \\ \vdots \\ \mathbf{y}_N \end{bmatrix} \tag{5.7}$$

and

$$\mathbf{H}(x,y) = \begin{bmatrix} \mathbf{H}_1(x,y) \\ \mathbf{H}_2(x,y) \\ \vdots \\ \mathbf{H}_N(x,y) \end{bmatrix}. \tag{5.8}$$

We call $\mathbf{H}(x,y)$ the linear propagation model matrix. The system of equations

$$\begin{cases} \mathbf{y}_1 = \mathbf{H}_1(x,y)\mathbf{D}\mathbf{s}_0 \\ \mathbf{y}_2 = \mathbf{H}_2(x,y)\mathbf{D}\mathbf{s}_0 \\ \vdots \\ \mathbf{y}_N = \mathbf{H}_N(x,y)\mathbf{D}\mathbf{s}_0 \end{cases} \tag{5.9}$$

can be written in matrix form:

$$\begin{bmatrix} \mathbf{y}_1 \\ \mathbf{y}_2 \\ \vdots \\ \mathbf{y}_N \end{bmatrix} = \begin{bmatrix} \mathbf{H}_1(x,y)\mathbf{D} \\ \mathbf{H}_2(x,y)\mathbf{D} \\ \vdots \\ \mathbf{H}_N(x,y)\mathbf{D} \end{bmatrix} \mathbf{s}_0 = \begin{bmatrix} \mathbf{H}_1(x,y) \\ \mathbf{H}_2(x,y) \\ \vdots \\ \mathbf{H}_N(x,y) \end{bmatrix} \mathbf{D}\mathbf{s}_0, \tag{5.10}$$

or yet,

$$\mathbf{y} = \mathbf{H}(x,y)\mathbf{D}\mathbf{s}_0. \tag{5.11}$$

If the source position were known, the problem of retrieving $\mathbf{s}_0$ could be solved via a sparse estimation algorithm using $\mathbf{y}$ as the measurement vector and $\mathbf{H}(x,y)\mathbf{D}$ as the dictionary. Unfortunately, the source position is not known, therefore we retrieve $\mathbf{s}_0$ at several possible source positions. In other words, we calculate dictionaries $\mathbf{H}(x,y)\mathbf{D}$ at several possible source positions (x,y) (for example, we choose positions that belong to a grid that cover

the region that is being monitored) and for each one we estimate $\mathbf{s}_0$ independently through the minimization of $J_\lambda(\mathbf{s};\lambda)$, obtaining a residue $J^*_\lambda(x,y) = J_\lambda(\hat{\mathbf{s}};\lambda)$ that depends on (x,y). Our estimated source position is the one that yields the minimum residue:

$$(x,y) = \arg\min_{x,y} J^*_\lambda(x,y), \qquad J^*_\lambda(x,y) = \min_{\mathbf{s}} \|\mathbf{y} - \mathbf{H}(x,y)\mathbf{D}\mathbf{s}\|_2^2 + \lambda \|\mathbf{s}\|_0 . \tag{5.12}$$

In other words, we choose the source position that makes the reconstructed signal $\mathbf{D}\mathbf{s}$ compatible with $\mathbf{H}(x,y)$.

Our method relies on minimizing a minimum – We first minimize the cost function with respect to the sparse representation $\mathbf{s}$, obtaining a minimum that depends on (x,y), and then we minimize this minimum with respect to (x,y) to obtain the source position estimate. Unfortunately, the function $J^*_\lambda(x,y)$ has several local minima, thus minimization algorithms that seek the point where the gradient is zero will not work unless the initial condition is very close to the true source position. For this reason, we define a grid of points and find $J^*_\lambda(x,y)$ for each one. Then, we choose its minimum and refine the grid so that the edges are close to the minimum found. This refinement procedure is repeated for a fixed number of iterations. After the refinements, the source position is estimated using a regular minimization algorithm whose initial condition is the chosen as the last (most refined) estimate. Our algorithm is detailed in Algorithm 2.

A least squares approach can be derived by setting $\lambda = 0$. In this case where the sparsity is not taken into account, it is straightforward to derive a closed-form expression for $J^*_\lambda(x,y)$:

$$J^*_\lambda(x,y) = \left\|\mathbf{y} - \mathbf{H}(x,y)\mathbf{H}^\dagger(x,y)\mathbf{y}\right\|_2^2 . \tag{5.13}$$

It is worth noting that our methods require a propagation model $\mathbf{H}(x,y)$. If the chosen propagation model requires parameters that are not available (for example, attenuation coefficient), they must be estimated. In this Chapter, we do not address the problem of estimating unknown parameters from the medium, but in our derivations we consider that the propagation model may be imprecise.

Algorithm 2: The proposed waveform-based source localization algorithm.

Data: Measurement vector $\mathbf{y}$; Dictionary $\mathbf{D}$; Sparsity-promoting parameters K, λ or ϵ; Linear model matrix $\mathbf{H}(x, y)$; Set $\mathcal{G}$ of points extracted from an initial grid; Number of grid refinements T.

Result: Estimated source position $(\hat{x}, \hat{y})$

Define the cost function $J(\mathbf{s}; x, y)$ as one the following options:

- $J(x, y) = \min_{\mathbf{s}} \|\mathbf{y} - \mathbf{H}(x, y)\mathbf{D}\mathbf{s}\|_2^2$ s.t. $\|\mathbf{s}\|_0 \leq K$
- $J(x, y) = \min_{\mathbf{s}} \|\mathbf{y} - \mathbf{H}(x, y)\mathbf{D}\mathbf{s}\|_2^2 + \lambda \|\mathbf{s}\|_0$
- $J(x, y) = \min_{\mathbf{s}} \|\mathbf{s}\|_0$ s.t. $\|\mathbf{y} - \mathbf{H}(x, y)\mathbf{D}\mathbf{s}\|_2 \leq \epsilon$
- $J(x, y) = \left\|\mathbf{y} - \mathbf{H}(x, y)\mathbf{H}^{\dagger}(x, y)\mathbf{y}\right\|$ (Least Squares approach)

for *i=1:T* **do**

  $(\hat{x}^{(i)}, \hat{y}^{(i)}) \leftarrow \arg\min_{(x,y)\in\mathcal{G}} J(x, y)$;

  Refine the grid $\mathcal{G}$ around $(\hat{x}^{(i)}, \hat{y}^{(i)})$;

Solve $(\hat{x}, \hat{y}) = \arg\min_{x,y} J(x, y)$ using $(\hat{x}^{(T)}, \hat{y}^{(T)})$ as initial condition through a conventional minimization algorithm;

5.1.2 Performance guarantees in the noiseless case

Let K be an integer such that the function $J_K(\mathbf{s}; K)$ is equivalent to the function $J_\lambda(\mathbf{s}; \lambda)$ used in the localization algorithm. Write the estimate for $\mathbf{s}_0$ as $\hat{\mathbf{s}} = \mathbf{s}_0 + \mathbf{h}$. Since $\mathbf{h} = \hat{\mathbf{s}} - \mathbf{s}_0$ and $\hat{\mathbf{s}}$ and $\mathbf{s}_0$ are K-sparse vectors, $\mathbf{h}$ has at most $2K$ nonzero elements.

At the source position (x_s, y_s), the cost function $J_K(\hat{\mathbf{s}}; K)$ is given by

$$J_K(\hat{\mathbf{s}}; K) = \|\mathbf{y} - \mathbf{H}(x_s, y_s)\mathbf{D}\hat{\mathbf{s}}\|_2^2 . \tag{5.14}$$

Considering our model is precise, $\mathbf{y}$ can be written as

$$\mathbf{y} = \mathbf{H}(x_s, y_s)\mathbf{D}\mathbf{s}_0. \tag{5.15}$$

Substituting (5.15) into (5.14), we have

$$J_K(\hat{\mathbf{s}}; K) = \|\mathbf{H}(x_s, y_s)\mathbf{D}\mathbf{s}_0 - \mathbf{H}(x_s, y_s)\mathbf{D}\hat{\mathbf{s}}\|_2^2 = \|\mathbf{H}(x_s, y_s)\mathbf{D}(\hat{\mathbf{s}} - \mathbf{s}_0)\|_2^2 = \|\mathbf{H}(x_s, y_s)\mathbf{D}\mathbf{h}\|_2^2 . \tag{5.16}$$

$J_K(\hat{\mathbf{s}}; K)$ is minimum and equal to zero for any $\mathbf{h} \in \ker\{\mathbf{HD}\}$ such that $\|\hat{\mathbf{s}}\|_0 \leq K$. Consequently, $\hat{\mathbf{y}} = \mathbf{HD}\hat{\mathbf{s}} = \mathbf{y}$ if and only if $\mathbf{HDh} = \mathbf{0}$.

Since $J_K(\hat{\mathbf{s}}; K) = 0$, $J_\lambda(\hat{\mathbf{s}}; \lambda)$ is a global minimum of $J_\lambda(\mathbf{s}; \lambda)$, thus (x_s, y_s) is a minimum of $J^*_\lambda(x, y)$ and thus the estimate source position is the true one. In other words, our method retrieves the true source position if there is no $2K$-sparse elements in the kernel of $\mathbf{H}(x_s, y_s)\mathbf{D}$.

5.2 Simulations

We used the first 50 samples of a waveform sampled at 1 MHz and collected during a tensile test performed by Embraer to synthesize a signal that is sparse in a dictionary but that is also similar to a real one. For this, we generated a wavelet-based dictionary as explained below and we ran the OMP algorithm with $K = 5$ samples (hence with a "sparsity rate" of 10%), obtaining a signal whose representation in $\mathbf{D}$ has only 5 nonzeros. The source is positioned at $\mathbf{x}_s = (0.2, 0.3)$ and the coordinates of the sensors are $(0, 0)$, $(1, 0)$, $(0, 1)$ and $(0.5, 0.5)$. We used $c = 5$ km/s for the wave velocity and, in the Power-Law Attenuation Model, we used $f_0 = 150$ kHz, $\alpha(f_0) = 2\text{m}^{-1}$ and $\gamma = 1.5$.

The dictionary we used is the default dictionary generated by the MATLAB function `wmpdictionary`, which is the concatenation of a sine subdictionary, a DCT-II matrix, a Daubechies wavelet dictionary with 4 vanishing moments generated with 5 iterations and a Daubechies wavelet packet dictionary with 4 vanishing moments generated with 5 iterations.

In the first simulation, the constant velocity model was used to generate the waveform with $\alpha = 2\text{m}^{-1}$, and the same model with the true parameters c and α were used as input for the localization algorithm. The noise variance at all sensors was the same, and was calculated as

$$\sigma^2 = \sigma^2_{\text{max}} 10^{-\text{SNR}/10}, \tag{5.17}$$

where σ_{max} is the standard deviation of the signal with the highest variance and SNR was swept from -10 dB to 30 dB. We used the Least Squares and the K-sparse methods with $K = 5$ to estimate the source position.

In the second simulation, although the model used by our algorithm was the constant velocity model with the same parameters as before ($\alpha = 2\text{m}^{-1}$ and $c = 5$ km/s), the model used to generate the waveforms received by the sensors was our causal approximation of the Power-Law Attenuation Model (1.26), with $\alpha(f_0) = 2m^{-1}$, $f_0 = 150$kHz and $\gamma = 1.5$.

For both simulations, 6 refinement iterations of a minimization over a 10×10 rectangular uniform grid whose edges are $\{(0, 0), (0, 1), (1, 0), (1, 1)\}$ were performed. Denote $\mathbf{x}_s$

the true source position and $\hat{\mathbf{x}}$ the estimated source position. The MSE was calculated as

$$\text{MSE} = 20\log_{10}(\|\hat{\mathbf{x}} - \mathbf{x}_s\|).$$

In most acoustic emission tests, the maximum deviation allowed from the true source position is about 1 cm, thus we can say the source position was correctly estimated if the MSE is lower than -40 dB.

We also calculated the accuracy of the position estimates obtained through the minimization of $J_{TOA}(x, y)$ and $J_{TDOA}(x, y)$, which used TOAs estimated with the fixed threshold algorithm. The performance of these cost functions depends on the choice of the threshold level because it impacts on the bias and variance of the estimated TOAs. In order to get rid of the problem of choosing an adequate threshold level, we generated position estimates with $J_{TOA}(x, y)$ and $J_{TDOA}(x, y)$ using several threshold levels and for each realization we used the optimal threshold, i.e. the one that yields the estimate that is closest to the actual source position.

Even though in practice it is not possible to calculate an optimal threshold because the actual source position is not known, we used the optimal one in this simulation to show that our waveform-based localization method yields more precise position estimates than the ones produced by the cost functions $J_{TOA}(x, y)$ and $J_{TDOA}(x, y)$ regardless of the threshold. Thus, the performance of $J_{TOA}(x, y)$ and $J_{TDOA}(x, y)$ would be worse if a single fixed threshold was used. For each SNR, we tested 1000 linearly spaced thresholds from 2σ (where σ is the noise variance) to the third largest value of $\{P_1, P_2, P_3, P_4\}$, where P_k is the maximum absolute value of $\mathbf{y}_k$. This maximum threshold was chosen because if a threshold above it were used, less than three hits would be detected and the source localization problem would not have a single solution.

The results are shown in Figures 42 and 43. Even at an SNR of 0 dB our method can successfully estimate the source position within a millimetric precision. When the model passed to the algorithm was exactly true, sparse regularization showed much better results than the Least-Squares at an SNR of -5 dB (in which case the MSE of all other methods is above -40 dB), and slightly better results for higher SNRs. On the other hand, when we generated the signals with the more complex model, but used the simpler model for the estimator, the sparse method presented better results than the least squares method only for SNRs above 15 dB, with the Least Squares being slightly better for lower SNRs. Both waveform-based localization algorithms perform better than the TOA-based methods in all cases, except when the localization error is very high for all algorithms (above -20

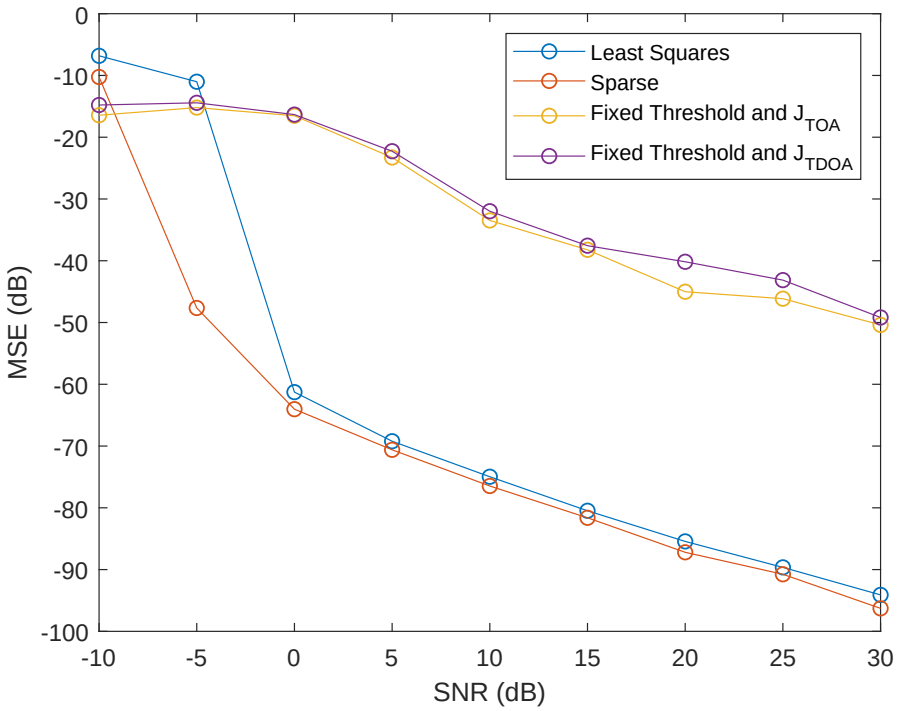

Figure 42: Source localization with noisy measurements using the least squares approach and the sparse regularization method. The constant velocity attenuation model was used both to generate the waveforms and to locate the source.

dB, or 10 cm), at SNRs lower than 0 dB.

5.3 Hit Grouping

Most source position estimation algorithms need as input the hits that will be used to localize the source. However, in actual acoustic emission tests, two or more sources may emit waves at very close instants. A hit grouping algorithm is a method that identifies which hits will be used in the localization and which hits will be discarded, and the group of hits that is used in localization is called an *event*.

In scenarios with multiple active sources, it is important to separate hits from different sources in order to avoid using hits generated by a different source in localization methods, which causes a large error in the position estimate. For this reason, hit grouping algorithms are developed and compared in this section.

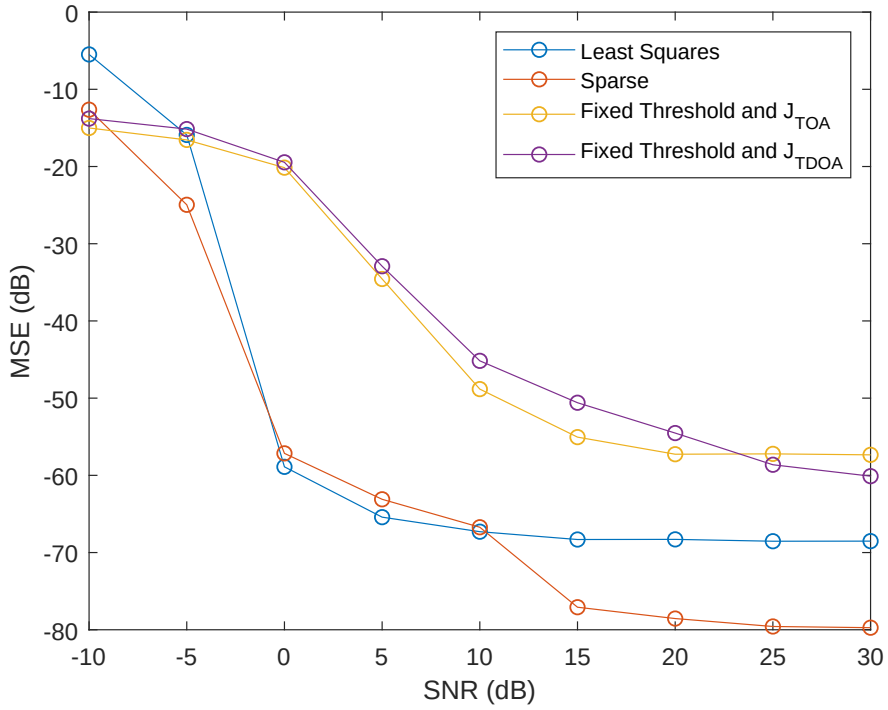

Figure 43: Source localization with noisy measurements using the least squares approach and the sparse regularization method. The constant velocity attenuation model was used to locate the source, but the Power-Law attenuation model was used to generate the waveforms.

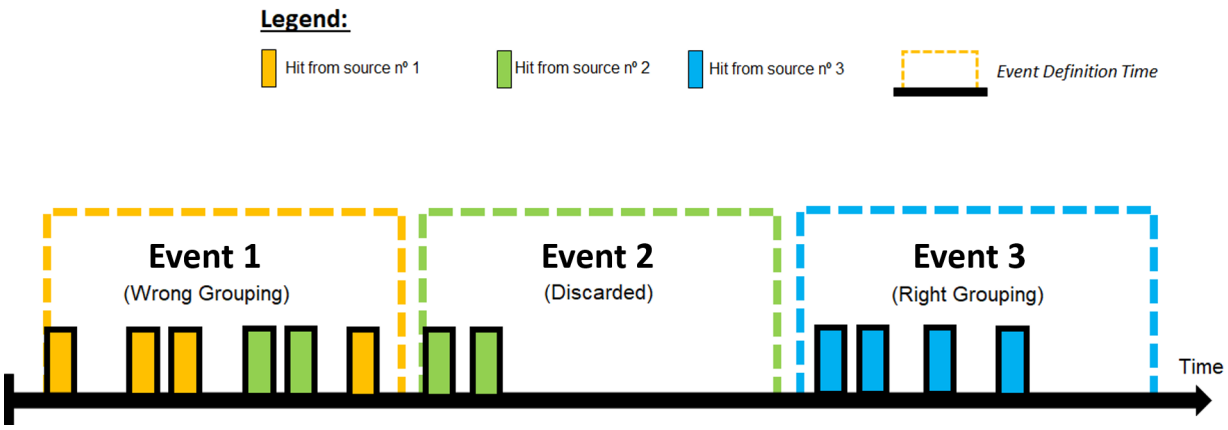

Figure 44: Hit grouping by Event Definition Time with different sources emitting waves at close instants.

5.3.1 Hit Grouping by Event Definition Time

Hit Grouping by Event Definition Time is a very popular hit grouping technique that is widely used in industry due to its simplicity and low complexity [28, 71]. This method receives as input the already segmented hits, a predefined constant called 'Event Definition Time' (EDT) and the maximum number of hits per group $K_{\max}$, and it uses these inputs to determine which hits belong to the group of the first hit, i.e. the hit with the smallest measured TOA.

The algorithm is shown in Algorithm 3. The selected hits are those whose TOAs are delayed from the minimum TOA by at most the interval EDT, and groups cannot contain two or more hits from the same sensor. However, if the number of hits grouped with the first hit is higher than $K_{\max}$, only the first $K_{\max}$ hits are selected. On the other hand, groups containing less than three hits are discarded because conventional localization algorithms cannot determine the source position with less than three sensors. After finding the group to which the first hit belongs, the algorithm is reapplied to the following ungrouped/undiscarded hits.

Even though this technique can be easily implemented in real time as it requires small computational power, it may not function properly if multiple sources are active simultaneously because only TOAs are used to group hits, thus hits from different sources cannot be distinguished.

An illustration of this method working with multiple active sources is shown in Figure 44. In this figure, the first and second sources emit signals at close instants, and for this reason two hits from source no. 2 (green) reach a sensor before the last hit from source no. 1 (yellow) is acquired. Thus, the first event contains hits that do not come from the first

source, lowering the accuracy of the localization method. The second event is discarded because contains less than three hits, thus the second source will not be detected. The third source (blue) is well grouped because sensors do not received hits from other sources during the Event Definition Time.

Algorithm 3: The Hit Grouping algorithm based on Event-Definition Time.

Data: TOAs $t_1, \cdots, t_N$ ordered in ascending order and their corresponding sensors $c_1, \cdots, c_N$; Event Definition Time (EDT); Maximum number of hits per group $K_{\max}$.

Result: Set $\mathcal{G}$ that contains the first hit.

Set $\mathcal{G} = \{1\}$, $\mathcal{C} = \{c_1\}$ and $k = 1$;

for $i = 2 : N$ **do**

  if $t_i \leq t_1 + EDT$ *and* $k < K_{max}$ *and* $c_i \notin \mathcal{C}$ **then**

    $\mathcal{G} \leftarrow \mathcal{G} \cup i$;

    $\mathcal{C} \leftarrow \mathcal{C} \cup c_i$;

    $k \leftarrow k + 1$

  if $|\mathcal{G}| < 3$ **then**

    $\mathcal{G} \leftarrow \{\}$ (the group is discarded).

5.3.2 Hit Grouping by Cross-Correlation

The hit grouping method based on EDT does not consider the waveform, and for this reason the existence of simultaneous sources may cause incorrect grouping. [72] proposes two methods to group hits based on their cross-correlation: The first method uses Basic Sequential Algorithm Scheme (BSAS) [73] to cluster hits into events, while the second one is a method designed for highly correlated signals and that generates groups with only 3 hits.

The cross-correlation coefficient between the signals $r_i[n]$ and $r_j[n]$ is defined as

$$\rho(r_i, r_j) = \begin{cases} \max_m \frac{1}{\|r_i\|_2 \|r_j\|_2} \sum_{k=0}^{N} r_i[k] r_j[m+k], & \text{channel}(r_i) \neq \text{channel}(r_j) \\ 0, & \text{channel}(r_i) = \text{channel}(r_j) \end{cases}, \quad (5.18)$$

where the ℓ_2-norm of a signal is given by

$$\|r_i\|_2 = \sqrt{\sum_{n=-\infty}^{+\infty} r_i^2[n]}, \quad (5.19)$$

channel(r_i) is the channel that sampled r_i, and the similarity between one hit waveform

$r_i[n]$ and a group of hits $\mathcal{G}$ is defined as the average cross-relation between $r_i[n]$ and each element from $\mathcal{G}$:

$$\rho(r_i, \mathcal{G}) = \frac{1}{|\mathcal{G}|} \sum_{g \in \mathcal{G}} \rho(r_i, g). \tag{5.20}$$

The cross-correlation between two hits from the same sensor is defined as 0 because the grouping methods based on cross-correlation cluster high-correlated hits, and we do not desire to have two hits from the same sensor in the same group.

The method based on BSAS, described in Algorithm 4, chooses the group of each hit by computing their similarity with respect to each group. If the maximum obtained similarity is higher than a predefined threshold $\Theta \in [0, 1]$, the hit is added to the group. Else, a new group is created.

This method does not work if all hits have very close similarity, as in the case where they are very correlated, since the choice of the groups may become very sensitive to noise. Therefore, [72] proposed to construct groups of three hits by clustering pairs of hits with maximum similarity. This method is described in Algorithm 5.

The main issue of the methods proposed by [72] is that they do not consider TOAs when adding a hit to a group. Hence, hits with very distant TOAs may be clustered in the same group. For this reason, this method must be applied to pre-selected hits whose TOAs are close. For example, it can be applied to hits belonging to the group returned by the EDT-based method with a high EDT value. Another issue is that the performance of this method is highly dependent on the similarity threshold θ. If Θ is not well-chosen, hits may be discarded or over-grouped.

Algorithm 4: Grouping Algorithm based on Cross-Correlation and BSAS (1st Wang et al. method)

Data: Hits $r_1[n], \cdots, r_N[n]$ ordered in ascending TOA order; Similarity Measure Threshold $\Theta \in [0, 1]$

Result: Set $\mathcal{G}_1, \mathcal{G}_2, \mathcal{G}_3, \cdots$ of grouped hits

Set $m \leftarrow 1$, $\mathcal{G}_1 = \{r_1\}$ and $k = 1$;

for $i = 2 : N$ **do**

  $k \leftarrow \arg\min_\ell \rho(r_i, \mathcal{G}_\ell)$;

  if $\rho(r_i, \mathcal{G}_k) < \Theta$ **then**

    $m \leftarrow m + 1$;

    Build a new cluster $\mathcal{G}_m \leftarrow \{r_i\}$

  else

    $\mathcal{G}_k \leftarrow \mathcal{G}_k \cup \{r_k\}$

Discard all groups that contain less than three hits;

Algorithm 5: Grouping algorithm based on cross-correlation for highly correlated hits (2nd Wang et al. method)

Data: Hits $r_1[n], \cdots, r_N[n]$ ordered in ascending TOA order;

Result: Set $\mathcal{G}_1, \mathcal{G}_2, \mathcal{G}_3, \cdots$ of grouped hits

Set $m \leftarrow 1$, $\mathcal{G}_1 = \{r_1\}$, $k = 1$, and calculate the similarity matrix $\mathbf{S}$ given by

$$\mathbf{S} = \begin{bmatrix} 0 & \rho(r_1, r_2) & \cdots & \rho(r_1, r_N) \\ \vdots & 0 & \ddots & \vdots \\ 0 & 0 & \cdots & \rho(r_N, r_N) \end{bmatrix};$$

while $\mathbf{S} \neq \mathbf{0}$ **do**

  $(i, j) = \max_{i,j} \mathbf{S}_{i,j}$;

  Find k such that $i \in \mathcal{G}_k$ or $j \in \mathcal{G}_k$. **if** k *was found* **then**

    $\mathcal{G}_k \leftarrow \mathcal{G}_k \cup \{i, j\}$;

    for $u \in \mathcal{G}_k$ **do**

      for $v = 1 : N$ **do**

        $\mathbf{S}_{u,v} \leftarrow 0$;

        $\mathbf{S}_{v,u} \leftarrow 0$;

  else

    $m \leftarrow m + 1$;

    Build a new cluster $\mathcal{G}_m \leftarrow \{i, j\}$;

Discard all groups that contain less than three hits;

Both methods proposed by [72] try to form groups that maximize the similarity between elements of the same group. However, since they are greedy algorithms, the groups returned by them may not be the ones that contain the most similar signals. As the number of hits that need to be grouped is very low (usually under 10 hits, even in actual acoustic emission tests), we propose a combinatoric algorithm that assigns a group to a hit by finding the group of K hits whose minimum similarity between elements of the group is maximum, where the number of hits per group K is fixed. The algorithm is shown in Algorithm 6.

Algorithm 6: Our proposed hit grouping method based on cross-correlation.

Data: Hits $r_1[n], \cdots, r_N[n]$ ordered in ascending TOA order; Number of hits per group K;

Result: Group $\mathcal{G}$ that contains the first hit.

Calculate the set $\mathcal{C}$ of all possible choices of K hits that contains the first hit and that does not contain two or more hits from the same sensor ;

$\mathcal{G} \leftarrow \arg\max_{\mathcal{G}\in\mathcal{C}} \min_{u,v\in\mathcal{G}} \rho(u,v)$;

5.3.3 Our proposed Hit Grouping method based on Least Squares

The source localization techniques presented in this chapter can be used to group hits into events, as the minimum of the cost function $J^*_\lambda(x,y)$ will be higher when one of the hits does not belong to the same event as the other ones. Suppose we want to choose L hits to locate a source from a set of $L' > L$ hits that possibly belong to that event. This can be done by generating all the $\binom{L'}{L}$ possible combinations of hits and for each one minimizing $J^*_\lambda(x,y)$. The combination that yields the smallest minimum for $J^*_\lambda(x,y)$ is the best grouping. Since in general L and L' are small numbers, this brute force search technique is feasible.

Minimizing $J^*_\lambda(x,y)$ for each possible group is actually a joint grouping and source localization technique, as the source position is also returned by the method. However, if we are only interested in grouping hits, the exact location of the source position is not important. In this case, it is possible to reduce the complexity of our method by computing $J_\lambda(\hat{x},\hat{y})$ instead of $J^*_\lambda(x,y)$, where $(\hat{x},\hat{y})$ is the source position estimated by any low-complexity localization method, as minimizing J_{TOA} using TOAs obtained from the Fixed Threshold Algorithm. For the same reason, in this work we test our hit grouping method using $\lambda = 0$ (that is, its least squares version) to further reduce complexity.

Our proposed hit grouping algorithm is described in Algorithm 7.

Algorithm 7: Our proposed hit grouping algorithm based on Least Squares.

Data: Hits $r_1[n], \cdots, r_N[n]$ ordered in ascending TOA order concatenated as a single vector $\mathbf{y}$; Propagation Model $\mathbf{H}$; Dictionary $\mathbf{D}$; Sparsity penalty factor λ;

Result: Group $\mathcal{G}$ that contains the first hit.

Calculate the set $\mathcal{C}$ of all possible choices of K hits that contains the first hit and that does not contain two or more hits from the same sensor ;

for *each* $\mathcal{G} \in \mathcal{C}$ **do**

  Estimate the source position (x_0, y_0) for group $\mathcal{G}$ using any low-complexity localization method;

  $E_{\mathcal{G}} \leftarrow \min_{\mathbf{s}} \|\mathbf{y} - \mathbf{H}(x_0, y_0)\mathbf{D}\mathbf{s}\|_2^2 + \lambda \|\mathbf{s}\|_0$;

$\mathcal{G} \leftarrow \arg\min_{\mathcal{G}} E_{\mathcal{G}}$;

5.3.4 Simulations

Using waveforms collected from an acoustic emission test on an aircraft performed by Embraer, we generated a synthetic source at $\mathbf{x}_1 = (0.2, 0.3)$ and $t_1 = 0$, which we aim to localize. Three sensors were positioned at $(0, 0)$, $(0, 1)$, $(1, 1)$, and the wave velocity in the medium is $c = 5$km/s. We chose to use only three sensors to allow the comparison of the grouping methods with Algorithm 5, which cannot form groups containing more than three hits. A spurious source with a different waveform than the one from the source of interested located at $(1.3, 1.3)$ was generated at several instants $t_2 \geq t_1$. A white Gaussian noise of standard deviation $K/5$ was added to the received signals, where $K = 0.02$ is the fixed threshold used to compute TOAs.

The stream at each sensor was converted into hits using the HDT/HLT technique with HDT = HLT = 15 μs and $K = 0.02$ (see Section 1.1.1 in Chapter 1). This way, each sensor detects one or two hits, depending if the waves from both sources arrive at close or distant instants. For each instant of emission of the second source t_2, hits were grouped using all presented grouping methods and the obtained groups were used to localize the source. The obtained groups were used to localize the source through the minimization of $J_{\text{TOA}}(x, y)$ and TOAs estimated by the fixed threshold method.

Figures 45 and 46 show the MSE for the presented hit grouping methods in terms of the instant of emission of the second source. In Figure 45, we generated a spurious source waveform that is not very correlated with the waveform of the source of interest, while in Figure 46 two similar (yet different) waveforms were used. Both EDT and Least

Squares present almost the same performance in both scenarios because they do not use cross-correlation to cluster hits, thus they are not affected by the choice of the waveform for the spurious source. In both scenarios, our method based on Least Squares has the smallest MSE between all other techniques.

The first hit always comes from the source of interest, but the second hit may come from the spurious source if $t_2 < 64\mu$s, in which case EDT cannot group signals correctly because it picks the three first hits to form an event. After $t = 64\mu$s, the first three hits come from the first source, thus EDT groups all hits correctly.

Figure 47 shows the number of hits detection by the HDT/HLT method over time for both simulations (recall that in our simulations all grouping algorithms receive the same hits as input). There are three sensors and two sources, thus ideally six hits should be detected. However, only five hits are detected for $t_2 \in [64, 194]\mu$s, which means that two waves from different sources are overlapped in a hit. That is why all three methods based on correlation do not perform well in this interval for both simulations.

There is a rise in MSE between $t_2 = 64$ μs and $t_2 = 129$ μs because the TOA from the overlapped hit cannot be accurately estimated: For $t_2 \in [64, 129]$ μs, the wave from the spurious source reaches the sensor before the wave from the source of interest, thus the picked TOA is actually from the spurious hit.

For low-correlated sources (Figure 45), all methods achieve the minimum MSE for large t_2, that is, very spaced hits. In this scenario, our combinatorial algorithm based on cross-correlation performs better than all other techniques from [72], and has the same performance as our grouping method based on Least Squares if hits are not overlapped. Note that our cross-correlation method has much less computational complexity than our LS-based method.

On the other hand, for high-correlated sources (Figure 46), all cross-correlation methods become very sensitive to noise, presenting high MSE for most values of t_2. Even the 2nd Wang et al. method (designed for highly-correlated sources) does not cluster hits correctly because of the noise. Our cross-correlation method finds the actual group at some instants, but it presents several spikes of high MSE at many instants.

From these simulations, we conclude that our LS-based hit grouping technique performs equal or better than all other methods in all situations. However, its complexity is much higher than the other methods, and it also requires the knowledge of the propagation model and its parameters. We also conclude that our proposed method based on similarity performs better than both methods from Wang et al, except in cases with

highly-correlated sources or overlapped hits, where none of the methods based on cross-correlation perform well.

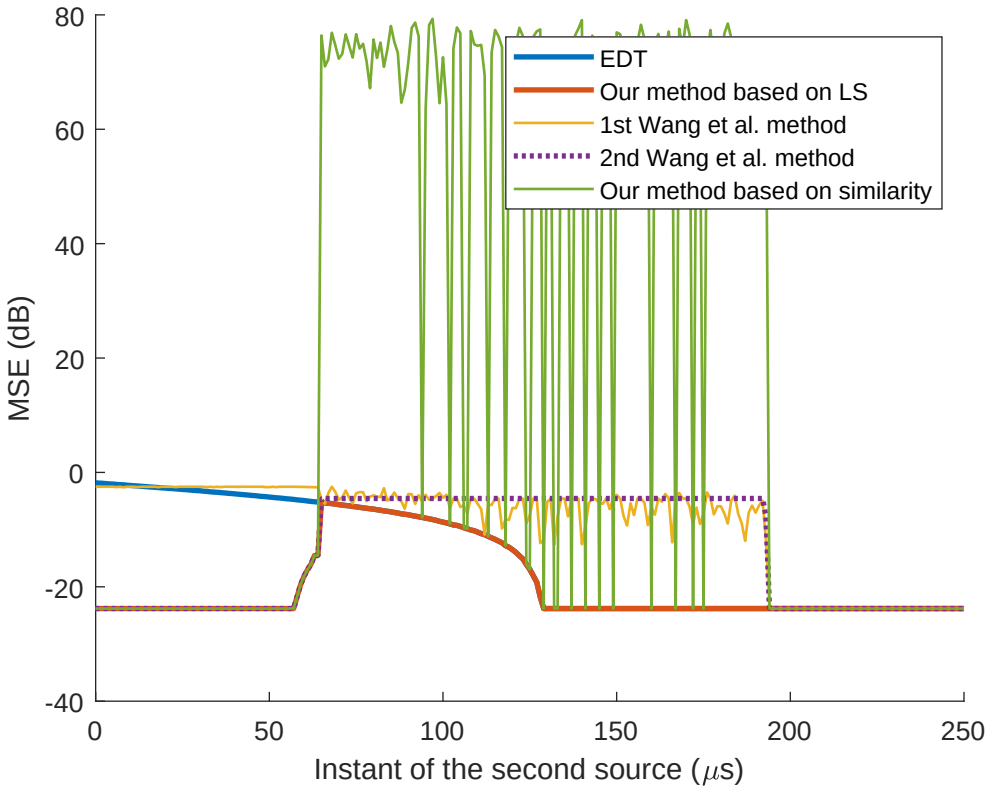

Figure 45: Comparison of hit grouping algorithms for two sources generating distinct waveforms. The first source emits elastic waves at $t = 0$, and the second one emits waves at different instants.

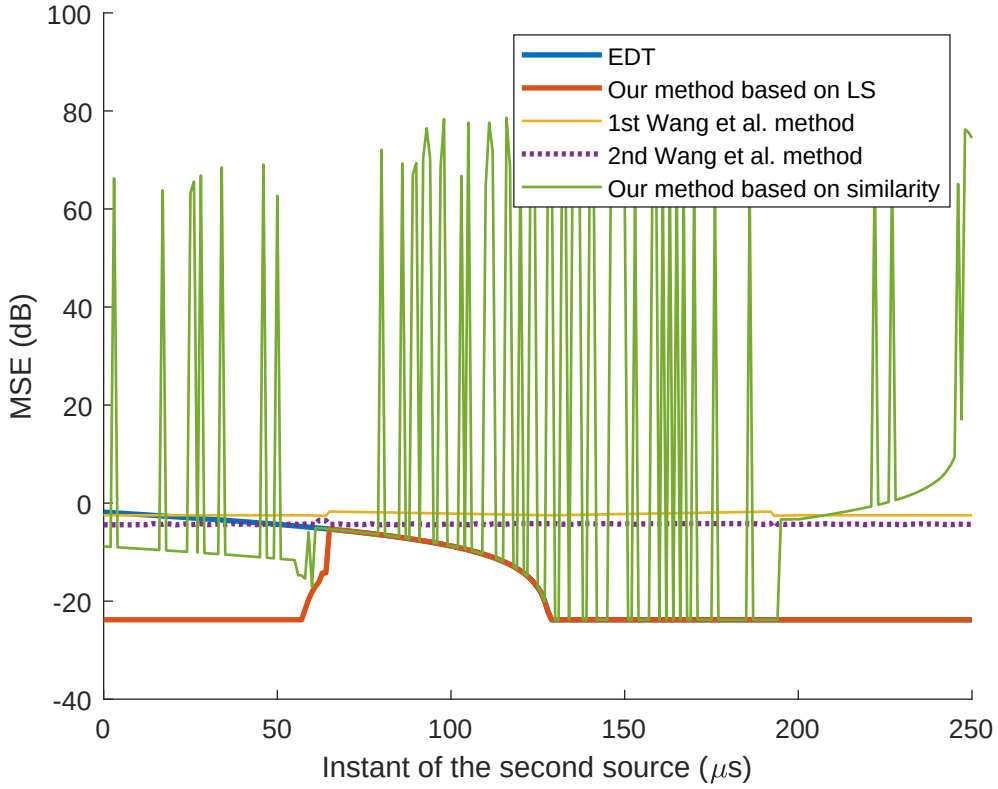

Figure 46: Comparison of hit grouping algorithms for two sources generating similar waveforms. The first source emits elastic waves at $t = 0$, and the second one emits waves at different instants.

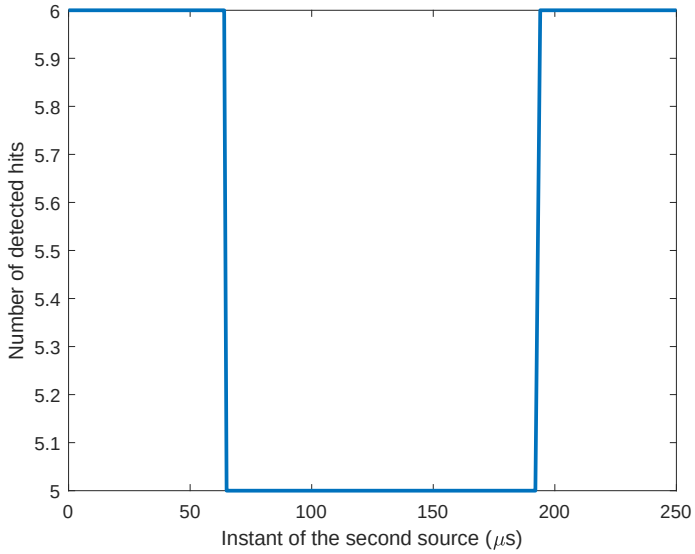

(a) Simulation from Figure 45

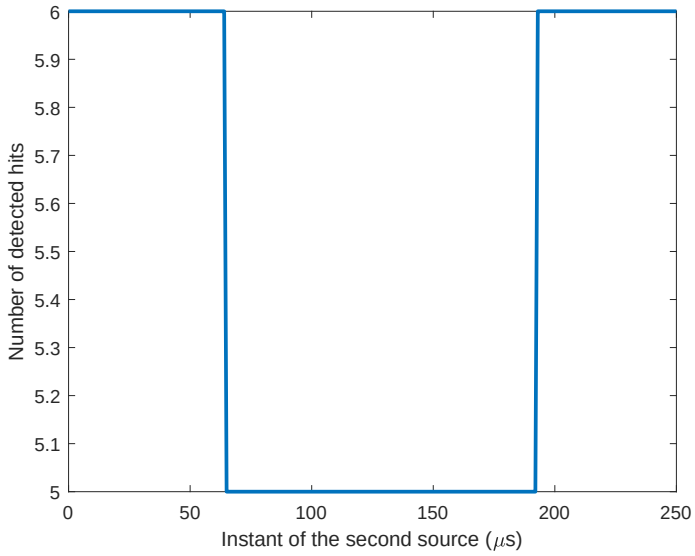

(b) Simulation from Figure 46

Figure 47: Number of detected hits in terms of the instant of the second source (t_2) for the HDT/HLT method. In our simulations, all grouping algorithms receive as input the hits extracted by the HDT/HLT method.

Concluding remarks

In this chapter, we presented a localization method that uses the waveforms instead of TOAs to estimate the source position. Even though the computational complexity of our method is much higher when compared to TOA-based methods, its accuracy is much better for most noise levels, even if TOAs are estimated using the best possible threshold for each realization of the noise. Our method requires a propagation model as input,

but it still shows higher accuracy than TOA-based methods when an imprecise model is used. It is also possible to exploit the information about the sparsity of the waveforms on a known dictionary to increase the performance of our method if a precise propagation model is used, even though using sparsity leads to accuracy gain for high SNRs if the model is not precise.

We also created two hit grouping algorithms — one method based on Least Squares and another method based on cross-correlation – and compared them with existing techniques in a scenario where a source emits a wave at instant $t = 0$ and a second source emits another wave at different instants. Our hit grouping algorithm based on Least Squares is an extension of our localization techniques presented in this chapter, and performs better than all other methods in all scenarios, even though it has high computational complexity. Our method based on cross-correlation has low complexity and performs better than the other algorithms based on cross-correlation in most cases, but this class of algorithms shows poor results if the waveforms emitted by the different sources are highly correlated.

6 CONCLUSION

In this work, we provided a brief introduction to acoustic emission and presented several new techniques whose ultimate goal is to improve the accuracy of localization methods. In Chapter 2, we deduced the TOA probability distribution expression assuming that TOAs were obtained using the fixed threshold method and that the instant of the first sample is a uniform random variable, allowing the development of new statistical TOA and source position estimators that may have better performance than usual methods. A simplified and approximate expression for the time of arrival pdf under low noise level condition was also developed, making it possible to test localization algorithms without the need to simulate the signals using a more precise model for the uncertainty on the time of arrival estimates than the Gaussian distribution.

Theoretical bounds for TDOA bias were calculated under small noise condition, and a TDOA bias model was derived from the new bounds. This model makes it possible to correct localization bias and thus reduce the distance between the estimated and the real source position. Eliminating the bias also allows the application of the Cramér-Rao Lower Bound and helps the search for better unbiased TDOA and source position estimators, as done in Chapter 4. Furthermore, we presented a TDOA debiasing technique for structures where the Constant Velocity Model is a good approximation of the propagation model.

In Chapter 3, we derived the closed-form solution in the case where only three sensors are used in isotropic medium and showed that for some geometries two sources at different positions may generate the same TOAs, in which case the localization problem has more than one solution. These secondary solutions may lead to local minima in cost function, causing a large localization error. We presented the TOA estimation method based on AIC, and we compared it with the fixed threshold method, concluding that AIC is more robust to noise and does not cause TOA bias, even though it may perform poorly for hits whose energy is not concentrated in the first samples. We also introduced the anisotropic cost functions J_{TOA} and J_{TDOA}, and showed they may perform better than their isotropic versions in anisotropic structures.

In Chapter 4, we derived an expression for the optimal source position estimator based on TOA estimates for the Gaussian Mixture case, which is a good approximation for the TOA pdf for high sampling frequency assuming that TOAs were estimated with the fixed threshold method. The derived estimator is optimal assuming that the noise level is not very high and the parameters of the mixtures are known, but we showed that it is possible to estimate these parameters from noisy signals, in which case our estimator may obtain better performance than other localization methods based on TOAs. Furthermore, we showed that $J_{TOA}(x, y)$ coincides with the optimal estimator if TOAs are i.i.d, unbiased and follow a Gaussian distribution.

Then, we derived in Chapter 5 a waveform-based localization method that uses directly the waveform instead of TOAs to localize the source. The propagation model is also an input of this method, which accepts any linear propagation model, such as the models presented in Chapter 1. The two versions of this method — one that relies on sparse estimation and another that uses a least-squares approach — showed great performance even when the model used by the algorithm is not the one used to generate the signals received by the sensors in simulation. Finally, we developed two hit grouping methods — one based in least squares, and other based on cross-correlation. The method based on least-squares performed better than all other grouping methods in all scenarios, and the our method based on cross-correlation performed better than techniques that also use cross-correlation is most cases.

REFERENCES

[1] W. H. Prosser, *Nondestructive Evaluation — Theory, Techniques, and Applications*. New York: Marcel Dekker, 2001.

[2] M. Rabiei and M. Modarres, "Quantitative methods for structural health management using in situ acoustic emission monitoring," *International Journal of Fatigue*, vol. 49, pp. 81–89, 2013.

[3] R. Pullin, K. M. Holford, S. L. Evans, M. Baxter, and J. Hensman, "Advanced location and characterisation of damage in complex metallic structures using acoustic emission," in *Proceedings of the 13th International Conference on Experimental Mechanics ICEM*, vol. 13, 2007, pp. 925–926.

[4] M. J. Eaton, R. Pullin, and K. M. Holford, "Towards improved damage location using acoustic emission," *Proceedings of the Institution of Mechanical Engineers, Part C: Journal of Mechanical Engineering Science*, vol. 226, no. 9, pp. 2141–2153, 2012.

[5] D. G. Aggelis, E. Z. Kordatos, and T. E. Matikas, "Acoustic emission for fatigue damage characterization in metal plates," *Mechanics Research Communications*, vol. 38, no. 2, pp. 106–110, 2011.

[6] C. Farrar and K. Worden, *Structural Health Monitoring: A Machine Learning Perspective*. Wiley, 2012.

[7] K. M. Holford, M. J. Eaton, J. J. Hensman, R. Pullin, S. L. Evans, N. Dervilis, and K. Worden, "A new methodology for automating acoustic emission detection of metallic fatigue fractures in highly demanding aerospace environments: An overview," *Progress in Aerospace Sciences*, vol. 90, pp. 1 – 11, 2017. [Online]. Available: http://www.sciencedirect.com/science/article/pii/S0376042116300768

[8] T. Kundu, "Acoustic source localization," *Ultrasonics*, vol. 54, no. 1, pp. 25–38, Jan. 2014, 00079.

[9] E. Y. Dris, R. Drai, A. Benammar, and D. Berkani, "Acoustic emission source localization in plate-like structure," in *2017 European Conference on Electrical Engineering and Computer Science (EECS)*, Nov 2017, pp. 193–197.

[10] S. K. Al-Jumaili, M. R. Pearson, K. M. Holford, M. J. Eaton, and R. Pullin, "Acoustic emission source location in complex structures using full automatic delta t mapping technique," *Mechanical Systems and Signal Processing*, vol. 72-73, pp. 513 – 524, 2016. [Online]. Available: http://www.sciencedirect.com/science/article/pii/S0888327015005439

[11] L. Sun and Y. Li, "Acoustic emission sound source localization for crack in the pipeline," in *2010 Chinese Control and Decision Conference*, May 2010, pp. 4298–4301.

[12] S. Gollob and T. Vogel, "Localisation of acoustic emission in reinforced concrete using heterogeneous velocity models," in *31st Conference of the European Working Group on Acoustic Emission (EWGAE)*. Eidgenössische Technische Hochschule Zürich, IBK, Institute of Structural Engineering, Chair of Structural Engineering, Structural Design and Conservation, 2014, 2014, 31st Conference of the European Working Group on Acoustic Emission (EWGAE 2014); Conference Location: Dresden, Germany; Conference Date: September 3-5, 2014.

[13] B. Dubuc, A. Ebrahimkhanlou, and S. Salamone, "Sparse reconstruction localization of multiple acoustic emissions in large diameter pipelines," *Sensors and Smart Structures Technologies for Civil, Mechanical, and Aerospace Systems*, 2017.

[14] A. Ebrahimkhanlou and S. Salamone, "Acoustic emission source localization in thin metallic plates: A single-sensor approach based on multimodal edge reflections," *Ultrasonics*, vol. 78, pp. 134 – 145, 2017. [Online]. Available: http://www.sciencedirect.com/science/article/pii/S0041624X16304097

[15] G. K. Kocur, E. H. Saenger, C. U. Grosse, and T. Vogel, "Time reverse modeling of acoustic emissions in a reinforced concrete beam," *Ultrasonics*, vol. 65, pp. 96 – 104, 2016. [Online]. Available: http://www.sciencedirect.com/science/article/pii/S0041624X15002693

[16] K. Grabowski, M. Gawronski, I. Baran, W. Spychalski, W. J. Staszewski, T. Uhl, T. Kundu, and P. Packo, "Time–distance domain transformation for acoustic emission source localization in thin metallic plates," *Ultrasonics*, vol. 68, pp. 142 – 149, 2016.

[17] A. Beck, P. Stoica, and J. Li, "Exact and approximate solutions of source localization problems," *IEEE Transactions on Signal Processing*, vol. 56, no. 5, pp. 1770–1778, May 2008.

[18] B. Friedlander, "A passive localization algorithm and its accuracy analysis," *IEEE J. Ocean. Eng.*, vol. 12, no. 1, pp. 234–245, Jan. 1987, 00354.

[19] L. Rui and K. C. Ho, "Bias analysis of source localization using the maximum likelihood estimator," in *2012 IEEE International Conference on Acoustics, Speech and Signal Processing (ICASSP)*, March 2012, pp. 2605–2608.

[20] K. C. Ho, "Bias reduction for an explicit solution of source localization using TDOA," *IEEE Transactions on Signal Processing*, vol. 60, no. 5, pp. 2101–2114, May 2012.

[21] The Japanese Society for Non-Destructive Inspection, *Practical Acoustic Emission Testing*, 01 2016.

[22] C. A. Prete Jr., V. H. Nascimento, and C. G. Lopes, "Modeling time of arrival probability distribution and TDOA bias in acoustic emission testing," in *2018 26th European Signal Processing Conference (EUSIPCO)*, Sep. 2018, pp. 1117–1121.

[23] H. Akaike, *Information Theory and an Extension of the Maximum Likelihood Principle*. New York, NY: Springer New York, 1998, pp. 199–213. [Online]. Available: https://doi.org/10.1007/978-1-4612-1694-0_15

[24] P. Sedlak, Y. Hirose, and M. Enoki, "Arrival time detection in thin multilayer plates on the basis of akaike information criterion," *28th European Conference on Acoustic Emission Testing" EWGAE-Kraków*, pp. 17–19, 01 2008.

[25] A. Carpinteri, J. Xu, G. Lacidogna, and A. Manuello, "Reliable onset time determination and source location of acoustic emissions in concrete structures," *Cement and Concrete Composites*, vol. 34, no. 4, pp. 529 – 537, 2012. [Online]. Available: http://www.sciencedirect.com/science/article/pii/S0958946511002149

[26] M. de Campos da Silva, "Monitoramento estrutural de aeronaves via redes de sensores — localização de falhas," Master's thesis, Escola Politécnica da USP, Em andamento, orientador: Prof. Vítor H. Nascimento; co-orientador: Prof. Cassio G. Lopes.

[27] R. D. Finlayson, "Acoustic emission testing," in *Handbook of Nondestructive Evaluation*, C. Hellier, Ed. McGraw Hill, 2003, ch. Acoustic Emission Testing, pp. 10.1–10.39.

[28] *DiST with AEwin User's Manual*, Physical Acoustics Corporation.

[29] M. Shateri, M. Ghaib, D. Svecova, and D. Thomson, "On acoustic emission for damage detection and failure prediction in fiber reinforced polymer rods using pattern recognition analysis," *Smart Materials and Structures*, vol. 26, no. 6, p. 065023, 2017. [Online]. Available: http://stacks.iop.org/0964-1726/26/i=6/a=065023

[30] R. Unnpórsson, "Hit detection and determination in ae bursts," *Acoustic Emission - Research and Applications*, 2013.

[31] M. Kharrat, E. Ramasso, V. Placet, and M. L. Boubakar, "A Signal Processing Method for Hits Detection and Separation in High AE Activity Systems: Application to Composite Materials under Fatigue Tests." in *EWSHM - 7th European Workshop on Structural Health Monitoring*, V. Le Cam, L. Mevel, and F. Schoefs, Eds. Nantes, France: IFFSTTAR, Inria, Université de Nantes, Jul. 2014. [Online]. Available: https://hal.inria.fr/hal-01022993

[32] K. Máthis and F. Chmelík, "Exploring plastic deformation of metallic materials by the acoustic emission technique," in *Acoustic Emission*, W. Sikorski, Ed. Rijeka: IntechOpen, 2012, ch. 2. [Online]. Available: https://doi.org/10.5772/31660

[33] M. C. Silva, V. H. Nascimento, and C. G. Lopes, "Localização de fontes por diferença de tempo de chegada em meios anisotrópicos," in *Anais do XXXVII Simpósio Brasileiro de Telecomunicações*, Petrópolis, 2019.

[34] M. Gresil and V. Giurgiutiu, "Prediction of attenuated guided waves propagation in carbon fiber composites using rayleigh damping model," *Journal of Intelligent Material Systems and Structures*, vol. 26, no. 16, pp. 2151–2169, 2015.

[35] P. He, "Simulation of ultrasound pulse propagation in lossy media obeying a frequency power law," *IEEE Transactions on Ultrasonics, Ferroelectrics, and Frequency Control*, vol. 45, no. 1, pp. 114–125, Jan 1998.

[36] W. Chen and S. Holm, "Modified Szabo's wave equation models for lossy media obeying frequency power law," *The Journal of the Acoustical Society*

of America, vol. 114, no. 5, pp. 2570–2574, 2003. [Online]. Available: https://asa.scitation.org/doi/abs/10.1121/1.1621392

[37] T. L. Szabo, "Causal theories and data for acoustic attenuation obeying a frequency power law," *The Journal of the Acoustical Society of America*, vol. 97, no. 1, pp. 14–24, 1995. [Online]. Available: https://doi.org/10.1121/1.412332

[38] Z. Nazarchuk, V. Skalskyi, and O. Serhiyenko, *Propagation of Elastic Waves in Solids*. Cham: Springer International Publishing, 2017, pp. 29–73.

[39] M. Bauccio, *ASM Metals Reference Book*. Ed. ASM International, 1993.

[40] S. P. Näsholm and S. Holm, "On a fractional zener elastic wave equation," *Fractional Calculus and Applied Analysis*, vol. 16, no. 1, pp. 26–50, Mar 2013. [Online]. Available: https://doi.org/10.2478/s13540-013-0003-1

[41] A. Deng, L. Zhao, and Y. Zhao, "A new algorithm of ae localization using subgradient projection," in *2009 International Conference on Computational Intelligence and Software Engineering*, Dec 2009, pp. 1–5.

[42] M. A. Torres Arredondo, "Acoustic emission testing and acousto-ultrasonics for structural health monitoring," 01 2013.

[43] V. Salinas, Y. Vargas, J. Ruzzante, and L. Gaete, "Localization algorithm for acoustic emission," *Physics Procedia*, vol. 3, no. 1, pp. 863 – 871, 2010, international Congress on Ultrasonics, Santiago de Chile, January 2009.

[44] M. A. Asiru, "Asymptotic formulas for sequence factorial of arithmetic progression," *International Journal of Mathematical Education in Science and Technology*, vol. 45, no. 6, pp. 947–952, 2014.

[45] P. Stoica and J. Li, "Lecture Notes - Source Localization from Range-Difference Measurements," *IEEE Signal Processing Magazine*, vol. 23, no. 6, pp. 63–66, Nov. 2006, 00141.

[46] A. Beck, P. Stoica, and J. Li, "Exact and Approximate Solutions of Source Localization Problems," *IEEE Transactions on Signal Processing*, vol. 56, no. 5, pp. 1770–1778, May 2008.

[47] T. Kundu, H. Nakatani, and N. Takeda, "Acoustic source localization in anisotropic plates," *Ultrasonics*, vol. 52, no. 6, pp. 740–746, Aug. 2012, 00079.

[48] M. D. Gillette and H. F. Silverman, "A linear closed-form algorithm for source localization from time-differences of arrival," *IEEE Signal Process. Lett.*, vol. 15, pp. 1–4, 2008.

[49] H. W. Wei and S. F. Ye, "Comments on "A Linear Closed-Form Algorithm for Source Localization From Time-Differences of Arrival"," *IEEE Signal Process. Lett.*, vol. 15, pp. 895–895, 2008.

[50] A. Le Duff, S. E. Hamdi, G. Plantier, A. Sourice, and R. Feron, "Cramer-Rao bounds for acoustic emission events localization in a flat plate," in *Acoustics 2012*, S. F. d'Acoustique, Ed., Nantes, France, Apr. 2012. [Online]. Available: https://hal.archives-ouvertes.fr/hal-00810842

[51] S. Spencer, "Closed-form analytical solutions of the time difference of arrival source location problem for minimal element monitoring arrays," *The Journal of the Acoustical Society of America*, vol. 127, pp. 2943–54, 05 2010.

[52] C. A. Prete Jr., "Estudo de ensaios de emissão acústica aplicados a testes de aeronaves," Escola Politécnica da USP / EMBRAER, Tech. Rep., 2015.

[53] H. C. So, *Handbook of Position Location*. John Wiley & Sons, Ltd, 2011. [Online]. Available: https://onlinelibrary.wiley.com/doi/abs/10.1002/9781118104750.ch2

[54] P. Stoica and J. Li, "Lecture notes - source localization from range-difference measurements," *IEEE Signal Processing Magazine*, vol. 23, no. 6, pp. 63–66, Nov 2006.

[55] M. R. Pearson, M. Eaton, C. Featherston, R. Pullin, and K. Holford, "Improved acoustic emission source location during fatigue and impact events in metallic and composite structures," *Structural Health Monitoring*, vol. 16, no. 4, pp. 382–399, 2017. [Online]. Available: https://doi.org/10.1177/1475921716672206

[56] S. M. Kay, *Fundamentals of statistical signal processing, volume I: estimation theory*. Upper Saddle River, NJ: Prentice Hall, 1993.

[57] H. C. So, Y. T. Chan, K. C. Ho, and Y. Chen, "Simple formulae for bias and mean square error computation [dsp tips and tricks]," *IEEE Signal Processing Magazine*, vol. 30, no. 4, pp. 162–165, July 2013.

[58] A. Ebrahimkhanlou and S. Salamone, "Single-sensor acoustic emission source localization in plate-like structures using deep learning," *Aerospace (ISSN 2226-4310)*, vol. 5, 05 2018.

[59] B. Dubuc, A. Ebrahimkhanlou, and S. Salamone, "Localization of multiple acoustic emission events occurring closely in time in thin-walled pipes using sparse reconstruction," *Journal of Intelligent Material Systems and Structures*, vol. 29, no. 11, pp. 2362–2373, 2018. [Online]. Available: https://doi.org/10.1177/1045389X18770857

[60] C. Boya, M. Ruiz-Llata, J. Posada, and J. A. Garcia-Souto, "Identification of multiple partial discharge sources using acoustic emission technique and blind source separation," *IEEE Transactions on Dielectrics and Electrical Insulation*, vol. 22, no. 3, pp. 1663–1673, June 2015.

[61] R. Ma, B.-M. Qiao, T.-J. Zhang, L. Wang, S.-N. Zhou, and L.-L. Zhang, "Application of discrete wavelet operations in the detection of acoustic emission of coal and rock rupture," *Journal of Coal Science and Engineering (China)*, vol. 19, no. 2, pp. 160–166, Jun 2013. [Online]. Available: https://doi.org/10.1007/s12404-013-0209-1

[62] D. Aljets, A. Chong, and S. Wilcox, "Acoustic emission source location in plate-like structures using a closely arranged triangular sensor array," vol. 28, 01 2010.

[63] M. Aharon, M. Elad, and A. Bruckstein, "K-SVD: An algorithm for designing overcomplete dictionaries for sparse representation," *IEEE Transactions on Signal Processing*, vol. 54, no. 11, pp. 4311–4322, Nov 2006.

[64] D. L. Donoho, "Compressed sensing," *IEEE Trans. Inf. Theory*, vol. 52, no. 4, pp. 1289–1306, Apr. 2006.

[65] J. A. Tropp and A. C. Gilbert, "Signal recovery from random measurements via orthogonal matching pursuit," *IEEE Transactions on Information Theory*, vol. 53, no. 12, pp. 4655–4666, Dec 2007.

[66] Y. Zakharov, V. Nascimento, R. de Lamare, and F. G. de Almeida Neto, "Low-complexity DCD-based sparse recovery algorithms," *IEEE Access*, 2017.

[67] M. Elad, *Sparse and Redundant Representations: From Theory to Applications in Signal and Image Processing*, 1st ed. Springer Publishing Company, Incorporated, 2010.

[68] R. Rubinstein, M. Zibulevsky, and M. Elad, "Double sparsity: Learning sparse dictionaries for sparse signal approximation," *IEEE Transactions on Signal Processing*, vol. 58, no. 3, pp. 1553–1564, March 2010.

[69] ——, "Efficient implementation of the K-SVD algorithm using batch orthogonal matching pursuit," *CS Technion*, vol. 40, 01 2008.

[70] K. Engan, S. O. Aase, and J. H. Husoy, "Method of optimal directions for frame design," in *1999 IEEE International Conference on Acoustics, Speech, and Signal Processing. Proceedings. ICASSP99 (Cat. No.99CH36258)*, vol. 5, March 1999, pp. 2443–2446 vol.5.

[71] W. S. Pires, "Processamento de dados para a eliminação de falsos positivos ao utilizar a técnica de emissão acústica," Master's thesis, Instituto Tecnológico de Aeronáutica, 2013.

[72] W.-K. Wang, Y.-B. Li, Y.-N. Li, and Y. Zhang, "An acoustic emission event determination method for acoustic emission testing of tank bottom based on cluster analysis," *IEEE/ASME International Conference on Advanced Intelligent Mechatronics (AIM)*, 2013.

[73] R. L. de Màntaras and J. Aguilar-Martín, "Self-learning pattern classification using a sequential clustering technique," *Pattern Recognition*, vol. 18, no. 3, pp. 271 – 277, 1985. [Online]. Available: http://www.sciencedirect.com/science/article/pii/0031320385900524